MECHANISTIC MODEL ENHANCES ESTIMATES OF SOLVENT-ASSISTED OIL RECOVERY IN UNCONVENTIONAL RESERVOIRS

A Thesis

by

RODRIGO MOREIRA MESSIAS

Submitted to the Graduate and Professional School of
Texas A&M University
In partial fulfillment of the requirements for the degree of

MASTER OF SCIENCE

Chair of Committee,	Maria A. Barrufet
Committee Members,	I. Yucel Akkutlu
	Mahmoud El-Halwagi
Head of Department,	Akhil Datta-Gupta

May 2023

Major Subject: Petroleum Engineering

ABSTRACT

In this project we developed a simulator to forecast solvent-assisted enhanced oil recovery using miscible solvents in unconventional reservoirs. We modeled oil recovery using a huff-n-puff process in ultra-low permeability oil reservoirs by including diffusion-dominated flow. We analyzed the swelling of dead and live oils, estimated the thermodynamic-limited recovery given solvent-in-oil solubility, assessed the impact of effective diffusion coefficient, flow length, pressure, and temperature on recovery, and explored the uncertainty and impact of fracture surface area.

Current conventional reservoir simulators do not consider all the complex rock-fluid interactions in unconventional reservoirs. Alternative published modeling techniques are computationally expensive and often require geological data that may not be available. Since flow is diffusion dominated, our simulator, by design, does not require geological data. Further, it was coded using only VBA and Microsoft Excel, making it viable for routine use in industry.

Prior to running the simulator, we estimate the ultimate achievable (thermodynamics-limited) recovery for a specified oil-solvent, which is rooted in complex interactions related to molecular size, individual critical points, and mutual solvent/oil solubility. Depending on the type of oil and solvent, increasing solvent concentration might result in a decrease in saturation pressure at the reservoir temperature, allowing for solvent to be added indefinitely and reach full miscibility at the specified reservoir pressure. And, a saturation point might not exist with increasing solvent concentration, as solvent might reach

full miscibility. For these scenarios maximum concentration must be restricted such that realistic injected pore volumes and gas oil ratios are achieved.

Increase in fracture surface area is equivalent to an increase in effective diffusion coefficient, allowing for recoveries to be estimated at any time. We can achieve the same result by decreasing fracture spacing, which can be modeled by decreasing stimulated flow length.

ACKNOWLEDGEMENTS

I would like to start by thanking my advisor and mentor, Dr. Maria Barrufet, for her constant support throughout my work. Her patience is beyond imaginable and her expertise in the field is nothing short of incredible. Without her guidance and assistance, this work would have never come to fruition.

I would like to thank my committee members, especially Dr. I. Yucel Akkutlu for piquing my interest in unconventional reservoirs, and providing me with in-depth, exciting, and thorough lectures, contributing to the background of this work.

I would also like to thank all the staff and faculty at Texas A&M University, for giving me an opportunity to gain experience and challenge myself. The countless seminars and the tough, yet rewarding courses I experienced, have given me a chance to prepare for the start of my career.

Last but foremost, I would like to thank my girlfriend, my friends and family for always being there for me and believing in me more than I ever could. Their endless support has made this possible.

CONTRIBUTORS AND FUNDING SOURCES

Contributors

This work was supported by a thesis committee consisting of Professor Maria A. Barrufet and Professor I. Yucel Akkutlu of the Department of Petroleum Engineering and Professor Mahmoud El-Halwagi of the Department of Chemical Engineering.

All other work for the thesis was completed by the student independently.

Funding Sources

Work was completed without financial support from Texas A&M University, or any other sources outside the University.

NOMENCLATURE

Symbols	Definition
c	Concentration of solvent in liquid phase (mole fraction)
c_i	Initial concentration of solvent in liquid phase (mol/cm^3)
$c_{0,j}$	Concentration of solvent in liquid phase at cell j (mol/cm^3)
$c_{0,jmax}$	Concentration of solvent in liquid phase at cell j_{max} (mol/cm^3)
c_0	Maximum concentration of solvent in liquid phase (mole fraction)
d_g	Average diameter of grain (m)
D_{eff}	Effective diffusion coefficient in liquid phase in porous medium (cm^2/s)
D_m	Average diffusion coefficient (m^2/s)
f^j_i	Fugacity of component i in phase j (psia)
$f^s_{v,SC}$	Oil with solvent vapor molar fraction at standard conditions (fraction)
$f^o_{v,SC}$	Oil vapor molar fraction at standard conditions (fraction)
$f^{o,sep}_{v,SC}$	Oil vapor molar fraction at standard conditions after separated from solvent (fraction)
G	Initial gas in place (SCF)
G_p	Produced gas (SCF)
h_R	Reservoir height (ft)
K_i	Vapor-liquid equilibrium constant (K-value)
L	Length of porous media (ft)
l_R	Reservoir length (ft)
N	Initial oil in place (STB)
N_c	Number of components
$n_{l\,o}$	Moles of oil in liquid phase (moles)
$n_{l\,s}$	Moles of solvent in liquid phase (moles)
n_o	Initial oil moles (moles)
N_p	Produced oil (STB)
n_p	Produced oil moles (moles)
N_{pe}	Peclet number
n^i_{ratio}	Ratio of oil+solvent mole fractions before and after mixing (fraction)
$n_{v\,o}$	Moles of oil in vapor phase (moles)
$n_{v\,s}$	Moles of solvent in vapor phase (moles)
P_b	Saturation pressure (psi)
$p_{c,i}$	Critical pressure of component i (psia)
P_{STC}	Standard pressure (psi)
P_R	Reservoir pressure (psi)
PV_{inj}	Pore volume injected (fraction)
RF_{max}	Maximum recovery factor (fraction)
S	Surface area (ft^2)
$SA{:}V$	Surface area to volume ratio (ft^{-1})
SR_{max}	Maximum swelling ratio (fraction)

s_{stor}	Solvent stored in matrix (ft^3)
t	Time (days, hours, years)
T_{STC}	Standard temperature (°F)
T_R	Reservoir temperature (°F)
$T_{r,\,i}$	Reduced temperature of component i
V	Volume (ft^3)
V_{frac}	Fracture volume (ft^3)
V_o	Initial volume of oil (ft^3)
V_s	Swollen volume of oil (ft^3)
V_p	Produced volume of oil (ft^3)
$V^s_{ml,sc}$	Oil with solvent liquid molar volume at standard conditions (ft^3/mol)
$V^o_{ml,sc}$	Oil liquid molar volume at standard conditions (ft^3/mol)
$V^{inj}_{mv,sc}$	Solvent gas molar volume at standard conditions (ft^3/mol)
$V^s_{ml,R}$	Oil with solvent liquid molar volume at reservoir conditions (ft^3/mol)
$V^o_{ml,R}$	Oil liquid molar volume at reservoir conditions (ft^3/mol)
$V^{o,\,sep}_{mv,R}$	Oil gas molar volume at reservoir conditions after separated from solvent (ft^3/mol)
$V^{o,\,sep}_{ml,R}$	Oil liquid molar volume at reservoir conditions after separated from solvent (ft^3/mol)
$V^{inj}_{mv,R}$	Solvent gas molar volume at reservoir conditions (ft^3/mol)
w_F	Fracture width (ft)
w_R	Reservoir width (ft)
x	Flow length (ft)
x_i	Liquid mole fraction of component i (EOS)
x_w	Reference length of a porous medium (ft)
y_i	Vapor mole fraction of component i (EOS)
z_i	Overall mole fraction of component i
z^i_{ini}	Initial mole fraction of solvent component *i* before mixing (mole fraction)
z^i_l	Mole fraction of solvent+oil component *i* after mixing in the liquid phase (mole fraction)
z^i_{l+v}	Mole fraction of solvent+oil component *i* after mixing in the liquid and vapor phase (mole fraction)
z^i_v	Mole fraction of solvent+oil component *i* after mixing in the vapor phase (mole fraction)

Greek Symbols	**Definition**
β	Fraction of total moles in vapor phase
μ_i	Fluid velocity (cm/s)
ϕ_R	Reservoir porosity (%)
$\hat{\phi}^j_i$	Fugacity coefficient of component i in phase j
τ	Dimensionless time
ΔV_e	Volume expansion of the oil phase (cm^3)
ω_i	Acentric factor

χ_i	Maximum concentration of solvent in liquid phase (mole fraction)
χ_{max}	Normalized concentration of solvent in liquid phase (fraction)

Subscripts	**Definition**
0	Initial conditions
b	Bubble (for pressure)
eff	Effective (for diffusion)
F	Fracture
v, SC	Gas phase, standard condition
i	Component *i*
ini	Initial conditions
l+v	Liquid + Vapor
max	Maximum
mg,SC	Molar gas, standard condition
mg,R	Molar gas, reservoir condition
ml,SC	Molar liquid, standard condition
ml,R	Molar liquid, reservoir condition
norm	Normalized
o	Oil phase
p	Produced oil
R	Reservoir conditions
ratio	Ratio – specific to mole fraction ratio
s	Swollen
STC	Standard conditions
v	Vapor phase
w	Width (for reference length)

Superscripts	**Definition**
i	Solvent component *i*
inj	Injection fluid
s	Solvent + Oil
o	Oil
o, sep	Oil (after separated from solvent)

Abbreviations	**Definition**
EIA	Energy Information Administration
EOR	Enhanced oil recovery
GC	Gas chromatography
GOR	Gas oil ratio
GUF	Gross utilization factor
MMP	Minimum miscibility pressure
SCF	Standard cubic feet
STB	Standard barrel

TABLE OF CONTENTS

Page

LIST OF FIGURES

Page

LIST OF TABLES

Page

CHAPTER I

INTRODUCTION

In the last few decades, as the United States has shifted to production from unconventional (shale) reservoirs, the oil and gas industry has learned that recovering large fractions of petroleum from these source rocks is not possible using conventional technology. Shale contains nanoscale pores, leading to extremely rapid declines in production. Combining the traditional recovery approaches of Enhanced Oil Recovery (EOR) and hydraulic fracturing provides more promising technology to improve recovery and economics. The approach we used in this study included a rigorous physics-based model, coupling thermodynamics, with diffusion to improve and scale up results from an in-house, VBA-based simulator. With the objective to model the performance of solvent-assisted oil recovery in tight reservoirs, where the dominant flow mechanism is molecular diffusion of solvent from the fracture network into the matrix.

Currently, miscible solvent injection is the most commonly used EOR method for tight oil formations in the United States, according to the U.S. Department of Energy. The best procedure for solvent injection is huff-n-puff, in which a single well is used as both injector and producer. Solvent is initially injected into the well, followed by a soaking period, allowing the solvent to penetrate the matrix and dissolve in the oil, causing an oil expansion referred to as swelling. This swollen volume is produced from the same well. Solvents impact recovery of the oil differently, as it is directly proportional to the solubility of the solvent in the oil. The goal is to reach the maximum recovery factor, corresponding to the

thermodynamic limit to which the oil will swell after contacting the solvent, provided injected pore volumes and GORs are not above industry standards.

Enhanced oil recovery is an effective method for improving recovery; however, to further facilitate the solvent injection and the oil production, hydraulic fractures should be created. These fractures serve as pathways for the injection of solvent, and these same pathways are used once the injection well is turned into a production well. Fractures accelerate production. Theloy (2014) performed a study in the Bakken formation and found that hydraulic fractures are not the only important form of improved pathways, but that secondary and natural fractures also play a significant role in the production from the reservoir. Assuming they do not close, the simulation of hydraulic, natural, and secondary fractures is complex. Liu et al. (2020) developed a procedure to estimate fracture surface area from hydraulic fracture treatment pressure falloff data. This procedure considers variables that are otherwise unknown (lack of data), such as hydraulic fracture geometry, average injection volume into a perforation cluster, leak-off coefficient, density, and closure stress of secondary fractures. High level of uncertainty currently exists when estimating fracture surface area. In this work, a planar fracture was assumed for simplicity, and, based on assumed fracture spacing, an effective surface area and an effective diffusion coefficient was defined. However, since the time to reach the maximum recovery is directly proportional to the fracture surface area, a planar fracture may be underestimating the real fracture surface area. By representing the same planar fracture acting on a "shoe-box" matrix, to a radial fracture acting on an arrangement of "rods", the impact of an increase in fracture surface area has on recovery was analyzed.

Type curves were created to analyze the impact of effective diffusion coefficient, flow length and fracture surface area on recovery. Increasing effective diffusion coefficient or decreasing flow length will lead to a more interconnected, or rather, a more stimulated reservoir. Similarly, increasing fracture surface area allows for a more stimulated reservoir volume without the need of increasing effective diffusion coefficient, allowing for increased recoveries as well.

1.1 Research Objectives

The goal of this project is to upscale the model to allow for design of a realistic fracture scheme, by evaluating effective diffusion coefficients and flow length combinations. Given reservoir characteristics (geometry, pressure, temperature, and production limitations, such as effective diffusion coefficient and time), solvent, and oil compositions, the simulator was used to estimate oil recovery, solvent stored, and solvent produced. From realizations, varying solvent and oil types, pressure, temperature, fracture surface area and flow length, type curves were created from simulated predictions. Results allow engineers to design realistic fracture schemes, estimate proper duration of soaking time, select best solvent for injection and predict production of huff-n-puff process, while maintaining physics-based constraints (effective diffusion coefficient/flow length) and industry standards (oil/solvent combination, injected pore volume, GOR, time) required to achieve feasible recovery factors. To meet these objectives, we :

1. Designed a diagnostic tool to evaluate the maximum recovery factor for specific solvent-oil combinations, pressures, and temperatures
2. Estimated the time required to reach the maximum recovery factor
3. Estimated number of cycles and duration of cycles required in a huff-n-puff project

4. Developed a diagnostic tool to evaluate proper length of soaking times
5. Limited solvent production by evaluating GOR and injected pore volumes as a function of solvent concentration
6. Calculated solvent produced and solvent stored from huff-n-puff process of any duration
7. Analyzed recovery factor as a function of different solvents, oils, pressure, temperature, fracture surface area and flow length

1.2 Description of Chapters

Chapter I contains the Introduction, states the problem, and provides a summary of the objectives

Chapter II summarizes published literature on solvent injection. Including the definition and example of unconventional, liquid rich reservoirs, methods of enhanced oil recovery (EOR), types of solvent used in solvent-assisted recovery, the specific transport of the fluid, and important characteristics of the reservoir.

Chapter III describes oils and solvents used for simulation, workflow of thermodynamic-limited recovery factor calculations, analysis of GOR and injected pore volume limits, modeling procedure and calculations that can be performed prior to running molecular simulator.

Chapter IV contains the analysis of pressure and temperature dependence on swelling, molecular diffusion flow, solvent concentration distribution within matrix, fracture surface area, as well as development of type curves.

Chapter V explains the conclusions of this work and future work recommendations. Including summary of results observed in this work, review of limitations of numerical simulator, and proposition of issues that can be overcome.

CHAPTER II

LITERATURE REVIEW

2.1 Shale Properties and Production from Tight Oil Formations

Shale has become an analogous term with unconventional reservoir. It is an umbrella term, describing different rock types with similar composition of silts and clay. The main difference from these types of source rocks and the conventional reservoir rocks is the extremely low permeability and pore size. Unconventional rocks have an average pore size in the nanometer range, compared to a conventional rock in the micrometer range. This difference in pore size, and permeability make unconventional reservoirs economically unfeasible to produce without assistance of improved recovery techniques (Glorioso and Rattia 2012).

The U.S. Energy Information Administration (EIA) estimated that in 2021, crude oil produced directly from tight oil formations made up 65% of the total U.S. crude oil production, in other words, 2.64 billion barrels, an increase of 5% in comparison to 2018 (**Figure 2.1**). About half of the daily oil crude oil production from tight formations come from the Eagle Ford and the Spraberry Trend (Section of the Permian basin) (**Figure 2.2**). Furthermore, the estimates for total recoverable oil in place in these, as well as other U.S. formations indicate large volumes of oil. Following current estimations, the Bakken formation, contains about 100-900 billion barrels of oil by itself (Alfarge et al. 2017a).

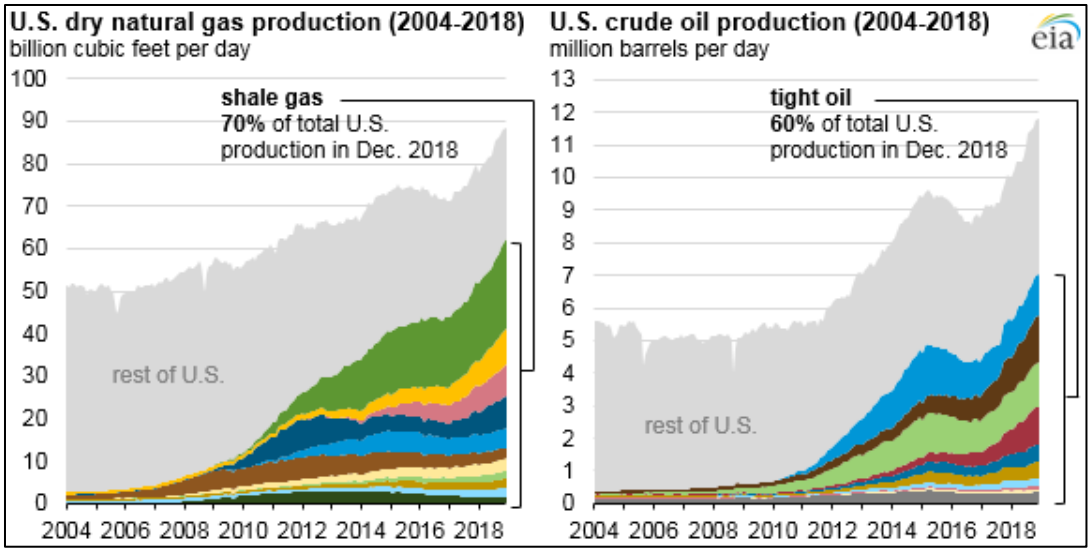

Figure 2.1 – United States natural and crude oil production from 2004-2018, showing the increase in tight oil and shale gas production over the years. Reprinted from the United States Energy Information Administration.

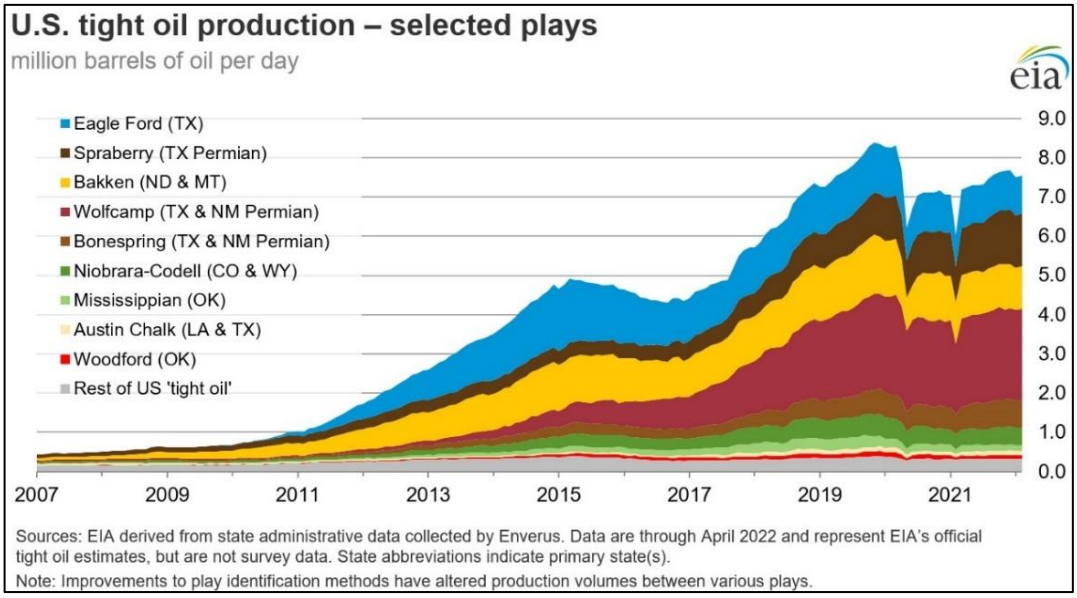

Figure 2.2 – United States tight oil production from selected plays. About half of the tight oil production comes from the Eagle Ford and the Spraberry formation. Reprinted from the United States Energy Information Administration.

Yet, primary oil recovery from these tight formations is typically less than 10% (Alfarge et al. 2017b). As the recovery mechanism for primary recovery is depressurization and solution gas drive, production will quickly decline due to the fast depletion of natural

fractures (Yu et al. 2014), resulting in low recoveries. As an example, the Bakken formation has a production decline rate of about 50% during the first year (Jia et al. 2019). Therefore, tight oil formations have shown to be great candidates for EOR methods, as even the minimal improvement in recovery can be potentially profitable. A 1% increase in recovery can yield 1.6 to 9 billion barrels of oil (Hawthorne et al. 2013), assuming the price of a barrel of oil to be around $90, this small increase could lead to $144 to $810 billion in revenue.

2.2 Solvent Assisted Oil Recovery

An operator can inject solvent into the matrix continuously or cyclically (huff-n-puff). In the continuous process, the injector and the producer are separate entities working together. As solvent is injected, oil is produced. In the cyclic process (**Figure 2.3)**, the injector and the producer wells are the same, and the process requires a "soaking time." When the well is shut in, the solvent swells the oil and lowers its viscosity. In either process, solvent (commonly CO_2, CH_4, or N_2) is injected, and partial miscibility is achieved through multiple contacts by vaporization and condensation. The injected solvent vaporizes light-to-intermediate hydrocarbons, and the presence of the oil will cause heavy components of the solvent to condense into the oil phase, referred to as forward and backward contacts, respectively (Hawthorne et al. 2013).

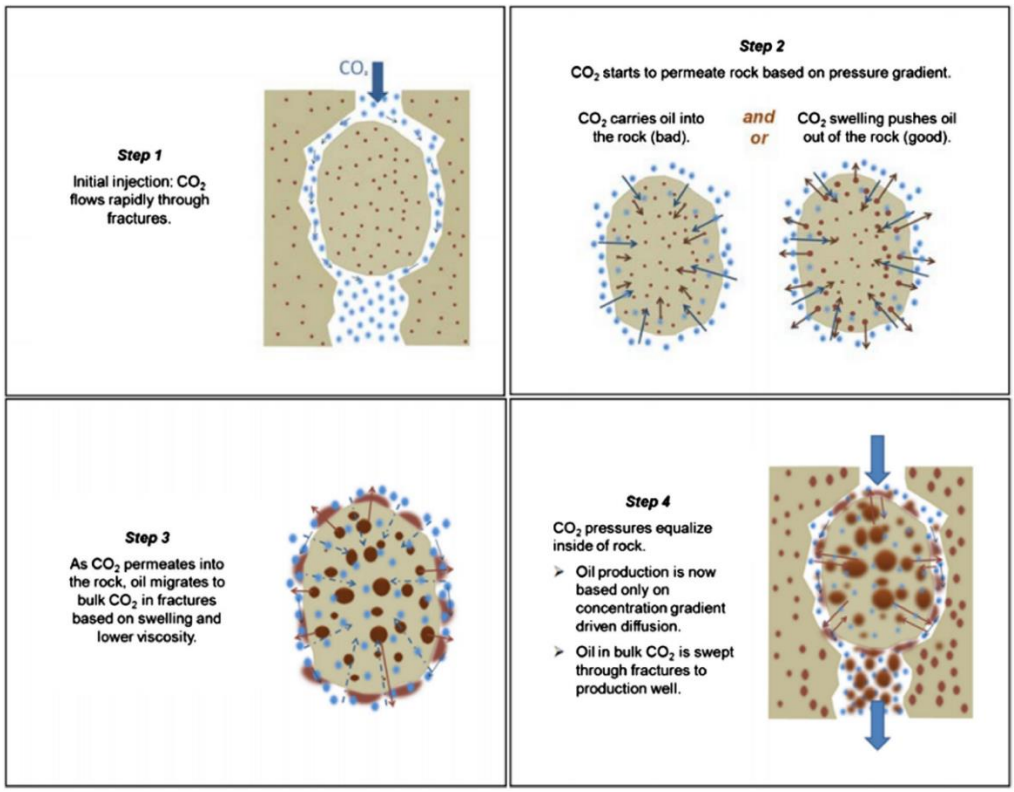

Figure 2.3 – Solvent injection process in low permeability media, using CO2. Reprinted from Hawthorne et al. (2013).

Huff-n-puff has become the preferred process in unconventional reservoirs due to their extremely low permeabilities (Burrows et al. 2020, Jia et al. 2018, Gamadi et al. 2014). Continuous solvent injection has proved to be effective in conventional plays as the solvent quickly propagates into the matrix, displacing and swelling the oil. The solvent, however, cannot flow into the matrix if the permeability is in the nano range, leading to a build-up of solvent at the injection point. Huff-n-puff aims to fix this issue by allowing time for the solvent to diffuse into the matrix.

2.2.1 Solvent Injection and Fracture Discretization Models

Unconventional modeling has improved in the last decade, due to the growing understanding of the physics underlying tight oil reservoirs, and the shift towards tight oil

production. Properly modeling flow in unconventional models often requires ample data describing geological properties of the reservoir, such as hydraulic fracture volume, surface area, closure, and reservoir permeability. On the other hand, simulating oil/solvent mixing accurately requires a dependable compositional model, considering thermodynamic interactions, temperature, and pressure dependence and limits using equations of state.

Recent studies have been using fully compositional models coupled with dual-porosity models to simulate solvent recovery in tight oil reservoirs, considering oil/solvent interactions with the prior and the flow within the reservoir with the latter. Reservoir properties are acquired through a Diagnostic Fracture Injection Test (DFIT), allowing for measurements of reservoir pressure, permeability, and fracture closure pressure. Microseismic data is also collected to be used in hydraulic propagation model, and hydraulic effectiveness and natural fracture network location. (Jia et al. 2019).

The most commonly used methodology to model highly complex fracture networks is using discrete fracture model (DFM), in which each individual fracture property, such as orientation, size, position, shape and aperture, is computationally and explicitly represented. As it requires a wide variety of geological data and geological mappings, stochastic realizations and geomechanical simulations must be performed prior to running the model. (Lei et al. 2017)

We focused on creating a mechanistic, fully compositional model, accurately simulating the thermodynamics of oil/solvent interactions. While also developing a simple discrete model to simulate the flow of the solvent within the reservoir, without needing real or simulated geological data, by assuming an effective diffusion coefficient, and a stimulated flow length.

2.2.2 Solvent Type

The choice of solvent is extremely important to plan a successful huff-n-puff project. Reservoir pressure and temperature and its effects on the oil/solvent pairing must be thoroughly analyzed. CO_2 and N_2 are among the most commonly used solvents. CO_2 has been used extensively in EOR laboratory studies showing high miscibility in comparison to alternatives, and N_2, while not as miscible as CO_2, at high pressures, has shown potential to increase recovery. Other gases, such as, methane, ethane, propane, and hydrogen have also shown to improve recovery when injected into tight oil reservoirs (Milad et al. 2021).

Gases are not the only solvents that can be used in EOR processes. Current experiments with heavier solvents are considered promising alternatives. Unrefined natural gases, or Y-grades, composed primarily of ethane, butane and natural gasolines are a cheap alternative, which may be used following the injection of the primary gas. Aqueous solutions may be used in unconventional formations with higher matrix permeability (Milad et al. 2021).

2.3 Diffusion in Porous Media

Oil recovery during solvent injection into conventional reservoirs is dominated by convective flow. Molecular diffusion will occur in high-permeability reservoirs, but it is insignificant as the flow velocity is high. The same cannot be said for unconventional plays, where oil recovery, will be dominated by molecular diffusion due to the low flow velocity in the matrix; in turn, making convection insignificant. Support for this concept comes from the Peclet number (**Eq. (2.1)**), defined as the ratio of the rate of advection to the rate of diffusion, where d_g is the average diameter of the grain [m], v is the average fluid velocity [m/s], and D_m is the molecular diffusion coefficient [m^2/s] (Lake et al. 2014). The Peclet

number will be small (< 1) for unconventional reservoirs and large (> 50) for conventional reservoirs due to the differing fluid velocities in the matrix. (Hoteit and Firoozabadi 2009, Sahimi 2009)

$$N_{Pe} = \frac{d_g v}{D_m} = \frac{convective\ transport}{dispersive\ rate} \tag{2.1}$$

Considering diffusion as the main flow mechanism, and assuming that the velocity gradient caused by the swelling of the oil to be negligible (Appendix B), we can simplify the convection-diffusion equation into the form of Fick's second law of diffusion (**Eq. (2.2)**). Fick's law describes the change in concentration due to diffusion in respect to time. Assuming the diffusion coefficient constant, this change in concentration will be a product of said coefficient and the Laplacian of the concentration.

$$\frac{\partial c}{\partial t} = D_{eff} \nabla^2 c \tag{2.2}$$

The effective diffusion coefficient, D_{eff}, is defined as the limiting rate of solvent diffusion, including the stimulation due to the hydraulic fracture, or rather, the areal flow of solvent divided by the time to reach that area. This coefficient considers the existence of secondary and natural fractures contributing to flow. Proper calculation of the effective diffusion coefficient is outside of the scope of this project; instead, we are interested on its impact on the time to achieve a certain recovery factor.

Our model assumes one-dimensional flow after injection of solvent. Valid because the entire fracture is planar and assumed to be the same height as the matrix. Assuming that

the entire fracture is saturated with solvent, flow of the solvent will be perpendicular to the length of the fracture (**Figure 2.4**), simplifying Eq. (2.2) to the following (**Eq. (2.3)**):

$$\frac{\partial c}{\partial t} = D_{eff} \frac{\partial^2 c}{\partial x^2} \tag{2.3}$$

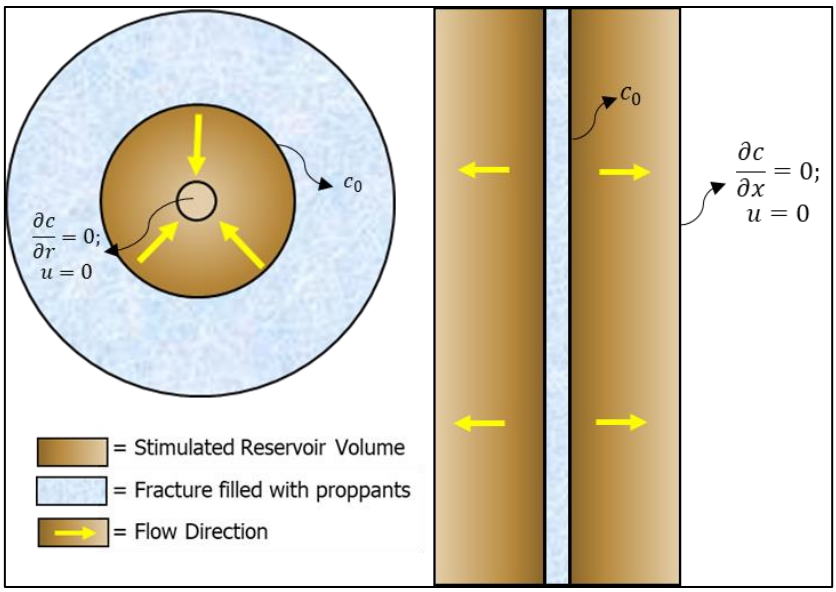

Figure 2.4 – Boundary conditions for radial and cartesian coordinates, showing the flow of solvent into the stimulated reservoir volume. Reprinted from Prawira (2021).

2.4 Reservoir Characteristics Impacting Recovery

Tight oil formations are geologically, widely different from conventional reservoirs, as such, geomechanical properties impacting existence of natural fractures and thermodynamic properties such as temperature and pressure play significant role in the development of a well (Elkady and Kovscek 2020). Temperature and pressure are also crucial variables that must be analyzed prior to the start of production, especially in production developments involving EOR. Temperature and pressure impact the swelling and

density of the oil and solvent, and maximum concentration of solvent produced, which can lead to different thermodynamically limited recoveries.

2.4.1 Reservoir Pressure

Ultra-tight formations such as shale often exhibit high average pressures as the pore fluid, usually located at depths ranging from 8000 to 9500 feet, is supporting the total rock column.

According to Elturki and Imqam (2020), pressures in most tight formations range from 2500 to 7500 psi, with the highest frequency range occurring from 5001 to 7500 psi. Furthermore, EOR may be used to repressurize formations that have dropped below desired pressures. As solvent is injected and begins to fill up the fracture, pressure continually builds up, pressurizing the surrounding matrix.

Tovar et al. (2017) performed core flooding tests of samples from preserved Wolfcamp sidewalls. After determining the CO_2-oil minimum miscibility pressure (MMP), tests were performed below, at and above the estimated MMP. The experiments showed that at high pressures, well above the MMP, recovery factor increased up to 40%, concluding that the highest recovery is achieved at the highest pressure.

The producing pressure for a huff-n-puff process is directly proportional to the injection pressure of the solvent. Tovar et al. (2017) also conducted a proof-of-concept experiment analyzing gas injectivity in organic rich shale matrix, attempting to observe convective flow of solvent (CO_2 and Hydrocarbons) into the core sample from the Bakken shale. The experiment was performed at a temperature of 240 °F, the backpressure regulator was set to 4,000 psig and the one inch in diameter core was subjected to an overburden pressure of 6,500 psig, with gas injected at a rate of 0.01 cm^3/min.

They concluded that no solvent penetrated the matrix, instead, the pressure inside of the fracture built up as the volume of solvent increased. As pressure within the fracture increases, so does the pressure within the matrix. Pressure travels within solid material at high velocities as a wave. Pressure waves are related to geological properties of the material it is traveling through such as the bulk modulus, shear modulus and the density. The U.S. Environmental Protection Agency (2016) conducted a study analyzing acoustic logs to determine the velocity at which pressure travels within samples of rock or fluid, the results are summarized in **Table 2.1**.

Table 2.1 – Compressional-wave velocity and transit time in rocks and fluids. Reprinted from the United States Environmental Protection Agency (2016).

Rock or Fluid Type	Velocity [m/s]	Velocity [ft/s]
Fresh Water	1,500	5,000
Brine	1,600	5,300
Sandstone		
Unconsolidated	4,600-5,200	15,000-17,000
Consolidated	5,800	19,000
Shale	1,800-4,900	6,000-16,000
Limestone	5,800-6,400	19,000-21,000+
Dolomite	6,400-7,300	21,000-24,000
Anhydrite	6,100	20,000
Granite	5,800-6,100	19,000-20,000
Gabbro	7,200	23,6000

Pressure travels through shale at 6,000 to 16,000 feet per second. Assuming that the fracture is in contact with the entire reservoir, it is safe to assume that the stimulated reservoir volume will be nearly instantly pressurized and equalized to the pressure of the fracture. Great care must be taken, however, when pressurizing a reservoir. As although producing at a higher pressure, results in higher recoveries, the injection pressure must not be higher than the fracturing pressure of the matrix, to avoid unnecessary fractures from being created.

2.4.2 Reservoir Temperature

Reservoir temperature is another important characteristic as it impacts density, viscosity, MMP and diffusion coefficient. According to Elturki and Imqam (2020) due to the previously mentioned average tight formations depths, temperatures range from 150 to 250°F, with the highest frequency range occurring between 151 to 200°F.

While unlikely to fluctuate during the huff-n-puff process, temperature has an impact on the recovery of the process. Milad et al. (2021) conducted a review of the progress and the gaps in huff-n-puff technology for tight reservoirs. One of the gaps the paper mentions is the lack of studies done on the gas phase miscibility at varying reservoir temperatures and the effects of solvent and reservoir temperatures. This project includes an analysis of the impact of temperature on the swelling and recovery of oil, to minimize the gap.

2.4.3 Natural and Secondary Fractures

Presence of natural and secondary fractures are also crucial characteristics worth debating. Natural fractures have many definitions, in this study we refer to them as pre-existing microfractures with width ranging from microns to a few millimeters in length, usually interconnecting with one another throughout the entire reservoir (Gale et al. 2014). Theloy (2014) attempted to analyze factors influencing production in the Bakken formation, including geological factors such as reservoir quality, thickness, structural and stratigraphic framework, rock mechanical properties, pore overpressure distribution, organic geochemical parameters, and trapping mechanisms. Among the many reservoir characteristics, Theloy also analyzed the impact natural fractures have on the overall production. Theloy found that the most common type of natural fractures in the Bakken sample cores were micro-scale fractures, occurring throughout the Bakken system interconnecting with one another forming

naturally occurring fracture networks (**Figure 2.5**). Based on the frequency and widespread distribution of the fractures, it was concluded that the entire network contributed to production as it enhanced the formation deliverability, allowing for greater movement of solvent and oil, creating conductive pathways to the hydraulic fracture, further increasing its contact area.

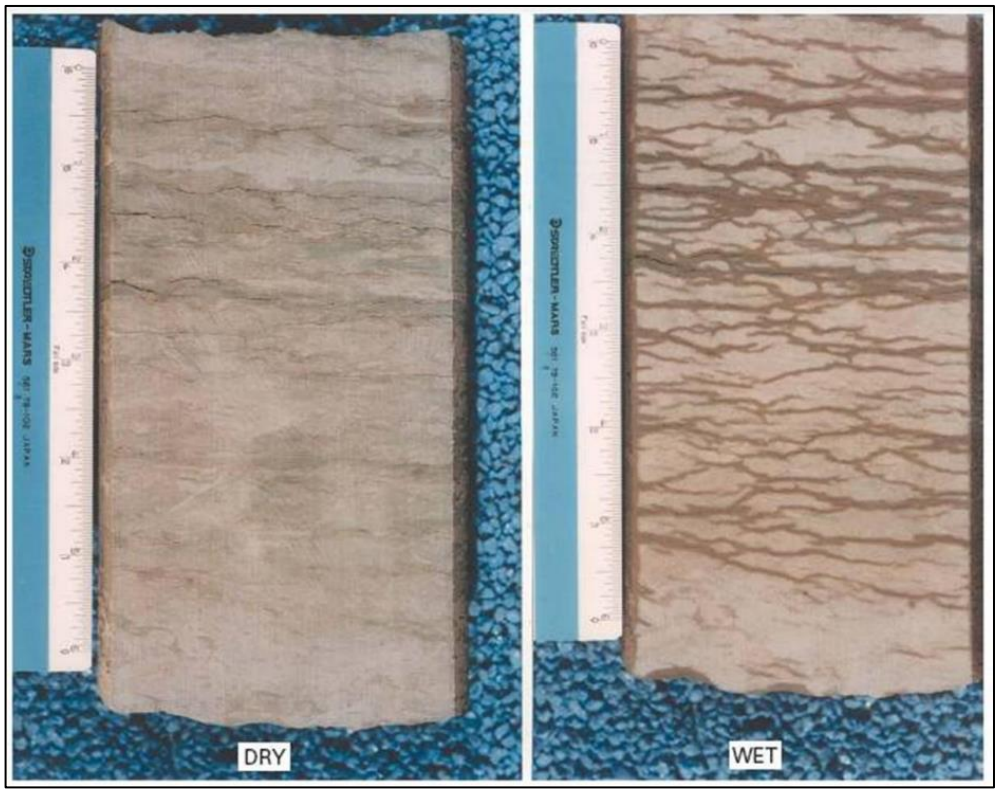

Figure 2.5 – Reticulated fracture network on wet surface of slabbed sandstone. Illustrating natural fractures not visible when surface is dry. Reprinted from Pitman et al. (2001).

Assuming natural fractures, along with secondary fractures that may be created due to hydraulic fracturing, do not close, their impact on the overall production of a field is irrefutable. As such, in this study, we used two strategies to analyze the increase of fracture surface area due to their existence. Firstly, as an increase to the effective diffusion coefficient, leading to higher recoveries as the reservoir is more stimulated due to the

increase in connectivity. Secondly, by transforming the "shoe-box" stimulated reservoir volume to an arrangement of "rods", which in turn, allow for a direct increase in the fracture surface area by increasing the number of rods (**Figure 3.11**). As such, we avoid assuming geological properties of the reservoir, and save on computational time that would be required to model a fracture network. Providing with an effective and simplified way to analyze the impact of an increase in fracture connectivity.

CHAPTER III

METHODOLOGY

3.1 Thermodynamic-Limited Recovery Factor

The expansion in oil volume after mixing with the solvent is related to the type of oil, the type of solvent, pressure, and temperature. There is a thermodynamic limit the oil can swell given a specific solvent, pressure and temperature. Once the solvent comes into contact with the oil, different situations may arise. For example, for a given oil to achieve the same solubility obtained with CO_2, using CH_4 would require a much higher pressure, and at a given pressure, CO_2 has a higher solubility which leads to larger oil swelling. For a given temperature, the saturation pressure of the oil can either increase or decrease with the solvent concentration, and in other cases, full miscibility may be reached at all proportions with no saturation pressure at the specified temperature.

If the saturation pressure decreases as the solvent concentration increases, and it is lower than the reservoir pressure the maximum recovery factor should be determined by an acceptable GOR or injected pore volume, since a limit in solvent concentration will not exist. Limiting GOR or injected pore volume based on available solvent allows us to calculate injected solvent volume, since the production is the saturated mixture at the allowed solvent concentration.

For either case, the oil produced has either the maximum or allowed concentration of solvent, and the GOR (acceptable) is constant throughout the procedure. This restriction allows us to use the simulator further as a diagnostic tool. When producing from a huff-n-puff well, the goal is to allow a long enough soaking time such that the solvent fully saturates

the oil, as we do not want to produce un-mixed solvent back. If the GOR is much higher than the simulated, this could indicate the mixture is not fully saturated, and the soaking time needs to be extended.

We developed a workflow to calculate the maximum recovery factor (**Figure 3.1**). The first step is to calculate the maximum solvent concentration such that the saturation pressure of the mixture is slightly below the reservoir pressure. We systematically calculate saturation pressures at increasing concentrations of solvent using the Peng-Robinson equation of state (Peng and Robinson 1976) until the desired pressure is reached.

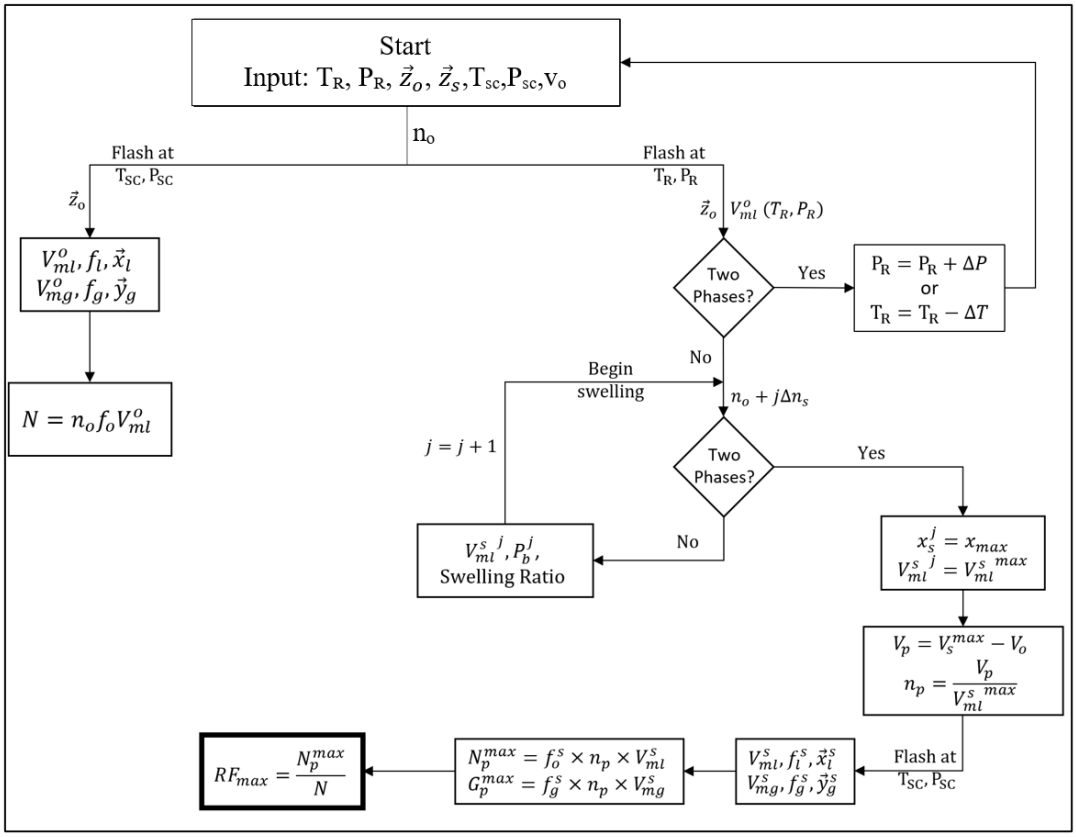

Figure 3.1 – Flow chart of oil-in-place and maximum-recovery-factor calculations. Nomenclature defined in Eq. (3.1) to Eq. (3.18).

The model analyzes oil swelling by gradually adding solvent to the oil until two phases form. Liquid molar volumes and saturation pressures are stored to be used in diffusion model. For the case in which the saturation pressure increases by adding solvent**,** the maximum concentration of solvent in the oil is determine, after a second phase forms. This process provides an array of liquid molar volumes at reservoir conditions for different solvent concentrations as the solvent penetrates the matrix. This array is used in the diffusion model, since concentration varies along the flow direction and time, as solvent continually swells the oil during the soaking period. The concentration of solvent in the matrix increases, allowing for solvent stored and the swelling ratio to be calculated at various distances within the matrix. While Figure 3.1 shows that swelling is a function of the number of moles of solvent added, this is an intensive property that can be evaluated as the ratio of molar volumes instead.

The recovery factor is unaffected by reservoir dimension since the number of moles is directly proportional to the reservoir volume as shown in **Eq. (3.1)**. The initial oil and gas in place are calculated using **Eqs. (3.2)** and **(3.3)**. **Eq. (3.4)** and **Eq. (3.5)** define the solvent concentration and the maximum swelling ratio respectively.

$$n_o = \frac{V_o}{V^o_{ml,\,R}} \tag{3.1}$$

$$N = n_o \times V^o_{ml,\,SC} \times \left(1 - f^{\,o}_{v,\,SC}\right) \tag{3.2}$$

$$G = n_o \times V^o_{ml,\,SC} \times f^{\,o}_{v,\,SC} \tag{3.3}$$

$$\chi_{max} = \frac{n_s}{n_o + n_s} \tag{3.4}$$

$$SR_{max} = \frac{V^s_{ml,R}}{V^o_{ml,R}} \times \frac{n_o + n_s}{n_o} = \frac{V^s_{ml,R}}{V^o_{ml,R}} \times \frac{1}{1 - \chi_{max}} \tag{3.5}$$

$$V_s = V_o \times SR_{max} \tag{3.6}$$

Using **Eq. (3.6)** to calculate the swollen volume, the volume produced is the difference between the swollen volume and the original oil volume (**Eq. (3.7)**). At this point, the moles produced (**Eq. (3.8)**) are calculated by taking the ratio of the volume produced and the liquid molar volume of the mixture.

$$V_p = V_s - V_o \tag{3.7}$$

$$n_p = \frac{V_p}{V^s_{ml,R}} \tag{3.8}$$

Great care must be taken when calculating the volume of produced oil from the total produced moles, especially in situations where moles produced include solvent components. Material balance must be used to separate the moles coming from the oil and the moles coming from the solvent. If the total produced moles are used instead, the predicted maximum recovery factor may be greater than 100%.

The molar ratio of a component in the feed is equal to the molar ratio of the same component in the gas and liquid phase once flashed (Appendix C). This ratio is a function of the maximum concentration of solvent, as well as its initial composition (**Eq. (3.9)**). The

moles coming from the solvent and the oil are now separated by phase and summed (**Eqs. (3.10) - (3.13)**).

$$n^{i}_{ratio} = \frac{z^{i}_{l+v} - \chi_{max} \times z^{i}_{ini}}{\chi_{max} \times z^{i}_{ini}} \tag{3.9}$$

$$n_{v_o} = \sum \left(\frac{z^{i}_{v}}{\left(1 + \frac{1}{n^{i}_{ratio}} \right)} \right) \times n_{p} \tag{3.10}$$

$$n_{l_o} = \sum \left(\frac{z^{i}_{l}}{\left(1 + \frac{1}{n^{i}_{ratio}} \right)} \right) \times n_{p} \tag{3.11}$$

$$n_{v_s} = \sum \left(\frac{z^{i}_{v}}{\left(1 + n^{i}_{ratio} \right)} \right) \times n_{p} \tag{3.12}$$

$$n_{l_s} = \sum \left(\frac{z^{i}_{l}}{\left(1 + n^{i}_{ratio} \right)} \right) \times n_{p} \tag{3.13}$$

We may now flash n_{lo} and acquire the molar volumes and gas fraction. The liquid and gas volume produced are now calculated using only the moles coming from the oil as seen in **Eq. (3.14)** and **Eq. (3.15)** respectively. The maximum recovery factor is now the ratio of the volume produced and the original oil volume (**Eq. (3.16)**). Likewise, the GOR and injected pore volume can now be calculated using **Eq. (3.17)** and **Eq. (3.18)**.

$$N_p = n_{l_o} \times V^{o,\ sep}_{ml,\ SC} \times \left(1 - f^{\ o,\ sep}_{v,\ SC}\right) \tag{3.14}$$

$$G_p = n_{v_o} \times V^{o,\ sep}_{mv,\ SC} \times f^{\ o,\ sep}_{v,\ SC} \tag{3.15}$$

$$RF_{max} = \frac{N_p}{N} \tag{3.16}$$

$$GOR = \frac{G_p}{N_p} \tag{3.17}$$

$$PV_{max} = \frac{V^{inj}_{mv,\ R} \times \frac{1}{1 - \chi_{max}}}{V^{o}_{ml,\ R}} \tag{3.18}$$

3.2 GOR and Injection Pore Volume Limits Due to Oil-Solvent Combination

Using the equations presented in the earlier section of this chapter (Eq. (3.1) - Eq. (3.18)), this section provides an analysis of the oil swelling, allowing for the determination at which solvent concentration the mixture should be produced at, in turn, impacting the GOR, the maximum recovery factor, injected pore volume and the number of cycles required. All of which should be constrained by the solvent's limitations (availability, cost), and the facility's ability to handle the mixture (GOR, number of cycles).

We classified oils into two categories: (1) dead oils, characterized by their low bubble point, little to no gas in solution, and a high percentage of heavy components, usually with an API gravity less than 20°, and (2) live oils, characterized by their high bubble point, low molecular weight, and gas in solution, with an API gravity greater than 31.5°. For a dead oil,

solvent concentration is limited because the saturation pressure of the mixture will reach the reservoir pressure as the solvent concentration increases; for a live oil, however, this limit may not be reached. An example of a swelling output can be seen on **Figure 3.2**. Nevertheless, if a limit of solvent concentration exists for a dead oil, the GOR at this concentration must still be deemed acceptable (< 10,000).

Swelling Data Output

Mixture	Solvent Moles/Total Mc	Swelling Factor (ratio)	Saturation Pressure (psi)	Swollen Volume (ft3)	Density (lb/ft3)	Viscosity (cp)	Molecular Weight (lb/lbmol)	Liq. Mol. Volume (ft3/lb-mol)
1	0.000	1.00000	3025.81	0.0000	38.2948	0.2727	70.4716	1.8402
2	0.009	1.00451	3023.83	0.0519	38.3207	0.2701	70.2140	1.8323
3	0.018	1.00911	3021.87	0.1047	38.3468	0.2674	69.9564	1.8243
4	0.026	1.01380	3019.94	0.1585	38.3730	0.2648	69.6988	1.8164
5	0.035	1.01857	3018.04	0.2133	38.3992	0.2622	69.4412	1.8084
.								
.								
.								
72	0.625	1.89503	2986.63	10.2826	39.9148	0.1054	52.1817	1.3073
73	0.634	1.93089	2988.19	10.6946	39.9176	0.1037	51.9241	1.3008
74	0.643	1.96860	2989.81	11.1279	39.9188	0.1020	51.6665	1.2943
75	0.652	2.00831	2991.49	11.5840	39.9182	0.1004	51.4088	1.2879
76	0.660	2.05017	2993.22	12.0649	39.9158	0.0988	51.1512	1.2815

Figure 3.2 – Example of selected swelling data output. Solvent concentration was set to a maximum value of 0.6 solvent moles/total moles. Solvent is incrementally added to oil until the maximum concentration is reached.

For a live oil, if the solvent concentration limit is reached, it may still require an unrealistic maximum injected pore volume, as it would require an almost infinite supply of solvent.

Figure 3.3 shows the preliminary analysis necessary prior to running the diffusion model. Temperature and pressure must be known, as well as the oil-solvent characterization.

The oil-solvent mixture swells until a specified pressure is reached, controlled by either fixed maximum solvent concentration or fixed in-situ pressure, at which the saturation pressure of the mixture is equal to the reservoir pressure.

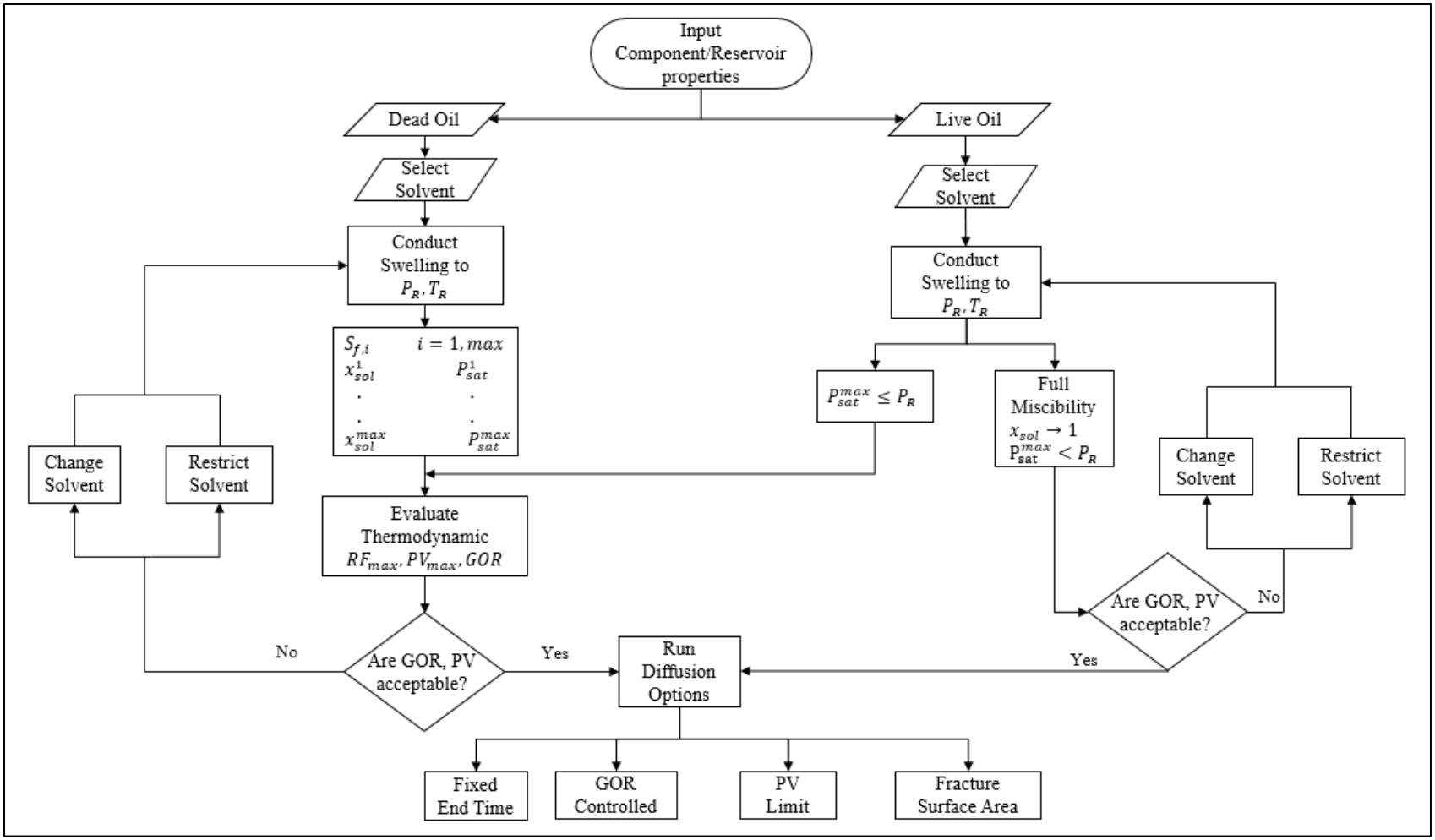

Figure 3.3 – Flow chart of preliminary analysis, separation of oil type and selection of solvent type and concentration. Estimated injected pore volume must realistic; if not, solvent volume is either reduced or solvent changed. Simulation option is then selected.

For a dead oil, if the maximum injected pore volume after solvent injection is deemed too high (> 1.2), the process will require an unrealistic amount of cycles (multiple cycles per day), defined as the ratio between the volume produced to the volume of the fracture. We may select a lower maximum solvent concentration such that realistic results are attained.

For a live oil, if there is no limit in the maximum solvent concentration, we analyze the GOR and maximum injected pore volume in a similar way. As the concentration of solvent approaches a molar fraction of unity, the saturation pressure may still be below the reservoir pressure and the swelling factor, (Eq. (3.5)), approaches infinity.

We analyzed two oils in this study, one is an analog of the dead oil used by Tovar et al. (2018). Components are characterized and lumped, matching the API gravity provided. Another oil is a live oil from a tight formation, acquired from the analog of Tianying (2021). The characterized oils are shown in **Table 3.1** and **Table 3.2**.

Table 3.1 – Analog of fluid from Tovar et al. (2018) - Dead Oil.

Compositional Information					
Component	M_{w_i}	P_{c_i} (psia)	T_{c_i} (°F)	ω_i	Zi
Pseudo1	46.000	616.000	206.060	0.152	1.38E-02
Pseudo2	107.000	413.206	573.489	0.338	5.67E-01
Pseudo3	275.000	204.942	958.894	0.780	2.65E-01
Pseudo4	402.000	159.142	1114.829	1.042	6.54E-02
Pseudo5	472.000	145.714	1176.062	1.155	8.87E-02

Table 3.2 – Analog of fluid from Tianying (2021) - Live Oil.

Compositional Information					
Component	M_{w_i}	P_{c_i} (psia)	T_{c_i} (°F)	ω_i	Zi
C1	16.043	667.400	-116.900	0.008	1.00E-05
N2	28.010	492.500	-232.800	0.040	1.00E-05
CO2	44.010	1070.200	87.600	0.225	1.98E-03
N2C1	16.258	661.784	-120.179	0.009	4.94E-01
C2-3	35.825	661.588	148.594	0.125	1.38E-01
C4-6	69.324	492.986	371.238	0.238	1.09E-01
F1	142.532	367.140	680.890	0.469	2.07E-01
F2	410.500	150.050	1064.180	1.267	4.94E-02

Three solvents were used to illustrate the possible interactions that may occur with lean, medium and rich solvents. These are labeled Injection Solvent (1), and Injection Solvent (2). The third solvent, known as a Y-grade or unrefined natural gas liquid (NGL), provided an example of a heavier mixture being used as injected solvent. Y-grades are commonly made up of ethane, propane, butane, and natural gasoline (C_{5+}), with varying compositions. There are studies and proof-of-concept projects (Moody (2020)) exploring the usage of Y-grades in solvent-assisted tight oil recovery, resulting in low GORs and high miscibility achieved at lower pressure, in comparison to CH_4 and N_2. **Table 3.3** shows the composition of the three solvents used in this study.

Table 3.3 – Solvents simulated: CO2 - Carbon Dioxide; C1 – Methane; C2 - Ethane; C3 - Propane; n-C4 - Butane; n-C5 - Pentane; n-C6 - Hexane. Noting that the solvents share components with the live oil.

Injection Solvent 1 (Medium)			Injection Solvent 2 (Lean)			Y-Grade (Rich)		
Name	mg-mol	Zi	Name	mg-mol	Zi	Name	mg-mol	Zi
C1	10	0.10	C1	40	0.40	C2	5	0.05
CO2	90	0.90	CO2	60	0.60	C3	27	0.27
						n-C4	32	0.32
						n-C5	16	0.16
						nC-6	20	0.20

3.3 Molecular Diffusion Modeling Procedure

Our model uses VLE calculations method by Rachford and Rice (1952) with additional use of the Wilson correlation. From the flash calculations, we acquire the liquid and vapor molar volumes and molar fractions, we then couple them with a numerical simulator, using finite differences to solve the molecular diffusion equations. Assuming a constant pressure and temperature, a horizontal well, ignoring gravitational force effects, and flow driven by molecular diffusion. Our model simplifies the complex fracture network into a planar fracture acting on a "shoe-box" stimulated reservoir for Cartesian coordinates, with options to model a radial fracture acting on a cylindrical stimulated reservoir volume or on an arrangement of "rods" allowing for an increase in fracture surface area.

Our model considers one-dimensional flow using **Eq. (3.19)**, describing molecular diffusion flow, and assumes single liquid-phase. The change in volume is a function of the solvent concentration change, the term $c_{x+\Delta x}^{t+\Delta t}$ refers to the concentration at distance $x+\Delta x$ and time $t+\Delta t$. (**Figure 3.4**)

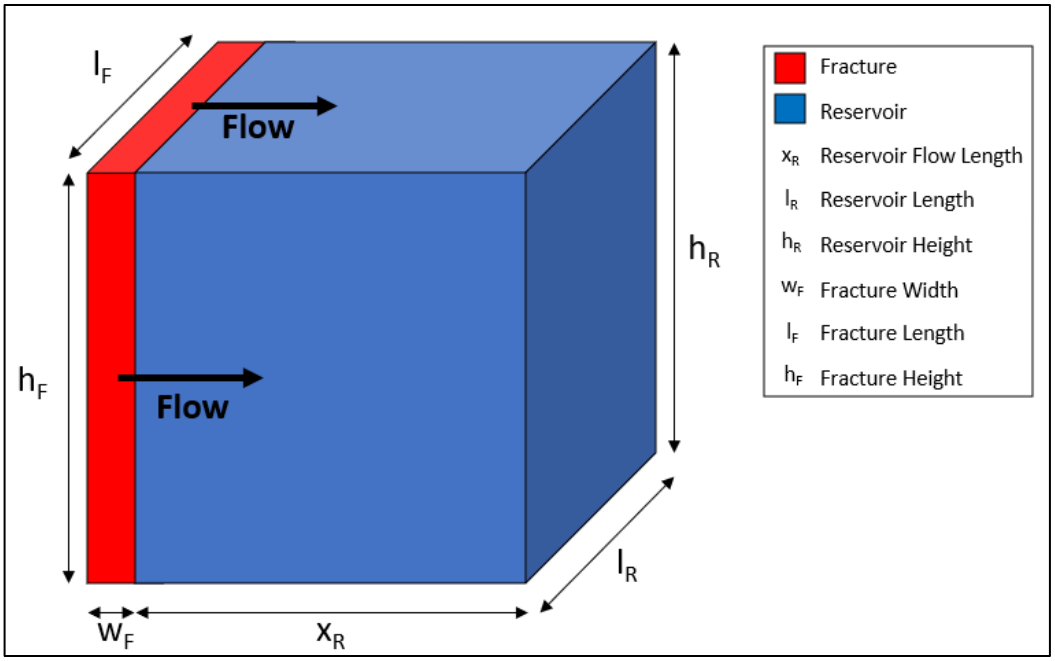

Figure 3.4 – Simplified simulated reservoir volume. Solvent flows from fracture into the matrix one-dimensionally following the flow length of the reservoir (x_R)

$$\Delta V_e = w \times h \times \phi \times \Delta x \left[f\left(\frac{c^{t+\Delta x}_{x+\Delta x} + c^{t+\Delta x}_{x}}{2} \right) - f\left(\frac{c^{t}_{x+\Delta x} + c^{t}_{x}}{2} \right) \right] \tag{3.19}$$

The boundary and initial conditions of the model are shown in **Eqs. (3.20)** to **(3.23)**. At $x = 0$, the solvent concentration is equal to the predetermined concentration when performing the swelling calculations, and at $x = L$, L being the maximum flow length of the reservoir, there is no flux.

Boundary Conditions:

$$c = c_0, \text{ at } x = 0 \tag{3.20}$$

$$\frac{dc}{dx} = 0, \text{ at } x = L \tag{3.21}$$

Initial Conditions:

$$c = c_0, \text{ at } x = 0,\ t = 0 \tag{3.22}$$

$$c = c_i, \text{ at } x > 0,\ t = 0 \tag{3.23}$$

Distance, time, and concentration (**Eq. (3.24)** to **Eq. (3.26)**) can be expressed in dimensionless form.

$$\bar{x} = \frac{x}{L} \tag{3.24}$$

$$\bar{c} = \frac{c - c_i}{c_0 - c_i} \tag{3.25}$$

$$\bar{\tau} = \frac{t}{L^2 / D_{eff}} \tag{3.26}$$

The boundary and initial conditions now become (**Eq. (3.27)** to **Eq. (3.30)**):

Dimensionless Boundary Conditions:

$$\bar{c} = 1, \text{ at } \bar{x} = 0 \tag{3.27}$$

$$\frac{d\bar{c}}{d\bar{x}} = 0, \text{ at } \bar{x} = L \tag{3.28}$$

Dimensionless Initial Conditions:

$$\bar{c} = 1, \text{ at } \bar{x} = 0, \tau = 0 \tag{3.29}$$

$$\bar{c} = \bar{c}_i, \text{ at } \bar{x} > 0, \tau = 0 \tag{3.30}$$

We now substitute the dimensionless variables into the molecular diffusion equation (Eq. (2.3)), as shown in **Eq. (3.31)**.

$$\frac{\partial \bar{c}}{\partial \tau} = \frac{\partial^2 \bar{c}}{\partial \bar{x}^2} \tag{3.31}$$

Eq. (3.31) can now be discretized and solved using finite difference. Forward difference expansion was used for time discretization and centered difference expansion was used for space discretization, as shown in **Eq. (3.32)** to **Eq. (3.34)**.

$$\frac{\partial \bar{c}}{\partial \tau} = \frac{1}{\Delta \tau}\left(\bar{c}_i^{n+1} - \bar{c}_i^{n} \right) + O(\Delta \tau) \tag{3.32}$$

$$\frac{\partial \bar{c}}{\partial \bar{x}} = \frac{1}{2\Delta \bar{x}}\left(\bar{c}_{i+1}^{n+1} - \bar{c}_{i-1}^{n+1} \right) + O\left(\Delta \bar{x}^2 \right) \tag{3.33}$$

$$\frac{\partial^2 \bar{c}}{\partial \bar{x}^2} = \frac{1}{\Delta \bar{x}^2}\left(\bar{c}_{i+1}^{n+1} - 2\bar{c}_{i}^{n+1} + \bar{c}_{i-1}^{n+1} \right) + O\left(\Delta \bar{x}^2 \right) \tag{3.34}$$

The discretized partial differential equation in Eq. (3.31) can now be simplified into **Eq (3.35)**, where the coefficients used are defined in **Eq. (3.36)** to **Eq. (3.39)**.

$$a_i \bar{c}_{i-1}^{n+1} + b_i \bar{c}_{i}^{n+1} + d_i \bar{c}_{i+1}^{n+1} = e_i \tag{3.35}$$

$$a_i = -\frac{\Delta \tau}{\Delta \bar{x}^2} \tag{3.36}$$

$$b_i = 1 + \frac{2 \times \Delta \tau}{\Delta \bar{x}^2} \tag{3.37}$$

$$d_i = -\frac{\Delta \tau}{\Delta \bar{x}^2} \tag{3.38}$$

$$e_i = \bar{c}_{i}^{n} \tag{3.39}$$

Applying the same discretization into the boundary conditions, it then become **Eq. (3.40)** and **Eq. (3.41)**. Substituting the newly defined boundary conditions into Eq. (3.35), **Eq. (3.42)** and **Eq. (3.43)** are developed. And the system of equations is then **Eq. (3.44)**.

$$\left.\frac{\partial \bar{c}}{\partial \bar{x}}\right|_{\bar{x}=1} = \frac{1}{2\Delta \bar{x}}\left(\bar{c}_{N}^{n+1} - \bar{c}_{N-2}^{n+1} \right) = 0 \tag{3.40}$$

$$\bar{c}_{N}^{n+1} = \bar{c}_{N-2}^{n+1} \tag{3.41}$$

$$\left(a_{N-1} + d_{N-1} \right) \bar{c}_{N-2}^{n+1} + b_{N-1} \bar{c}_{N-1}^{n+1} = e_{N-1} \tag{3.42}$$

$$b_1 \bar{c}_{1}^{n+1} + d_1 \bar{c}_{2}^{n+1} = e_1 - a_1 \tag{3.43}$$

$$\begin{bmatrix} b_1 & d_1 & 0 & 0 & 0 \\ a_2 & b_2 & d_2 & 0 & 0 \\ 0 & a_3 & b_3 & d_3 & 0 \\ 0 & 0 & \ddots & \ddots & \ddots \\ 0 & 0 & 0 & a_{N-1}+d_{N-1} & b_{N-1} \end{bmatrix} \begin{bmatrix} \bar{c}_{1}^{n+1} \\ \bar{c}_{2}^{n+1} \\ \bar{c}_{3}^{n+1} \\ \vdots \\ \bar{c}_{N-1}^{n+1} \end{bmatrix} = \begin{bmatrix} e_1 - a_1 \\ e_2 \\ e_3 \\ \vdots \\ e_{N-1} \end{bmatrix} \tag{3.44}$$

We can model using field or lab units, allowing for simulation of large-scale reservoirs for industry use, as well as small samples for laboratory use. End time, number of time steps, number of cells and output frequency allows for production to be visualized at any period of time and for computational efficiency to be controlled.

Reservoir and fracture geometry, such as matrix and fracture porosity, height, length, and width may also be modified prior to simulation. Production constraints, such as effective diffusion coefficient and volume of solvent per cycle may be varied, limiting diffusion rate and solvent availability, respectively.

Our model can be run with or without advection, which was found to be negligible (Appendix B), and with one of three simulation options. “Fixed End Time”, in which the user inputs a desired final time for the huff-n-puff process in hours, days or years, “Fixed Injected Pore Volume”, where the user inputs a target injected pore volume and the simulator runs until the target is reached, and lastly “Until Ultimate Recovery Factor”, in which the huff-n-puff process runs until the recovery factor plateaus, allowing the flow length or the effective diffusion coefficient to be varied. Using the live oil and solvent 1 (90/10 CO_2-CH_4) as an example, **Figure 3.5** to **Figure 3.7**, illustrate recovery factor and injected pore volume for all three simulation options.

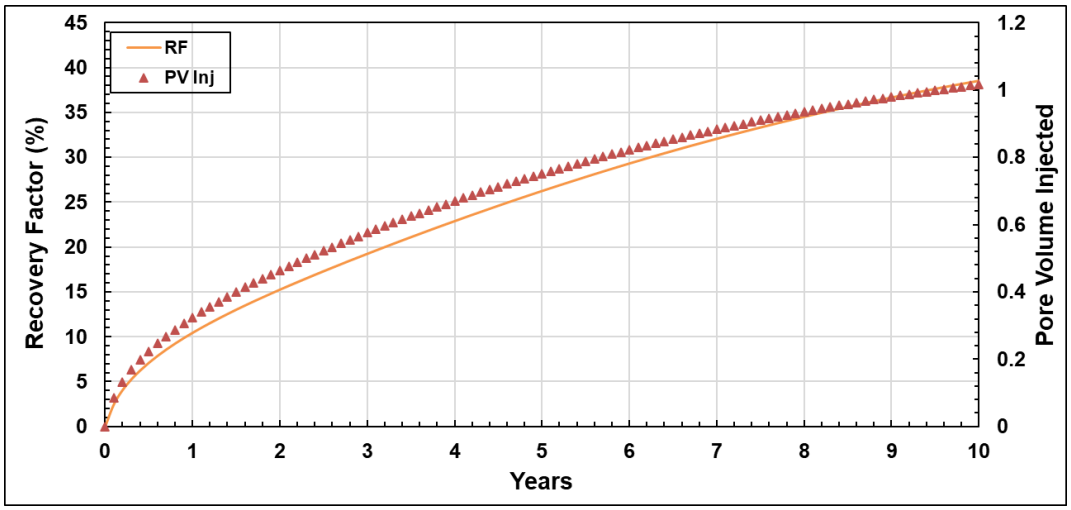

Figure 3.5 – Recovery factor using "Fixed End Time" set to 10 years, for the live oil and with 90/10 CO_2-CH_4 solvent. Simulator will run until final time is reached. Reservoir pressure of 3750 psi and temperature of 175 °F, D_{eff} of 1.00×10^{-3} cm^2/s, flow length of 20 ft.

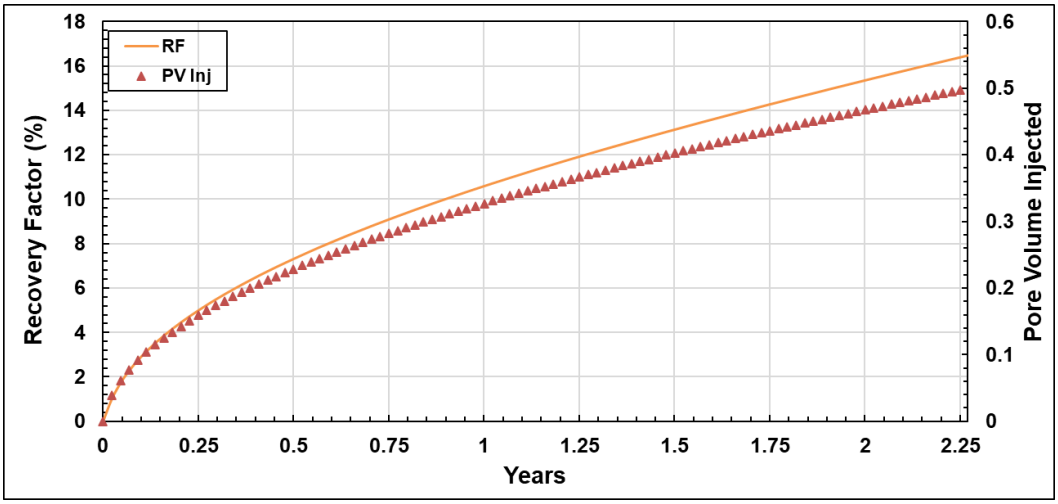

Figure 3.6 – Recovery factor using "Fixed Injected Pore Volume" set to 0.5, for the live oil and with 90/10 CO_2-CH_4 solvent. Simulator will run until injected pore volume is equal to the selected value. Reservoir pressure of 3750 psi and temperature of 175 °F, D_{eff} of 1.00×10^{-3} cm^2/s, flow length of 20 ft.

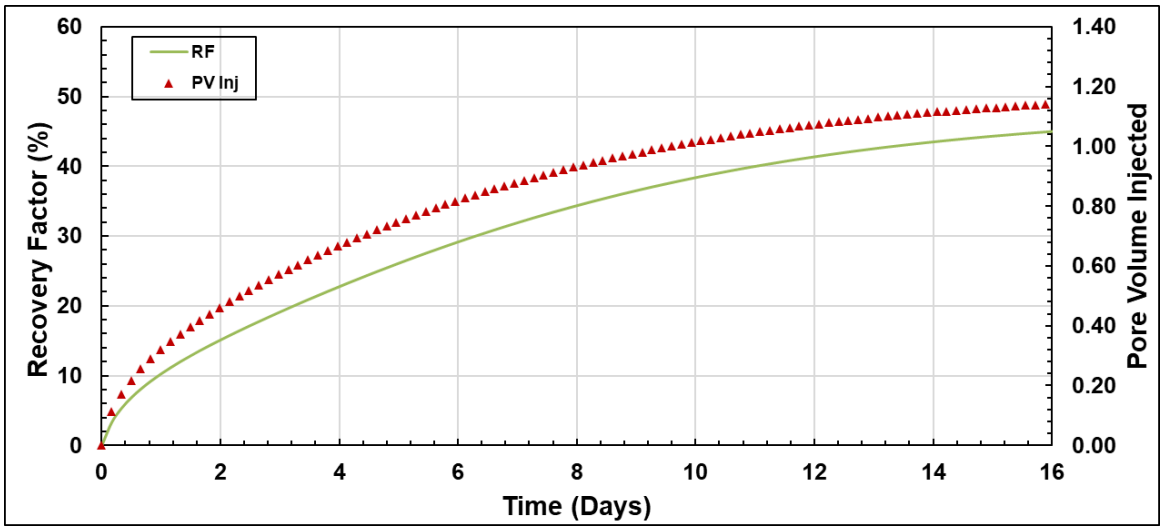

Figure 3.7 – Recovery factor using "Until Ultimate Recovery Factor", for the live oil and with 90/10 CO_2-CH_4 solvent. Simulator will run until recovery factor reaches a plateau, indicating its maximum value. Reservoir pressure of 3750 psi and temperature of 175 °F, D_{eff} of 1.00×10^{-3} cm^2/s, flow length of 20 ft.

Noting that effective diffusion coefficient will proportionally impact time as it increases or decreases (i.e. increasing effective diffusion coefficient by 10, will increase the time to reach ultimate recovery factor by 10). **Table 3.4** illustrates this proportional relationship between D_{eff} and the time to reach the ultimate recovery factor.

Table 3.4 – Impact of effective diffusion coefficient on time to reach ultimate recovery factor. Decreasing effective diffusion coefficient by a factor result in an increase by the same factor on the final time. Results using live oil with the 90/10 CO_2-CH_4 as an example.

Time for ultimate RF (years)	D_{eff} (cm^2/s)
31.556	1×10^{-3}
63.112	5×10^{-4}
315.56	1×10^{-4}
632.12	5×10^{-5}

Solvent concentration profile can also be kept in the matrix at the end of the simulation. As such, processes in which solvent is switched after a period of time can also

be modeled. In this option, the solvent concentration within the entire matrix is assumed to be equal to the average concentration throughout the flow length at the end time.

The last simulation option we provide is allowing the user to transform the "shoe-box" stimulated reservoir volume into an arrangement of "rods", essentially increasing the fracture surface area while maintaining a constant reservoir volume. Users can input number of rods, decide if the rods have randomly generated flow lengths or are all equal, and if the fracture volume is the same as the planar fracture. **Figure 3.8** displays the simulation options when allowing for the transformation of the planar stimulated reservoir volume to an arrangement of rods.

☑ Rods	
Number of Rods	64
Equivalent Pore Volume (CF)	40000
Random sized rods?	☐
Radius per Rod (ft)	9.97
Equal fracture width as ☐ shoe-box? (mm)	0.623315362
Fracture Volume (CF)	32.81

Figure 3.8 – Simulation options of rods transformation. Options include: number of rods and random sized rods, and equal fracture width as shoe-box reservoir volume (If set to variable, fracture spacing will be calculated from the rods, and will be smaller than the original fracture width).

3.4 Fracture Surface Area

Natural and secondary fractures increase the contact area between the fracture network and the impermeable matrix. **Figure 3.9** shows the comparison between a planar fracture (a) and a simulated fracture network (b), showing the complex behavior and

geometry of fractures. As the figure suggests, simply assuming a planar fracture may be underestimating the fracture connectivity, leading to lower recovery estimates.

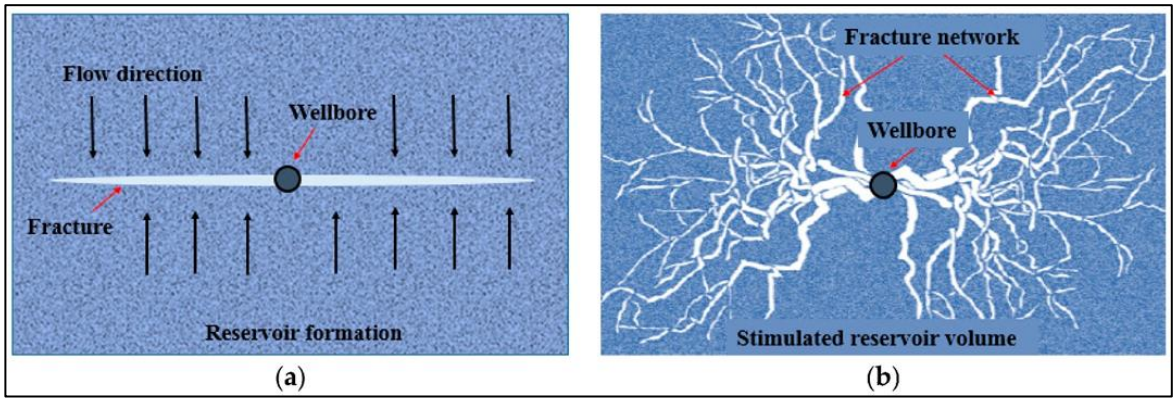

Figure 3.9 – Top view of reservoir formation and of Stimulated Reservoir with secondary fractures present. Illustrating the increase in fracture surface area when comparing a planar fracture (a.) to a fracture network (b.). Reprinted from Yu et al. (2019).

We can analyze the impact on recovery by transforming a planar fracture within a "shoe-box" matrix to a 'radial' fracture within an arrangement of "rods". **Figure 3.10** and **Table 3.5** shows how transforming a shoebox into a group of cylinders while maintaining the pore volume constant, results in solely a change in surface area. Noting that the surface area of the cartesian coordinate is only a single face of the box, and the surface area of the cylinders does not include the base, only the width and the radius.

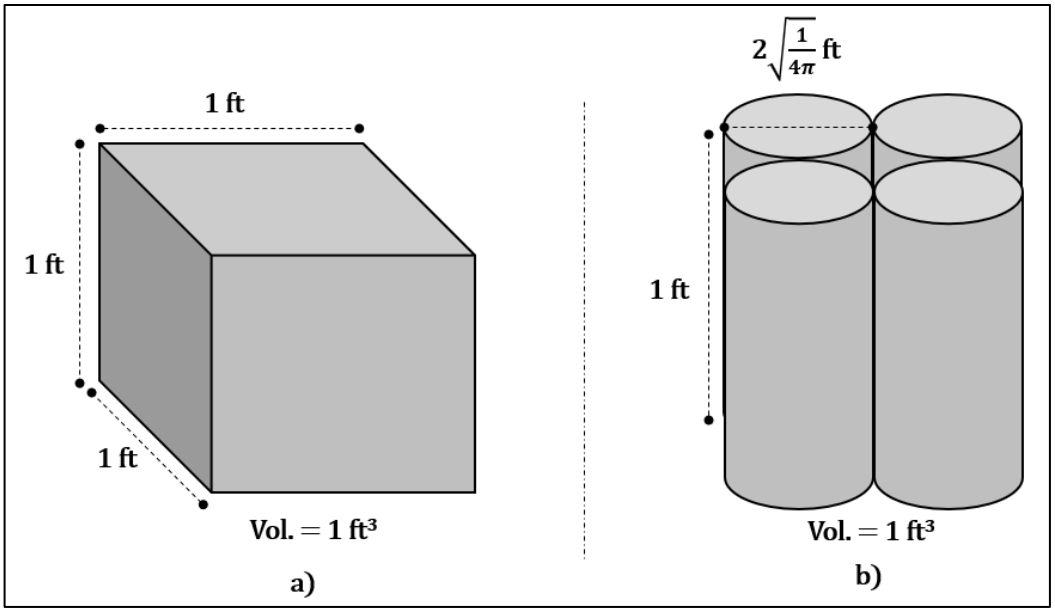

Figure 3.10 – Illustration of transforming a "shoe-box" matrix (a.) into an arrangement of "rods" (b.) by maintaining the original's pore volume.

Table 3.5 – Example calculation of fracture surface area increase of a "shoe-box" matrix and an arrangement of "rods", with a constant volume. Fracture surface area of rods does not include base, only width and radius.

	Shoe-Box	Rods
Height	1 ft	1 ft – per rod
Width	1 ft	$2\sqrt{\frac{1}{4\pi}}$ ft – per rod
Length	1 ft	$2\sqrt{\frac{1}{4\pi}}$ ft – per rod
Volume		1 ft³
Surface Area	1 ft²	1.77 ft²

Figure 3.11 shows how we could represent a shoe-box matrix in radial geometry. A planar fracture might result in an underestimation of the actual fracture surface area. A "radial" fracture causes an increase in surface area, which can then be simulated, and the change of recovery factor can be evaluated.

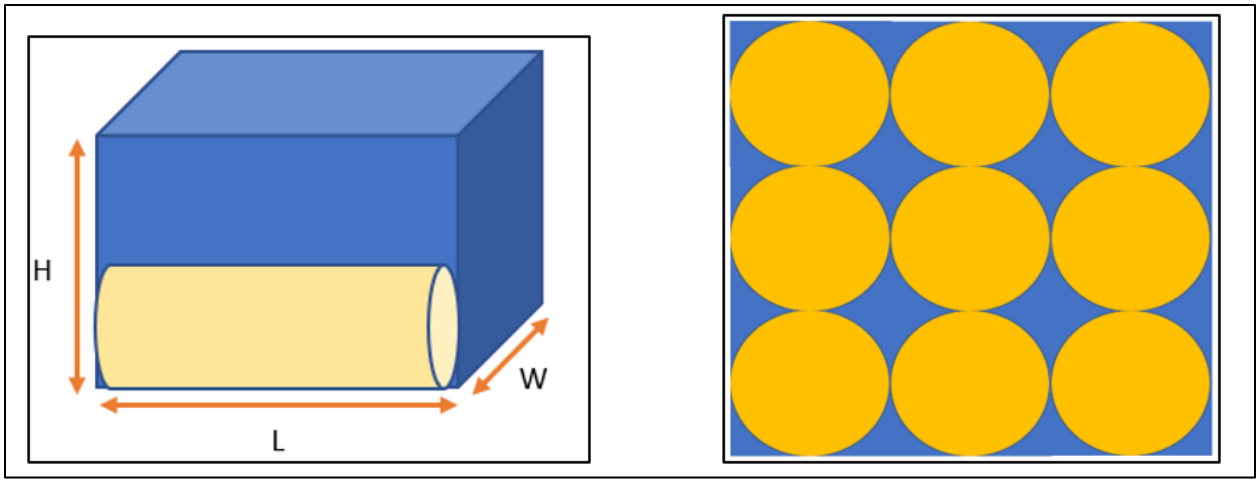

Figure 3.11 – Shoe-box matrix, represented in cylindrical geometry with the same volume. In a rectangular geometry, fractures are planar and in contact with only one side of the matrix. A cylindrical representation of the matrix allows for greater fracture contact area.

Figure 3.12 shows the recovery factor over a 10-year period for seven representations of a matrix with constant bulk volume, using the live oil with the 90/10 CO_2-CH_4 solvent as an example. We changed the number of rods, changing the radius of each rod, such that the volume of the aggregate rods is equal to the volume of the rectangular matrix. Summing the surface area of each rod allows us to calculate the total fracture surface, and the increase in surface area to volume can be assessed with **Eq. (3.45)**. **Table 3.6** shows the results of the six cylindrical representations of the matrix.

$$SA:V = \frac{S}{V} \tag{3.45}$$

Table 3.6 – Results of cylindrical rod representation of planar fracture with constant bulk volume (400,000 ft^3). Ranging from four rods, illustrating a minor increase in surface are to sixty-four rods showing a significant increase.

# of rods	W_{rods} (ft)	Radius (ft)	V/rod	Surface area per rod (ft^2)	SA:V (ft^{-1})	Increase in surface area (%)
4	20	39.89	100000	5013	0.05	0.27
8	20	28.21	50000	3544	0.07	41.80
12	20	23.03	33333	2894	0.09	73.66
16	20	19.95	25000	2506	0.10	100.53
32	20	14.10	12500	1772	0.14	183.59
64	20	9.97	6250	1253	0.20	301.06

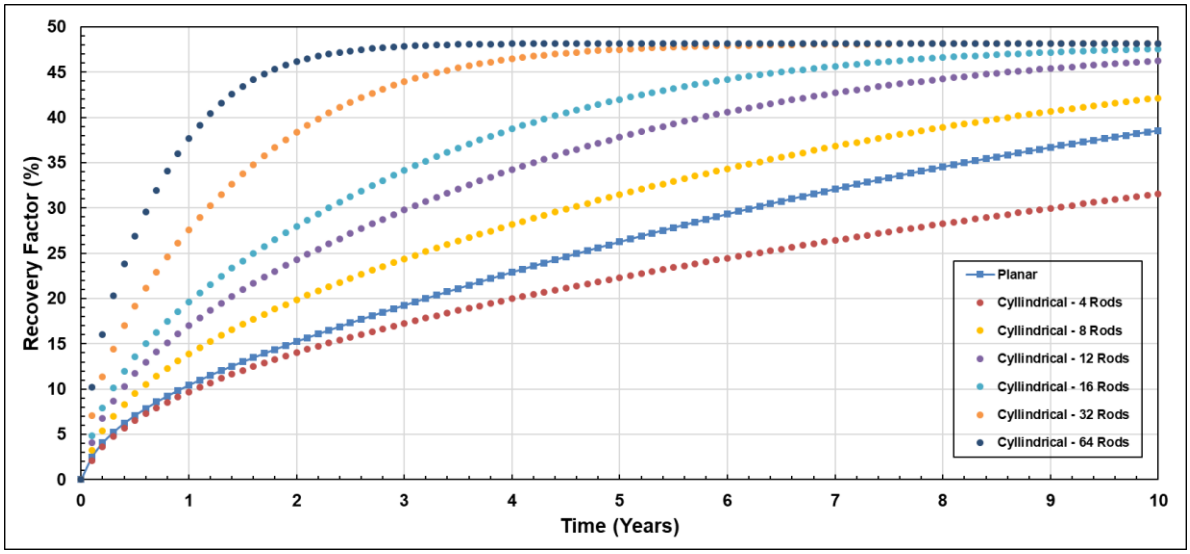

Figure 3.12 – Recovery Factor for multiple representations of a 10-year huff-n-puff injection process, with the live oil and 90/10 CO_2-CH_4 solvent. Noting that with four rods, led to a decrease in recovery as the increase in surface area did was not substantial to account for the increaes in flow length. Reservoir pressure of 3750 psi and temperature of 175 °F, D_{eff} of 1.00×10^{-3} cm^2/s.

If there is a substantial increase in surface area of the fracture, the time required to reach the limiting recovery factor will be shorter. However, for four rods, the recovery factor decreased, even though there was an increase in surface area. This increase in surface area was not substantial enough in comparison to the increase in flow length. The radius of each rod resulted in a much longer flow path required for the solvent to reach the center of the rods. However, by maintaining the flow length constant, the increase in surface area due to the rods is substantial. With sixteen rods, the flow length is about twenty feet, equaling the flow length of the planar fracture model, in such scenario, the surface area doubled.

A planar fracture might result in an underestimation of the actual surface area. Representing the same stimulated reservoir volume as an arrangement of a high number of rods, may overestimate the fracture surface area. As such, we have the lower and the higher

bound respectively, of our recovery estimation. Laboratory work with samples or fracture propagation models may help narrow the expected surface area of fracture, with our methodology we can then estimate the recovery (Milad et al. (2021)).

We may also predict recovery using rods of unequal sizes. By varying the flow length of each rod, such that the volume of the different sized rods is equal to the volume of the original shoe-box reservoir. An array of rods can be created, each contributing differently to the total recovery of the field. Using VBA's pseudorandom number generator, we calculate the fraction that a rod contributes to the total volume of the reservoir and solve for the respective flow length.

While the impact of the pseudorandom rods does not impact the final recovery greatly, it adds an uncertainty to the reservoir transformation, which may allow for a more realistic depiction of the reservoir (**Figure 3.13**).

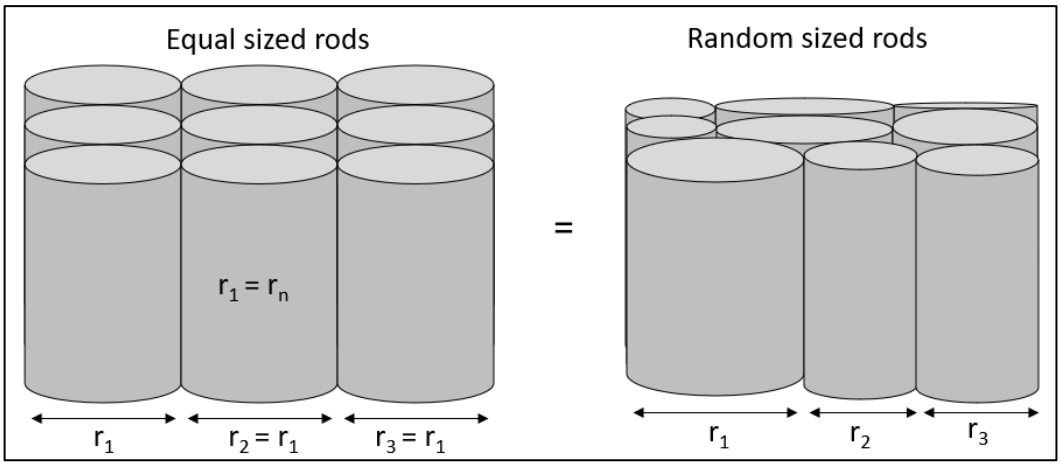

Figure 3.13 – Equal sized rods and random sized rods representation. Random sized rods require calculation of each individual rod, each of which will have a different contribution to the total recovery of the field.

CHAPTER IV

RESULTS AND DISCUSSION

4.1 Solvent Maximum Concentration

Solvent concentration is directly proportional to the swelling factor of the original oil, as such, increasing it leads to an increase in recovery. By plotting recovery factor and injected pore volume, as a function of normalized concentration (**Eq. (4.1)**), the maximum thermodynamic-limited recovery factor may be predicted as seen in **Figure 4.1** for live (a.) and dead (b.) oil, using injection solvent 1, 2 and Y-grade, both oils at a pressure of 3750 psi and a temperature of 175 °F.

$$\chi_{norm} = \frac{\chi_i}{\chi_{max}} \qquad \textbf{(4.1)}$$

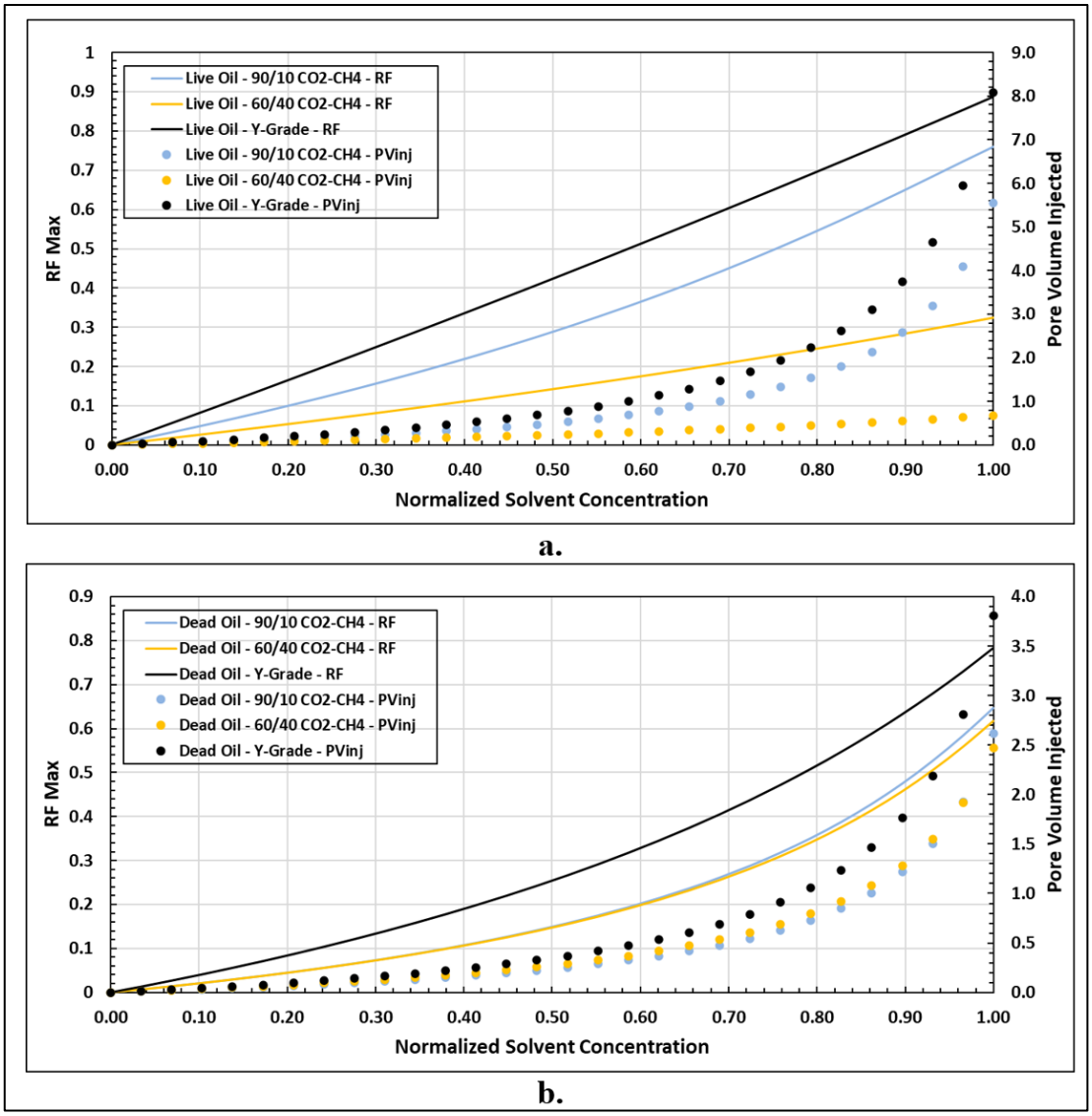

Figure 4.1 – Maximum recovery factor and Maximum pore volume injected at increasing normalized solvent concentration for live (a.) and dead (b.) oil. Dotted lines represent injected pore volumes while solid lines represent recovery factor. 60/40 CO_2-CH_4 solvent reached a maximum solvent concentration. Mixtures under pressure of 3750 psi and a temperature of 175 °F.

From looking at the figures above, it is easy to assume that wells should be producing solvent at the highest solvent concentration to yield the highest recovery. While this is true, it may not be economically feasible to inject so much solvent.

Increasing solvent concentration of injection solvent 1 (90/10 CO_2-CH_4) and Y-grade, for the live oil, and all three for the dead oil, eventually leads to unrealistic injected pore volumes. Requiring economically unfeasible amounts of solvent. By setting the maximum injected pore volume to a value of 1.2, as it is commonly done in the industry, we can limit the solvent concentration to be used. Noting that, injection solvent 2, composed of 60/40 CO_2-CH_4, reached a maximum allowable concentration to maintain liquid phase behavior when introduced to the live oil, as such, it resulted in much lower injected pore volumes.

The maximum recovery factor and pore volume calculations only required the oil and solvent compositions, and the solvent concentration at the producing well. However, to predict the maximum number of cycles required for the huff-n-puff process, defined in **Eq. (4.2),** where V_p is the volume of oil produced at reservoir pressure and temperature, the volume of the fracture (V_{frac}) must be provided. We assumed both geometries which are summarized in **Table 4.1**. **Figure 4.2** shows normalized solvent concentration as a function of the maximum number of cycles required for the live (a.) and dead (b.) oil.

$$\#\ of\ \ Cycles = \frac{V_p}{V_{frac}} \tag{4.2}$$

Table 4.1 – Cartesian stimulated reservoir and fracture geometry example. Including porosity, length, width, and height.

Stimulated Reservoir Geometry		Fracture Geometry	
ϕ_R (%)	10	ϕ_F (%)	40
l_R (ft)	200	l_F (ft)	200
w_R (ft)	20	w_F (mm)	2.5
h_R (ft)	100	h_F (ft)	100

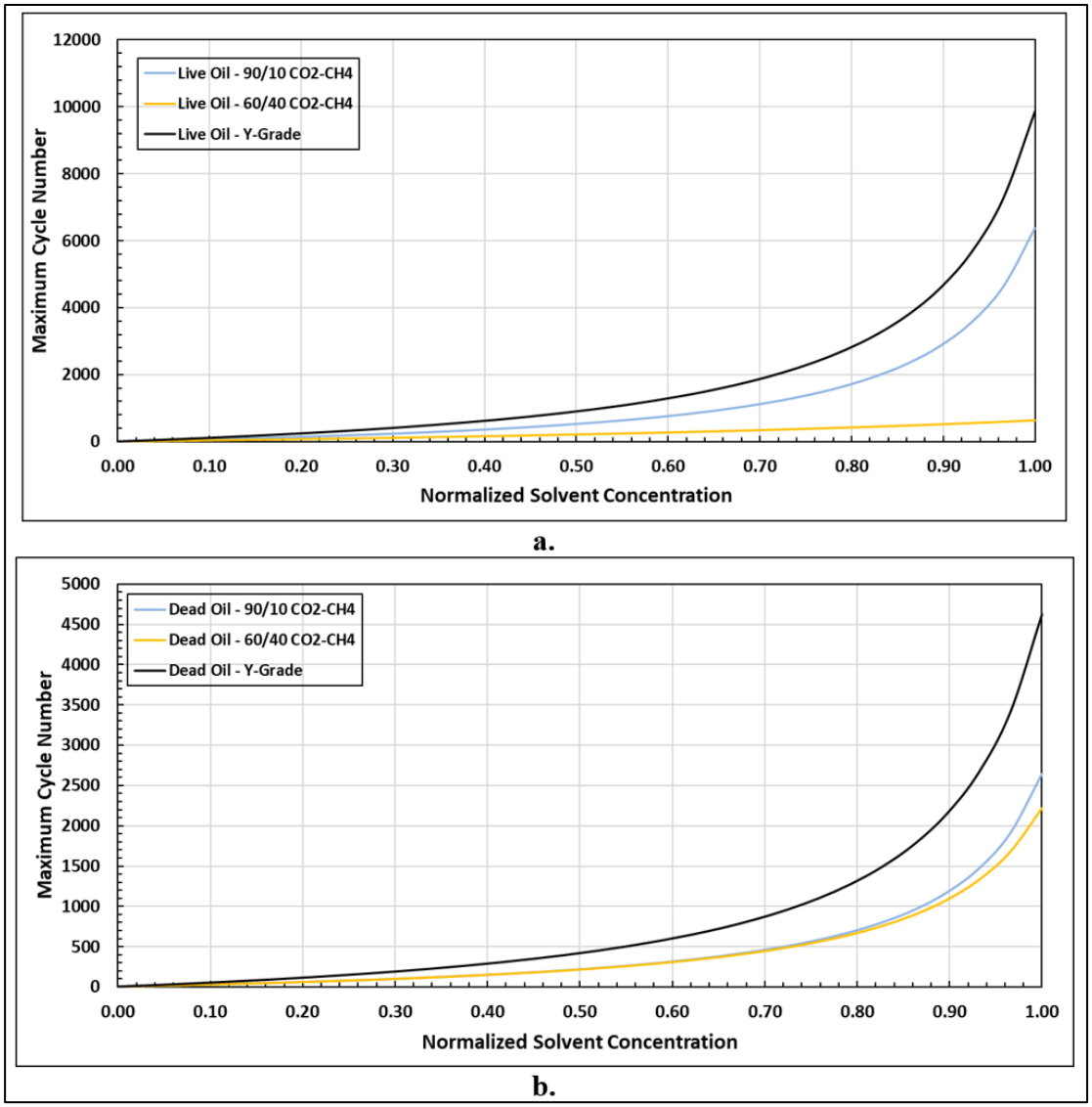

Figure 4.2 – Maximum Number of Cycles at increasing normalized solvent concentrations for live (a.) and dead (b.) oil. Mixtures under pressure of 3750 psi and a temperature of 175 °F.

On all cases illustrated above, the Y-grade resulted in the largest number of cycles required for the process. Reaching upwards of almost ten thousand cycles at its maximum normalized concentration with the live oil. Y-grade is a liquid solvent, as such it will cause higher liquid volume produced in comparison to the other solvents. On the other hand, the 60/40 CO_2-CH_4 solvent, showed the least maximum number of cycles at all normalized

concentration values. The 60/40 CO_2-CH_4 solvent is the lightest solvent of all, as well as the least effective at expanding the initial oil volume. Once it combines with the oil it will not lead to such increase in liquid volume produced, allowing for less cycles required at the same normalized concentration. Furthermore, we may want to decrease the number of cycles after selecting a solvent. Increasing solvent injection pressure, or rather, pressurizing the reservoir, can not only increase oil recovery, but also decrease number of cycles required for the process. Alternatively, combining light natural gases with heavy solvent, will lead to lower cycles at the cost of an increase in GOR.

The maximum number of cycles required follow a similar trend to the maximum injected pore volumes. Consequently, it also approaches infinity as the concentration of solvent approaches a molar fraction of unity. As a result, the solvent concentration at which the producing well, can be limited on a desired number of cycles instead.

Table 4.2 and **Table 4.3** illustrate the resulting maximum recovery factor, realistic GOR and injected pore volumes after limiting the solvent concentration based on an injected pore volume of 1.2, if necessary (Injection solvent 2 (60/40 CO_2-CH_4) was limited to a maximum concentration of 0.476, increasing it any further would lead to the saturation pressure of the mixture to be greater than the pressure of the reservoir leading to two phases), for the live and dead oil respectively.

Table 4.2 – Preliminary analysis of live oil recovery at increasing solvent concentration. Injected pore volumes were limited to 1.2 as industry standard, or lower if mixture reached two-phases at high solvent concentrations. At a reservoir pressure of 3750 psi and a temperature of 175 °F.

Live Oil - 90/10 CO2-CH4					Live Oil - 60/40 CO2-CH4					Live Oil - Y-Grade				
Solvent Moles/Total Moles	GOR (SCF/STB)	RF Max	Cycle	Pore Volume Injected	Solvent Moles/Total Moles	GOR (SCF/STB)	RF Max	Cycle	Pore Volume Injected	Solvent Moles/Total Moles	GOR (SCF/STB)	RF Max	Cycle	Pore Volume Injected
0.000	1409	0.000	0	0.000	0.000	1409	0.000	0	0.000	0.000	1409	0.000	0	0.000
0.100	1656	0.053	69	0.069	0.053	1534	0.029	36	0.041	0.100	1480	0.091	122	0.100
0.200	1965	0.112	156	0.154	0.106	1674	0.059	78	0.088	0.200	1559	0.184	274	0.225
0.300	2363	0.177	270	0.265	0.159	1831	0.091	124	0.140	0.300	1648	0.278	470	0.385
0.400	2894	0.249	424	0.412	0.212	2010	0.125	178	0.199	0.400	1747	0.375	731	0.599
0.500	3636	0.330	643	0.617	0.265	2214	0.161	240	0.267	0.500	1860	0.473	1097	0.898
0.600	4752	0.421	978	0.926	0.318	2450	0.198	312	0.345	**0.572**	**1951**	**0.545**	**1465**	**1.200**
0.660	**5744**	**0.482**	**1280**	**1.200**	0.371	2726	0.238	398	0.436	0.600	1989	0.573	1644	1.347
0.700	6614	0.524	1549	1.440	0.424	3052	0.281	501	0.544	0.700	2137	0.676	2557	2.095
0.800	10358	0.639	2726	2.469	**0.476**	**3444**	**0.325**	**627**	**0.674**	0.800	2312	0.781	4382	3.592
0.900	21749	0.761	6375	5.555						0.900	2520	0.888	9857	8.082

Table 4.3 – Preliminary analysis of dead oil recovery at increasing solvent concentration. Injected pore volumes were limited to 1.2 as industry standard. At a reservoir pressure of 3750 psi and a temperature of 175 °F.

Dead Oil - 90/10 CO2-CH4					Dead Oil - 60/40 CO2-CH4					Dead Oil - Y-Grade				
Solvent Moles/Total Moles	GOR (SCF/STB)	RF Max	Cycle	Pore Volume Injected	Solvent Moles/Total Moles	GOR (SCF/STB)	RF Max	Cycle	Pore Volume Injected	Solvent Moles/Total Moles	GOR (SCF/STB)	RF Max	Cycle	Pore Volume Injected
0.000	0	0.000	0	0.000	0.000	0	0.000	0	0.000	0.000	0	0.000	0	0.000
0.100	51	0.023	29	0.032	0.097	53	0.023	29	0.038	0.100	0	0.044	56	0.047
0.200	129	0.051	65	0.073	0.195	128	0.050	65	0.084	0.200	0	0.094	127	0.106
0.300	229	0.084	112	0.125	0.292	224	0.083	111	0.144	0.300	14	0.152	218	0.181
0.400	362	0.125	176	0.194	0.389	350	0.123	173	0.223	0.400	54	0.217	339	0.282
0.500	548	0.177	265	0.291	0.487	524	0.174	260	0.331	0.500	114	0.294	509	0.423
0.600	829	0.245	401	0.436	0.584	781	0.239	390	0.490	0.600	204	0.384	765	0.635
0.700	1300	0.336	634	0.679	0.681	1197	0.326	605	0.747	**0.739**	**423**	**0.540**	**1450**	**1.200**
0.800	2255	0.464	1114	1.163	**0.775**	**1940**	**0.441**	**1004**	**1.200**	0.700	345	0.491	1192	0.987
0.805	**2329**	**0.472**	**1151**	**1.200**	0.779	1988	0.447	1030	1.229	0.800	585	0.622	2048	1.692
0.900	5227	0.647	2645	2.617	0.876	4080	0.617	2218	2.471	0.900	1077	0.783	4621	3.808

4.1.1 Pressure and Temperature Dependance

In this section, the impact of pressure and temperature on the thermodynamic properties of oil-solvent mixtures was analyzed by using the realistic injected pore volumes from the previous sections. It is important to note however, pressure and temperature affect the amount at which an oil swells differently for any combination of oil and solvent. Therefore, swelling data from laboratory experiments should be gathered and analyzed prior to production of any well.

Pressures were set from 5000 psi to 7500 psi with 100 psi increments, as those are the lowest and highest-pressure points for most shales and tight oil formations (Elturki and Imqam 2020), at a constant temperature of 175 °F. Maintaining an arbitrary solvent concentration of 0.6 solvent moles/total moles, the impact of pressure on the swelling factor and injected pore volumes can be seen in **Figure 4.3** for the live and dead oil.

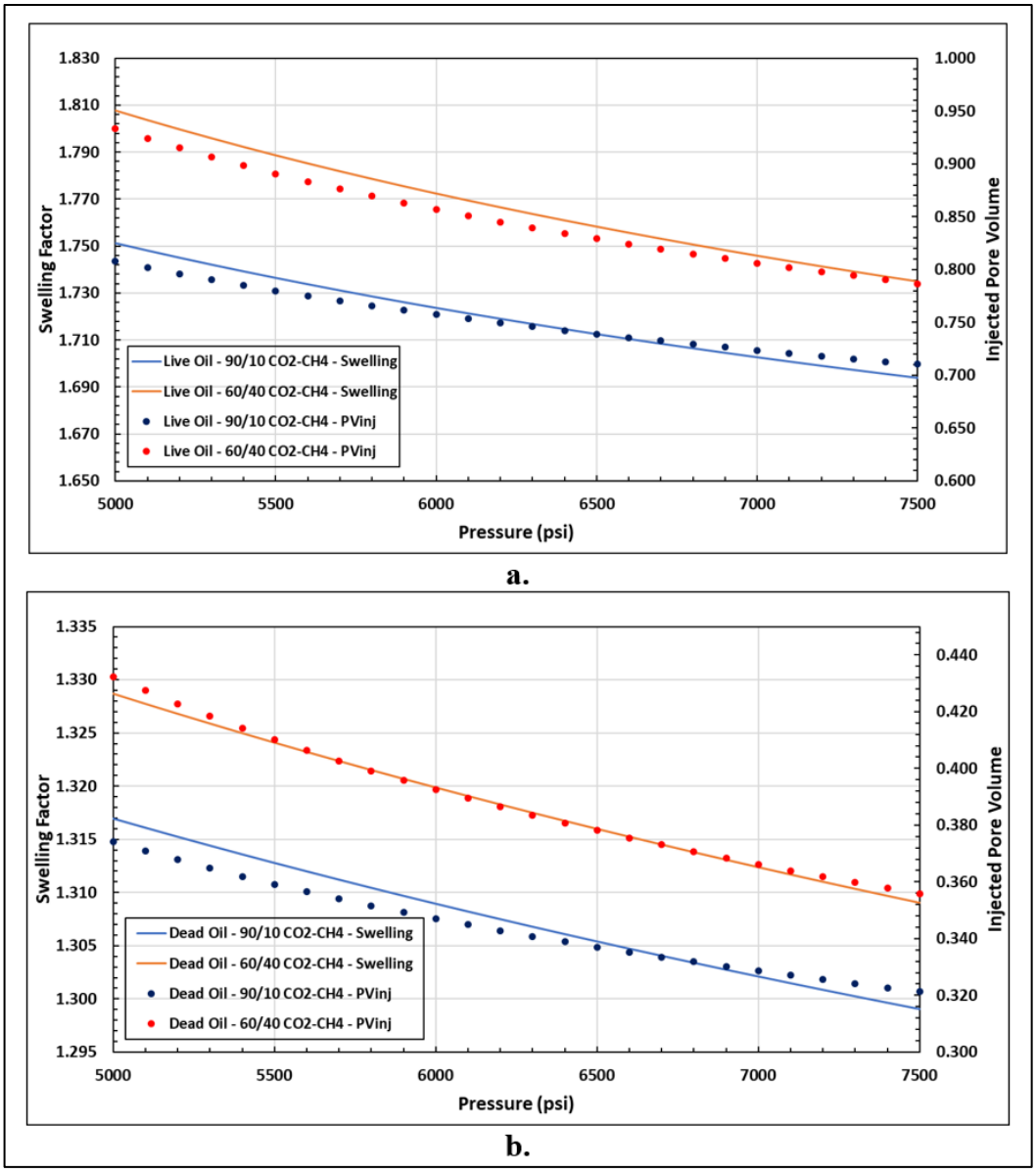

Figure 4.3 – Impact of pressure on swelling factor of live (a.) and dead oil (b.), and injected pore volume, following mixing of solvent at a constant concentration of 0.6 solvent moles/total moles, and constant temperature of 175 °F.

At a constant solvent concentration, swelling factor decreases as a function of pressure; however, at higher pressures, solvent density increases, improving oil recovery (Milad et al. 2021). Consequently, solvent can be produced at a higher concentration while maintaining a reasonable injected pore volume. Using the same realistic injected pore

volume of 1.2, the impact on maximum recovery and solvent concentration by keeping it constant at 1.2 can be seen in **Figure 4.4** for the live oil and dead oil.

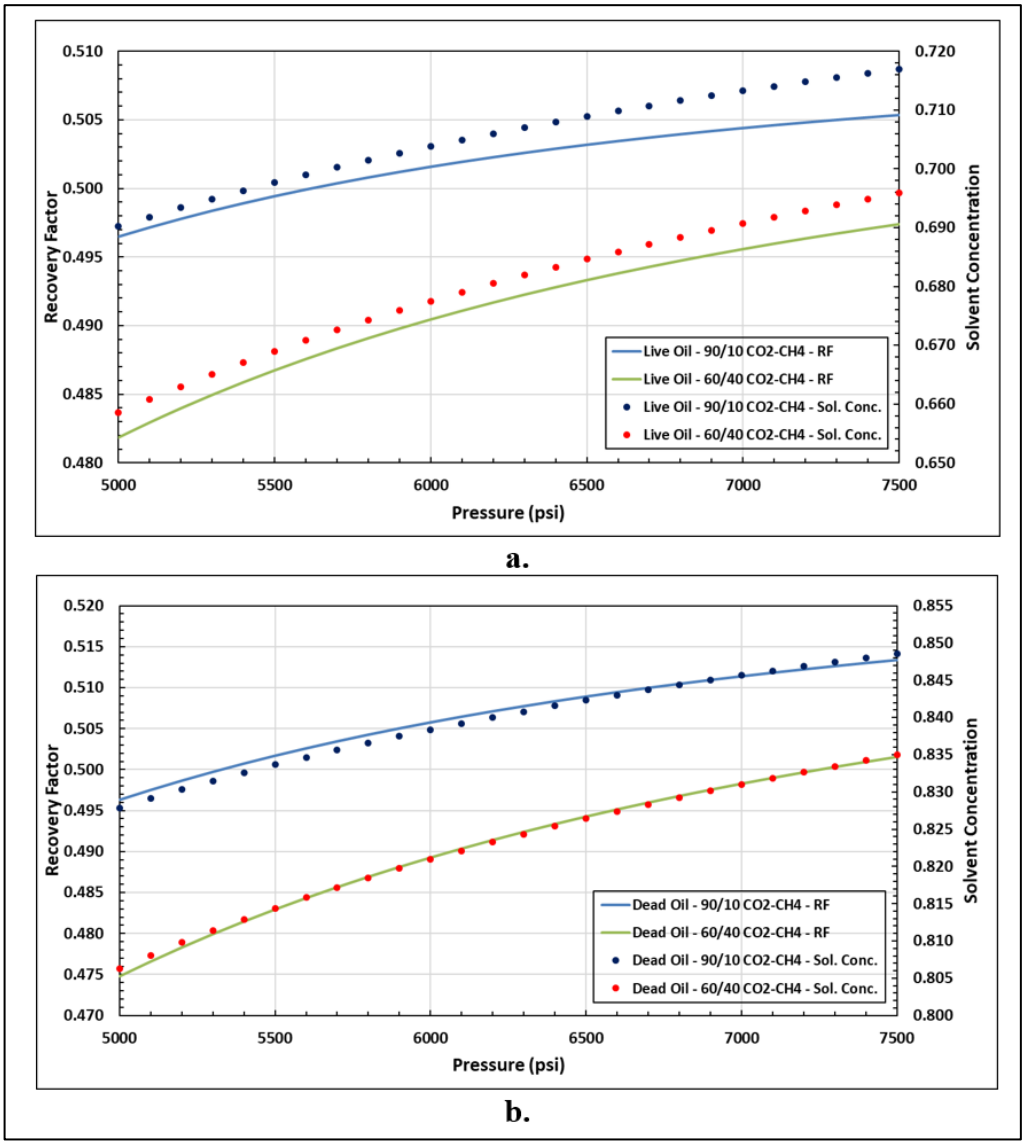

Figure 4.4 – Impact of pressure on recovery of live (a.) dead (b.) oil, following mixing of solvent at a constant injected pore volume of 1.2, and constant temperature of 175 °F.

Figure 4.4 shows the same trend Tovar et al. (2017) observed in their experiment. Maintaining a constant injected pore volume, recovery factor has a positive relationship with pressure. And, as explained in Chapter II, the reservoir pressure is directly proportional to

the injection pressure, as such, it can be pressurized during injection allowing for greater oil recoveries.

The Y-grade solvent was omitted from the above figures as it showed less than 1% change in the swelling factor due to the increase in pressure, allowing for the assumption that the solvent is unaffected by pressure. **Figure 4.5** and **Figure 4.6 i**llustrate the impact of pressure on Y-grade.

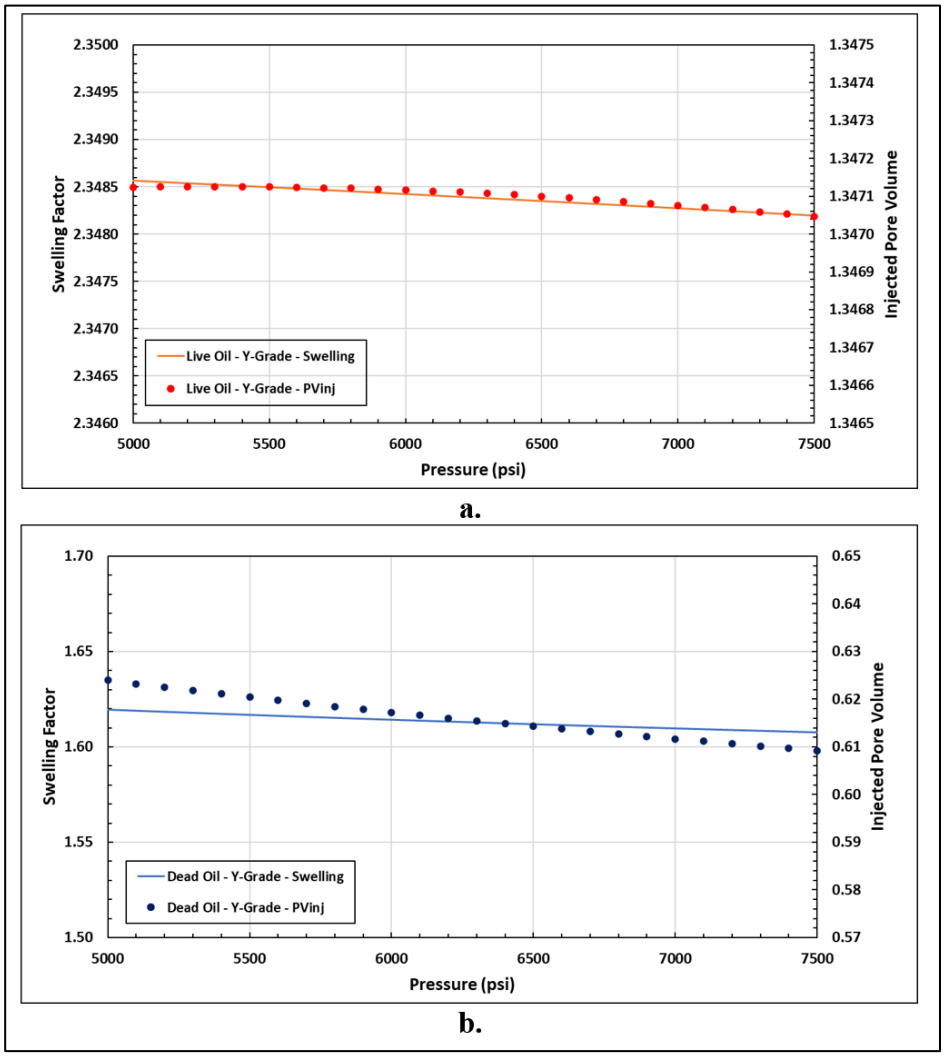

Figure 4.5 – Impact of pressure on swelling factor of live (a.) and dead oil (b.), and injected pore volume, following mixing of Y-Grade at a constant concentration of 0.6 solvent moles/total moles, and constant temperature of 175 °F.

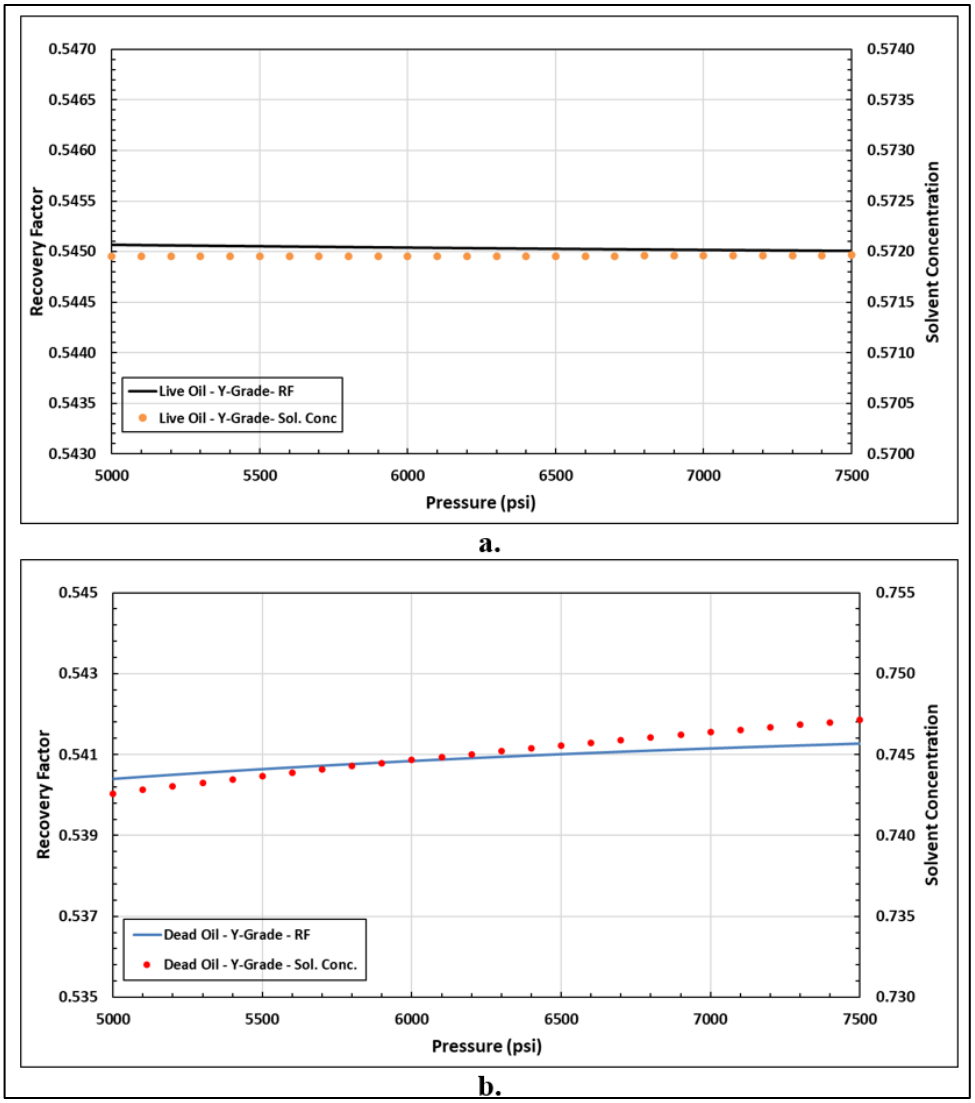

Figure 4.6 – Impact of pressure on recovery of live (a.) dead (b.) oil, following mixing of Y-Grade at a constant injected pore volume of 1.2, and constant temperature of 175 °F.

The same methodology can be performed to analyze recovery due to the impact of temperature changes, while temperature is more difficult to control than pressure, its effects on the oil and solvent should be analyzed prior to production. Temperatures were set from 150 psi to 250°F with 5°F increments, as those are the lowest and highest temperature points for most shales and tight oil formations (Elturki and Imqam 2020), at a constant pressure of 6000 psi. Maintaining an arbitrary solvent concentration of 0.6 solvent moles/total moles,

the impact of temperature on the swelling factor and injected pore volumes can be seen in **Figure 4.7** for the live and the dead oil.

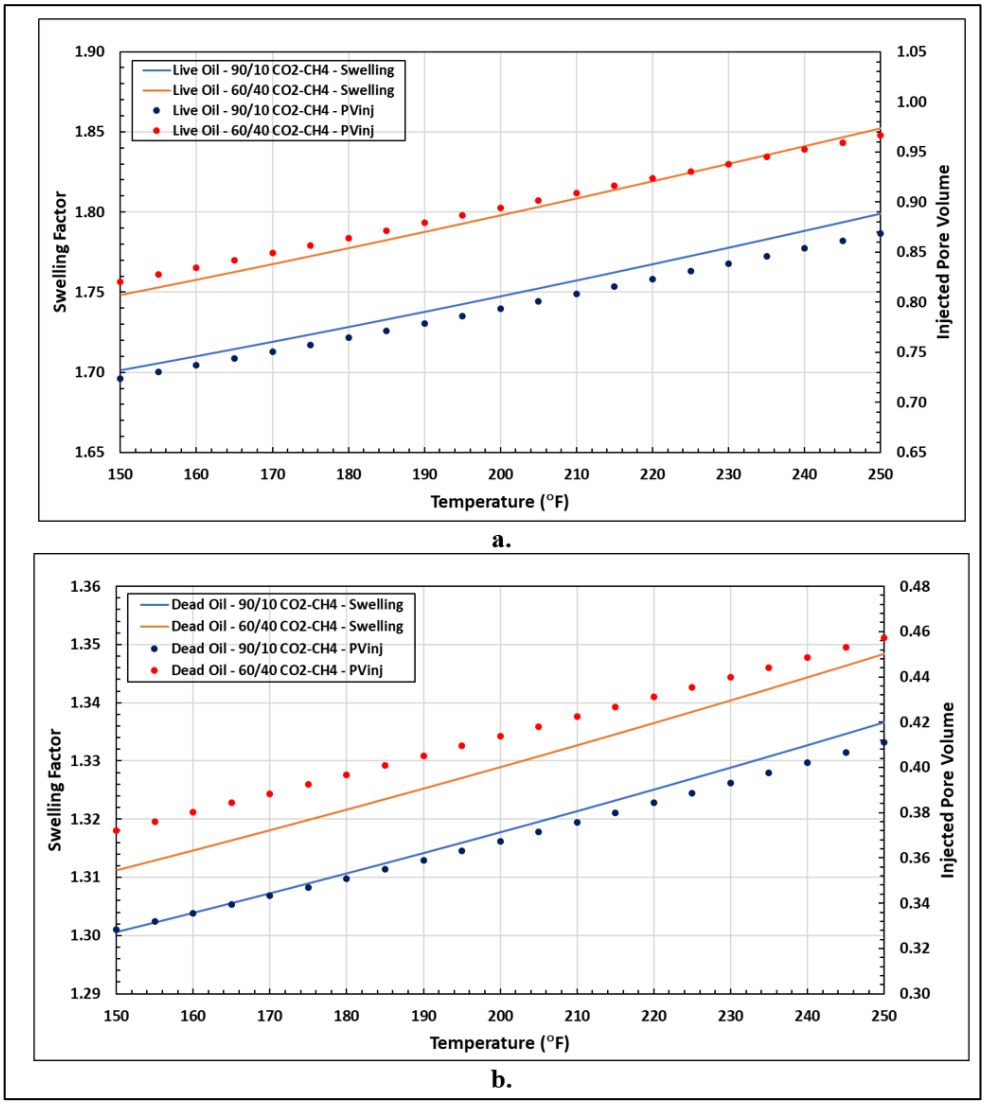

Figure 4.7 – Impact of temperature on swelling factor of live (a.) and dead oil (b.), and injected pore volume, following mixing of solvent at a constant concentration of 0.6 solvent moles/total moles, and constant pressure of 6000 psi.

Swelling factor and injected pore volumes show an increase at higher temperatures, an opposite relationship when comparing to pressure changes. Consequently, it can be expected that maintaining a constant injected pore volume will lead to lower recoveries as

the fluid is expanding with rising temperatures, allowing for less fluid to be injected into the reservoir, as seen in **Figure 4.8**.

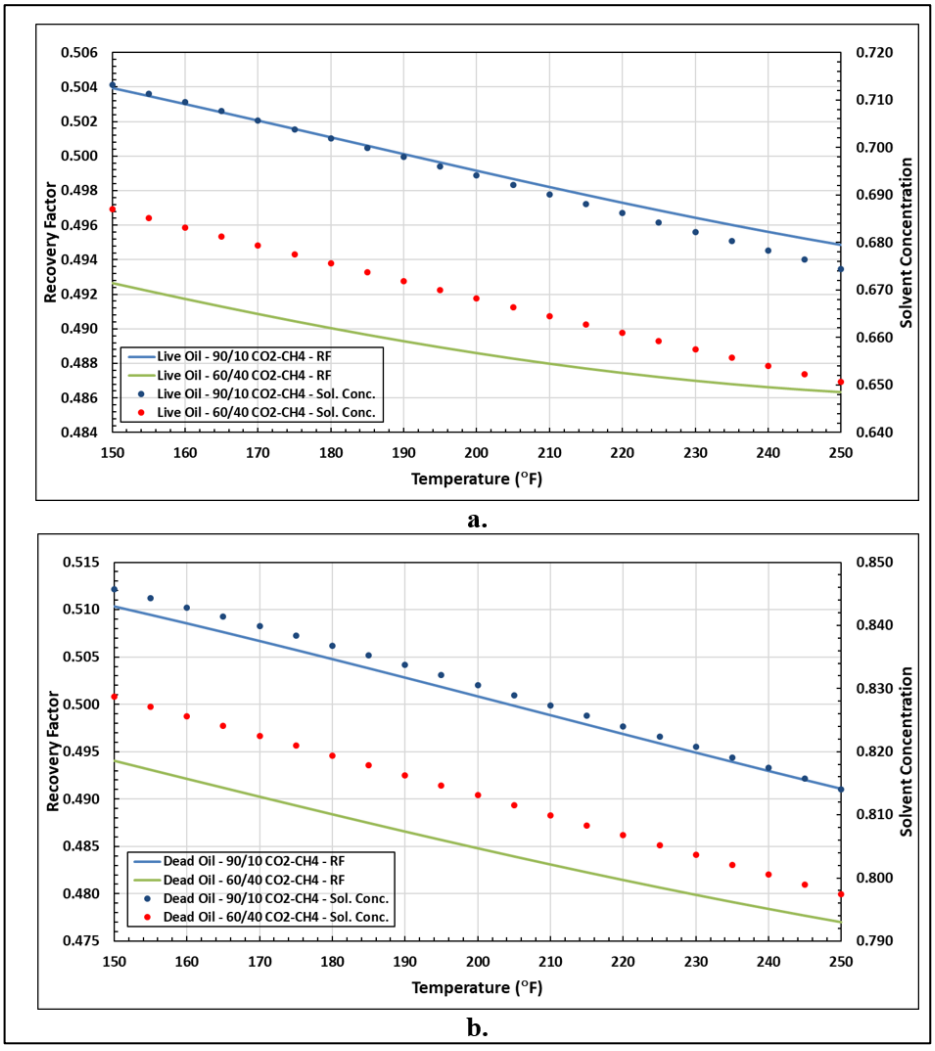

Figure 4.8 – Impact of temperature on recovery of live (a.) and dead (b.) oil, following mixing of solvent at a constant injected pore volume of 1.2, and constant pressure of 6000 psi. Shows opposite trend in comparison to pressure changes.

As temperatures are unlikely to fluctuate during production, its analysis and impact on recovery factor has been neglected by researchers, allowing Milad et al. (2021) to label effects of temperature on reservoirs as one of the "gaps" that exist in the general knowledge of huff-n-puff technology. Yet, thorough analysis of its impact using a simple methodology

as presented on this study can allow for that gap to cease. Trends shown above can seem trivial but provide meaningful understandings of variables affecting oil production in tight reservoirs.

The Y-grade solvent was once again omitted from the analysis above as it showed negligible (< 1%) change in swelling as a result of temperature changes, deeming it unaffected by it. **Figure 4.9** and **Figure 4.10** illustrate the impact of temperature on Y-grade.

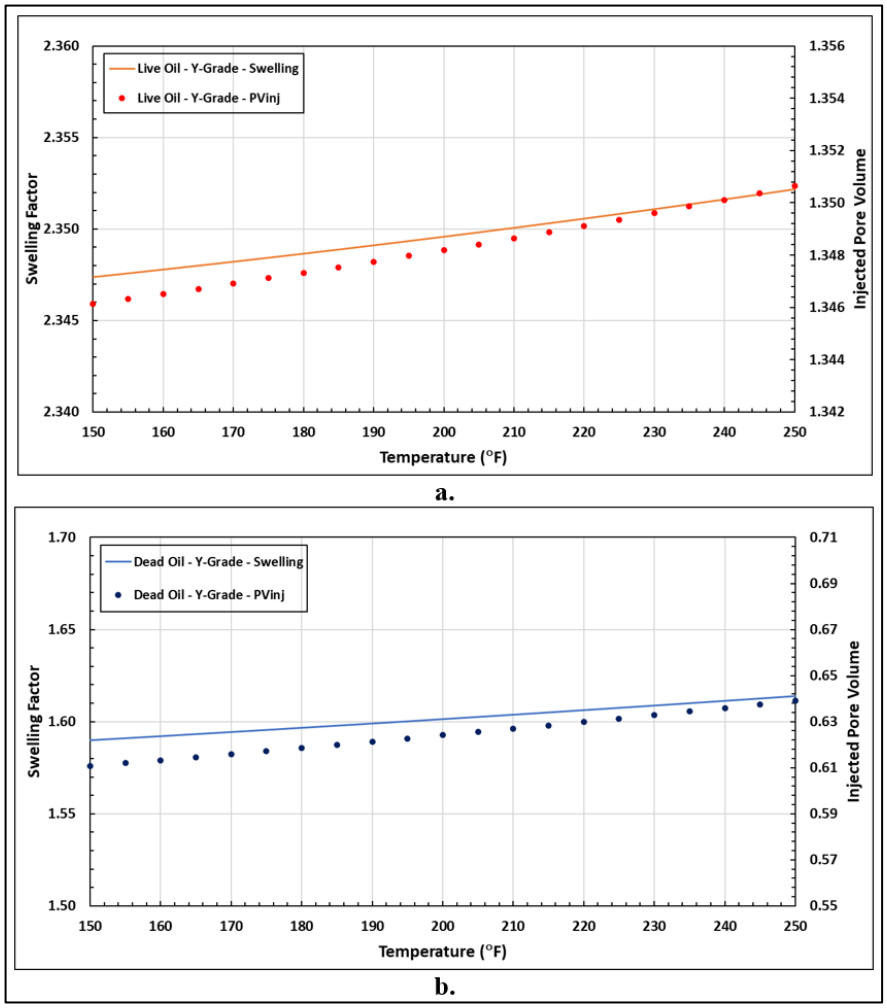

Figure 4.9 – Impact of temperature on swelling factor of live (a.) and dead oil (b.), and injected pore volume, following mixing of Y-Grade at a constant concentration of 0.6 solvent moles/total moles, and constant pressure of 6000 psi.

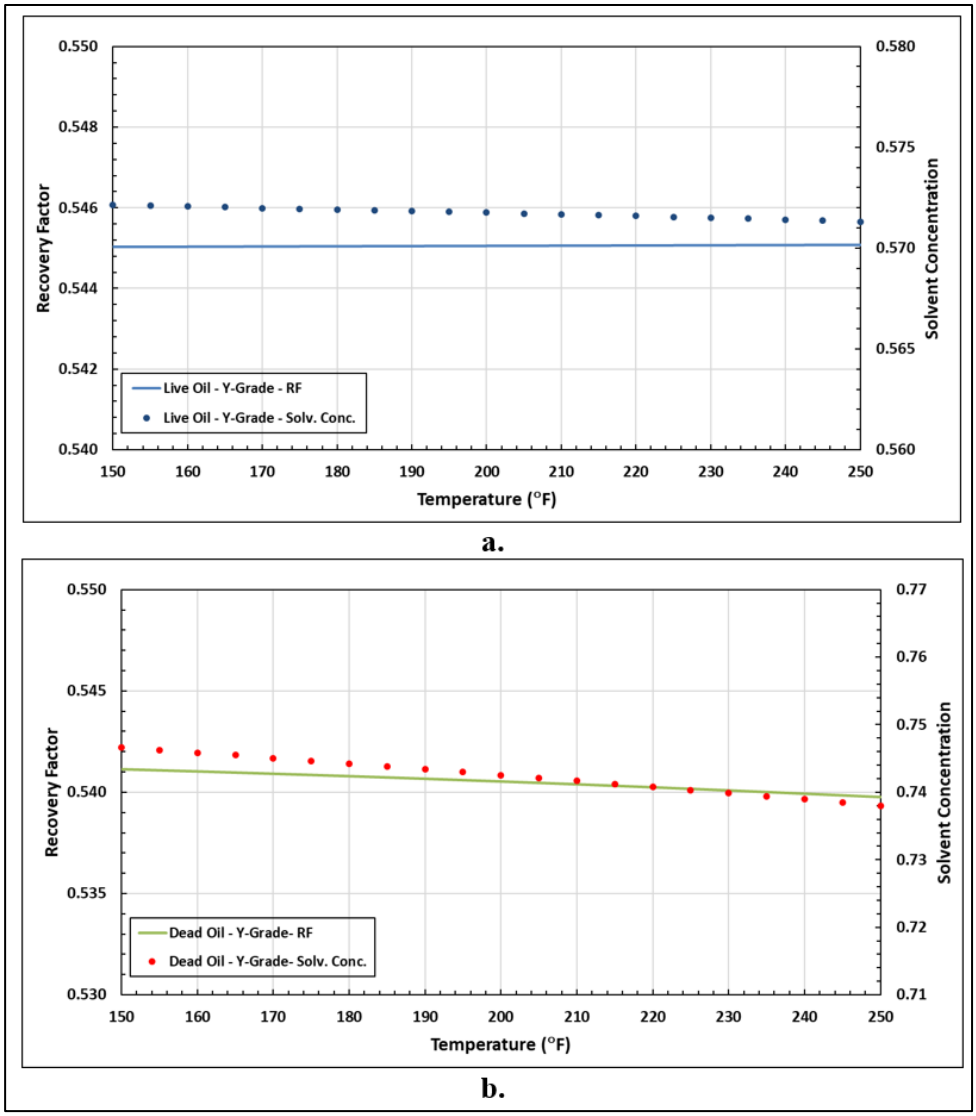

Figure 4.10 – Impact of temperature on recovery of live (a.) and dead (b.) oil, following mixing of Y-Grade at a constant injected pore volume of 1.2, and constant pressure of 6000 psi.

Y-Grade shows vastly different results when analyzing its dependence to temperature and pressure changes after comparison to the other two solvents (90/10 CO_2-CH_4 and 60/40 CO_2-CH_4). Y-Grade is shown to be nearly unaffected by pressure and temperature changes, making it an ideal choice of solvent for low-pressure and/or high-temperature reservoirs. Furthermore, as Y-Grade is nearly an incompressible liquid solvent, it may be used in high-

pressure reservoirs at the same concentration (solvent moles/total moles) as used on low-pressure reservoirs and maintaining the same final recovery factor. A lighter solvent, such as 90/10 CO_2-CH_4 or 60/40 CO_2-CH_4, will need to be produced at a higher concentration, to maintain an injected pore volume of 1.2.

4.2 Molecular Diffusion Flow

We used a molecular diffusion model driven by concentration gradient to simulate flow within a shale or tight oil reservoir. Conventional advective transport, like Darcy's Law cannot be applied in this situation due to the tight pore space. Studies from Tovar et al. (2018) and Hawthorne et al. (2013) have further proven that the soaking time is impacted by the molecular diffusion flow of the solvent, as it is limited solely by the diffusion coefficient.

Diffusion coefficients are commonly calculated using empirical correlations, such as Wilke and Chang (1955) correlation or Scheibel (1954) correlation for binary liquid diffusion, of which are both a modification of the Stokes-Einstein equation. However, multicomponent diffusion cannot be calculated using empirical correlations and there are very few physics-based studies of diffusion coefficient in tight oil reservoirs (Jia et al. 2019). Instead, laboratory methods can be used to estimate diffusion coefficients, using experiments such as PVT cell method, pressure-decay method, and CT-scan method. (Prawira, 2021)

4.2.2 Recovery with Fixed End Time

The simulator features can be illustrated using the live oil from Tianying (2021) and the dead oil from Tovar (2018), in conjunction with the three solvents described in the earlier sections. Each solvent concentration set corresponding to the maximum 1.2 pore volumes injected, while maintaining single-phase. **Table 4.4** shows the fracture and stimulated

reservoir volume characteristics and geometry. A 10-year injection project life was simulated using the "Fixed End Time" option.

Table 4.4 – Diffusion simulation input, including cartesian stimulated reservoir and fracture porosity, height, length, width, pressure, temperature, and production constraints.

Stimulated Reservoir Properties		Fracture Properties	
ϕ_R (%)	10	$\boldsymbol{\phi_F}$ (%)	40
l_R (ft)	200	l_F (ft)	200
w_R (ft)	20	w_F (mm)	2.5
h_R (ft)	100	h_F (ft)	100
P_R (psi)	3750	Constraints	
T_R (°F)	175	D_{eff} (cm^2/s)	1×10^{-3}
		End Time (years)	10

It is important to note that effective diffusion coefficient considers the fracture surface area, the oil-solvent interaction, pressure and temperature. Varying this coefficient only changes the time to reach the ultimate recovery factor, as the coefficient is what limits the rate of solvent diffusion. We assumed a high effective diffusion coefficient to allow for visualization of a scenario in which the reservoir is greatly stimulated by the fracture.

The fracture is assumed to be initially fully saturated with solvent. As the solvent diffuses into the matrix, it contacts and swells the oil. The swollen volume flows into the fracture space and, when the oil concentration in the fracture is equal to the maximum solvent concentration, the oil is produced, and the solvent is replenished. **Figure 4.11** shows the recovery factor as a function of time for the live oil and the dead oil. As time increases, the production eventually reaches a plateau value, which is the thermodynamic maximum recovery factor determined earlier.

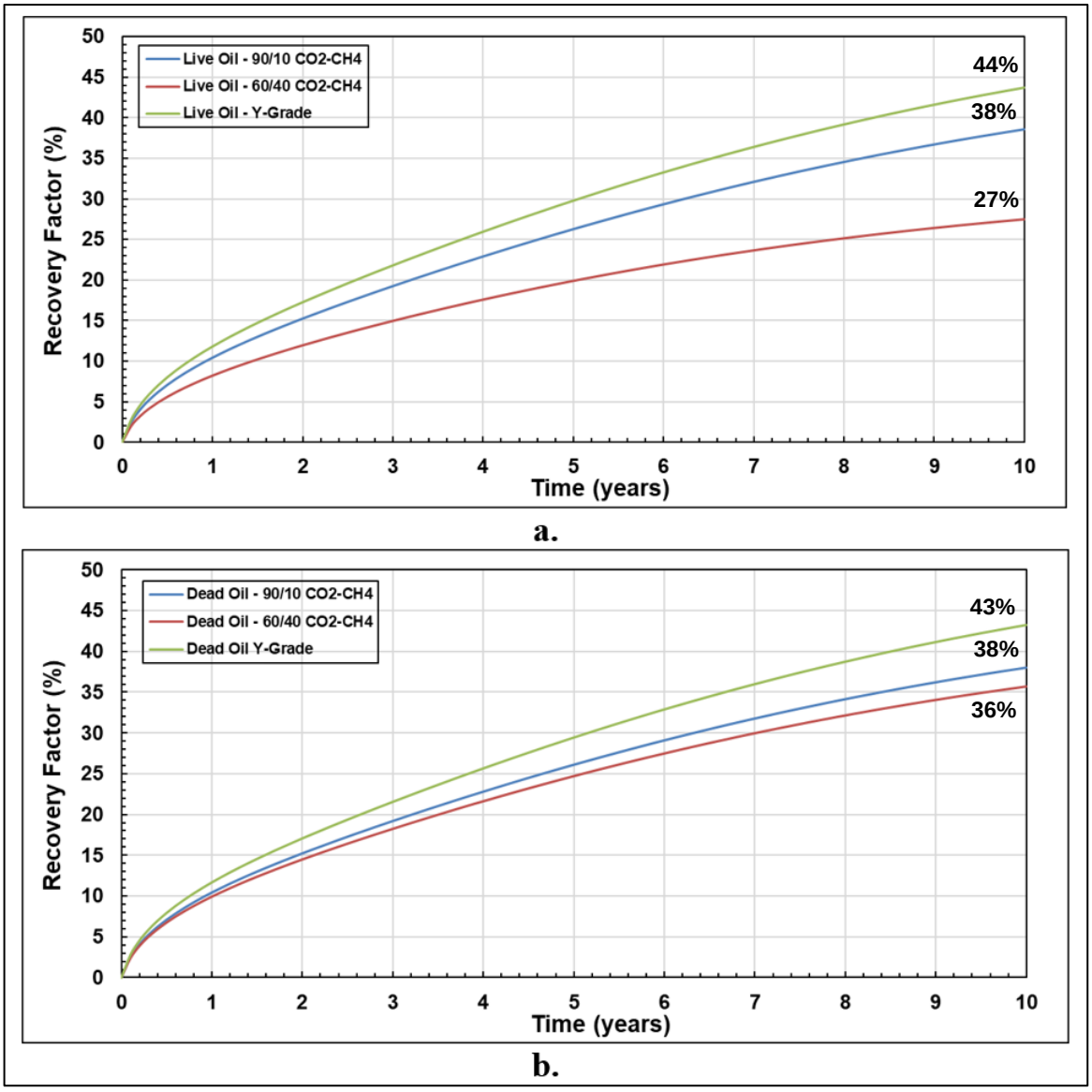

Figure 4.11 – Recovery factor following a 10-year huff-n-puff injection process, for live (a.) and the dead (b.) oil. Recovery approaches a plateau as it reaches the maximum swelling of the original oil.

The effectiveness of solvent 1 (90/10 CO_2-CH_4) and Y-grade at swelling the original oil is similar when comparing the live and dead oil. Solvent 2 (60/40 CO_2-CH_4) showed an improvement in recovery factor for the dead oil. As, for the live oil, at the specified solvent concentration, the saturation pressure of the mixture equated the pressure of the reservoir. On the other hand, the dead oil allows for a much higher concentration of solvent to be added

while keeping it at a single liquid phase, as a result, it was limited by the injected pore volume.

Figure 4.12 show the change in injected pore volume as a function of time. As the field did not reach the thermodynamic-limited recovery, the maximum injected pore volumes were lower than the predetermined limit of 1.2.

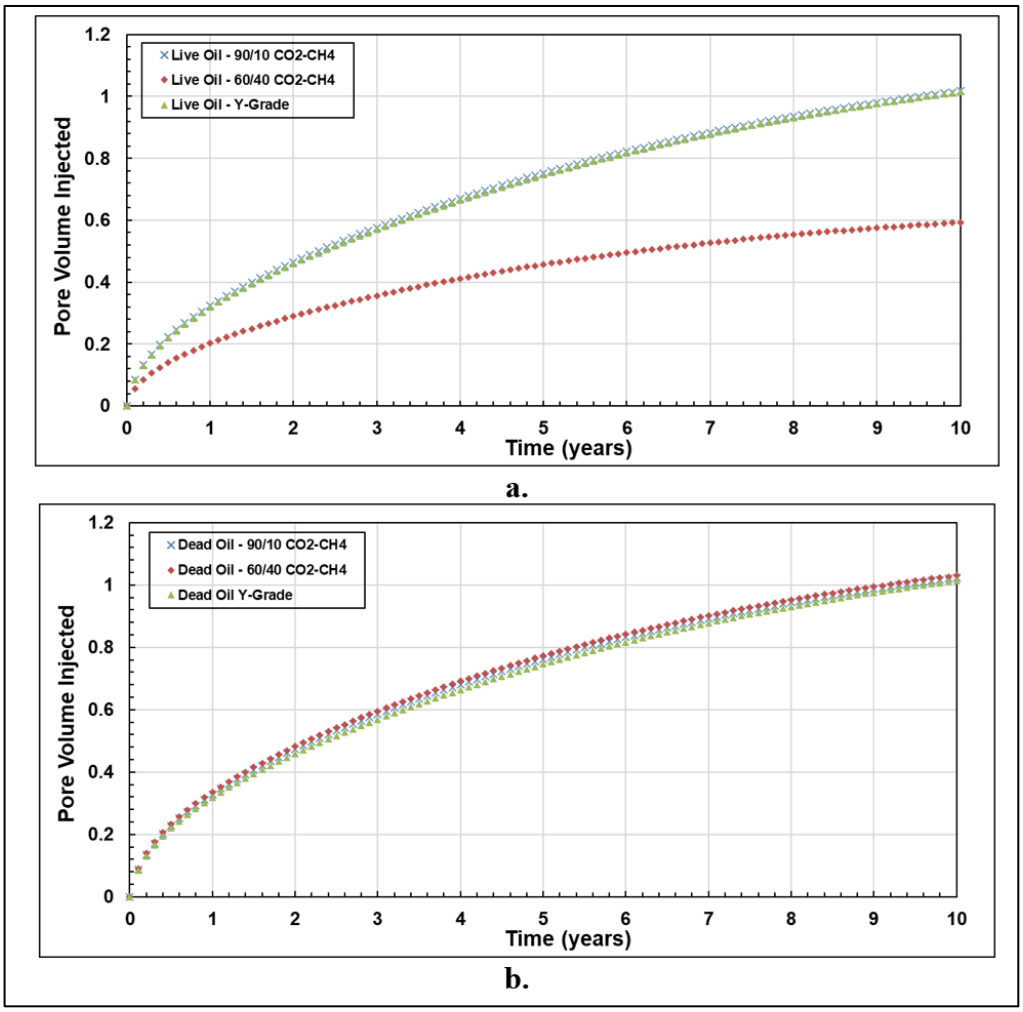

Figure 4.12 – Pore volume injected for a 10-year huff-n-puff injection process for live (a.) and the dead (b.) oil. Solvent produced at concentration such that the maximum injected pore volume is 1.2, if possible.

We can simulate a scenario in which the solvent is switched after a set period of time. As an example, we used the same reservoir and fracture geometry, and effective diffusion

coefficient from Table 4.4, except we produced live oil in conjunction with 90/10 CO_2-CH_4 solvent for a period of 5 years, next, the solvent was switched for the Y-grade and the process ran for 15 years. Both solvents' concentrations were limited to a maximum injected pore volume 1.2, the resulting recovery factor change for the 20-year process can be seen in **Figure 4.13**. Refer to Appendix A for the estimation of solvent concentration after the initial 5 years.

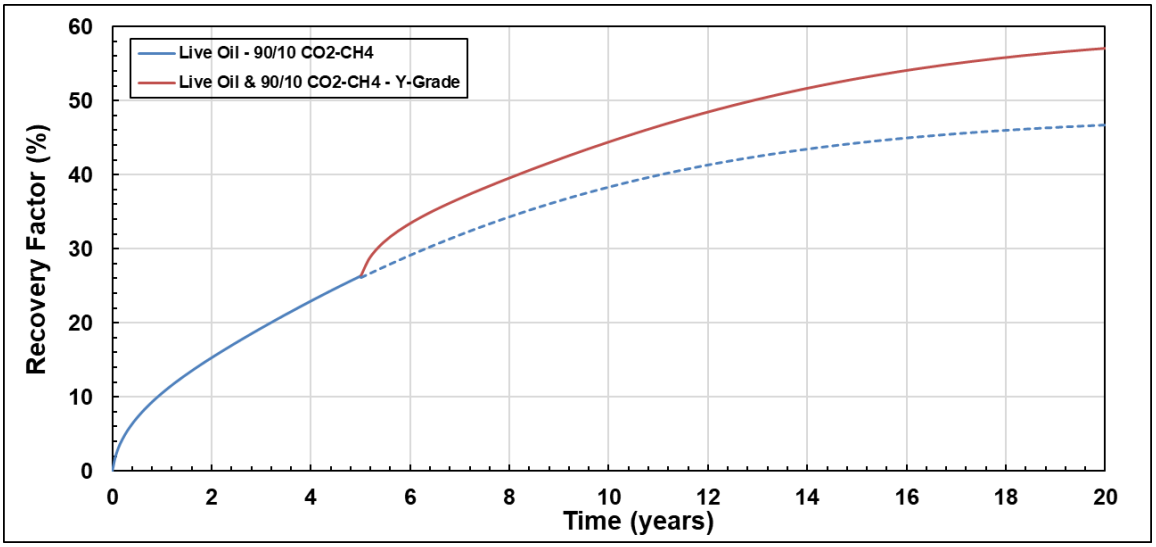

Figure 4.13 – Recovery factor of 20-year huff-n-puff injection process, for the live oil. Including a solvent change after the initial 5 years of injection from 90/10 CO_2-CH_4 solvent to Y-Grade solvent for 15 more years.

Results above show that recovery of a huff-n-puff process are dependent on the solvent used. A more dramatic impact on the performance of the process can be seen when a solvent that is not as soluble is used, such as N_2. Tovar et al. (2017) conducted huff-n-puff injections with pure CO_2 and N_2. We can further validate those findings and our model by replicating their laboratory huff-n-puff experiment using our simulator.

Table 4.5 shows the fracture and stimulated reservoir volume characteristics and geometry Tovar et al. (2017) used. A 22-hour injection project life was simulated. The

effective diffusion coefficient was varied until recoveries matched the experiment. The resulting recovery factor and injected pore volume with time is seen in **Figure 4.14**.

Table 4.5 – Diffusion simulation input of Tovar et al. (2017)'s laboratory experiment, including radial stimulated reservoir and fracture porosity, length, width, pressure, temperature, and production constraints. Varying effective diffusion until recovery was matched.

Stimulated Reservoir Properties		Fracture Properties	
ϕ_R (%)	10.3	ϕ_F (%)	40
l_R (cm)	4.093	l_F (ft)	4.093
r_R (cm)	1.27	w_F (mm)	2.5
P_R (psi)	2500	Constraints	
T_R (°F)	150	D_{eff} (cm^2/s)	2.5×10^{-6}
		End Time (hours)	22

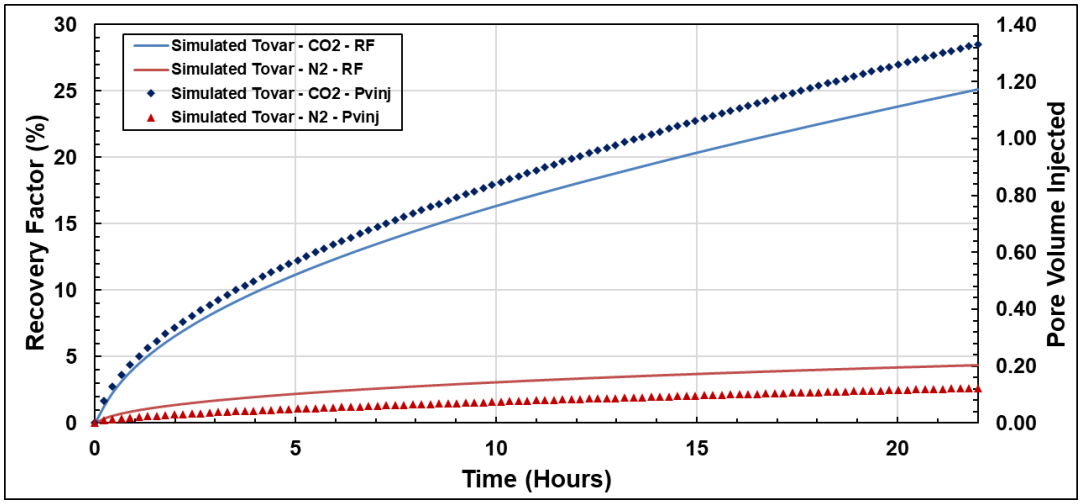

Figure 4.14 – Simulation of recovery factor and pore volumes injected for Tovar et al. (2018)'s laboratory experiment. Injection period of 22-hours using CO_2 and N_2 as solvents.

For the specified time period of 22 hours, N_2 resulted in a final oil recovery of about 4% whereas Tovar et al. (2017) observed 0% recovery. On the other hand, our simulation resulted in an oil recovery of 25% using CO_2, compared to Tovar et al. (2017)'s laboratory experiment resulting in 24% oil recovery. The difference in effectiveness stems from the

miscibility of both solvents in the oil. N_2 has a lower miscibility in the oil, and a lower potential to vaporize hydrocarbons in comparison to CO_2, as such, little can be added to the oil while maintaining liquid-phase. A higher concentration of N_2 would lead to partial miscibility, which is a mechanism outside of the scope of this study. Furthermore, we want to avoid the formation of two-phase as it would lead to an increase in liquid density, lowering oil production. Using a live oil instead would lead to an even less recovery when using N_2, as a result, it is not recommended to be used as a solvent for huff-n-puff processes.

4.2.3 Solvent Concentration Distribution and Storativity

Oil is produced at a constant solvent concentration, as such, the process will have a constant GOR; however, since the diffusion is limited by the effective diffusion coefficient rate, there will be a concentration profile within the matrix as time progresses. Using the array of increasing concentrations of solvent along the flow direction solvent, we can then plot dimensionless solvent concentration as a function of space and time (**Figure 4.15** and **Figure 4.16**) to visualize the solvent concentration within the matrix, using the live oil with the 90/10 CO_2-CH_4 solvent as an example.

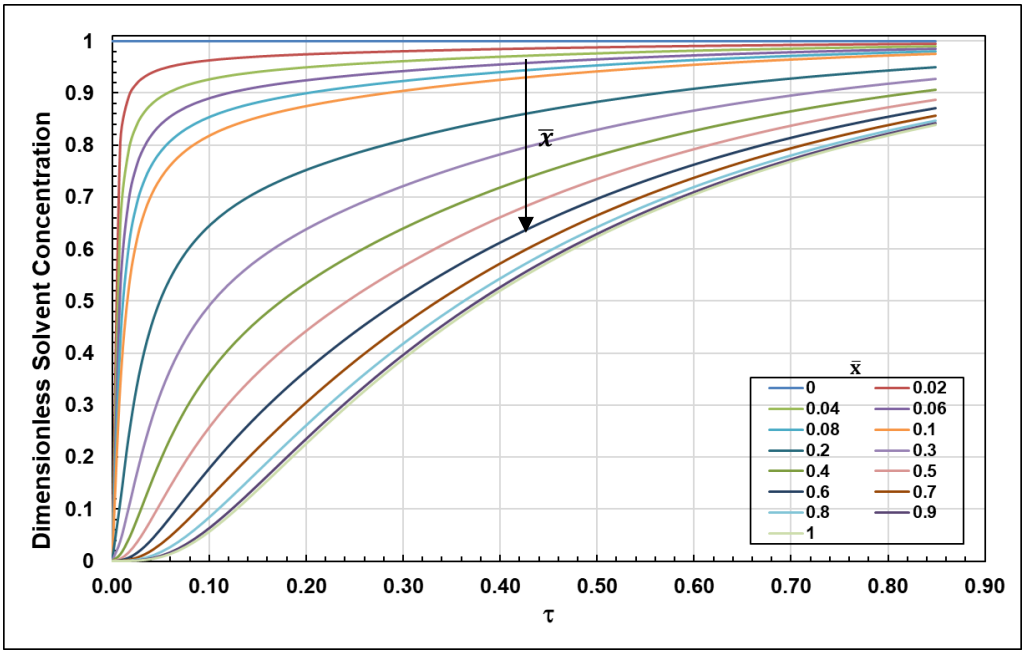

Figure 4.15 – Dimensionless solvent concentration profile as a function of dimensionless time for the live oil and 90/10 CO_2-CH_4 solvent.

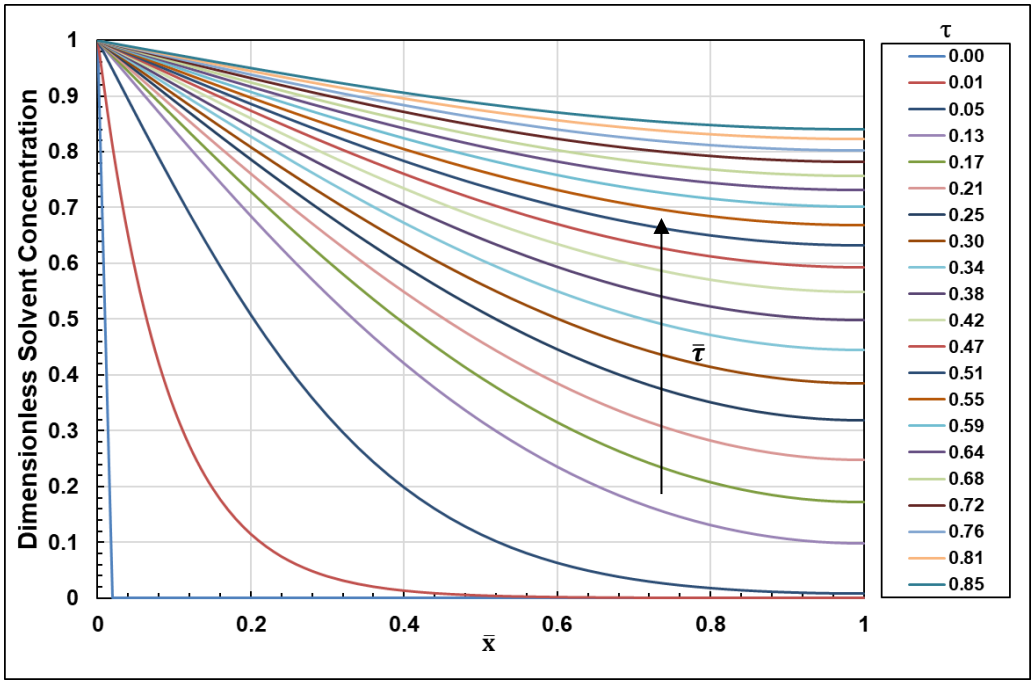

Figure 4.16 – Dimensionless solvent concentration profile as a function of dimensionless flow length of stimulated reservoir volume for the live oil and 90/10 CO_2-CH_4 solvent. Width zero representing the fully saturated fracture and one being the entire flow length. Integrating profile at the end of simulation provides solvent stored in the matrix.

The concentration profile curve is integrated, and multiplied by the reservoir height, length, and porosity, as seen in **Eq. (4.3)**. Allowing for the solvent stored within the matrix to be calculated at any time step. **Figure 4.17** illustrates solvent produced, and solvent stored for the 10-year period.

$$S_{stor} = \frac{1}{2}\left(x_i \times c_{0,j} + 2\left(\sum (c_i) + c_{i,j_{max}}\right)\right) \times h_R \times l_R \times \phi_R \qquad \textbf{(4.3)}$$

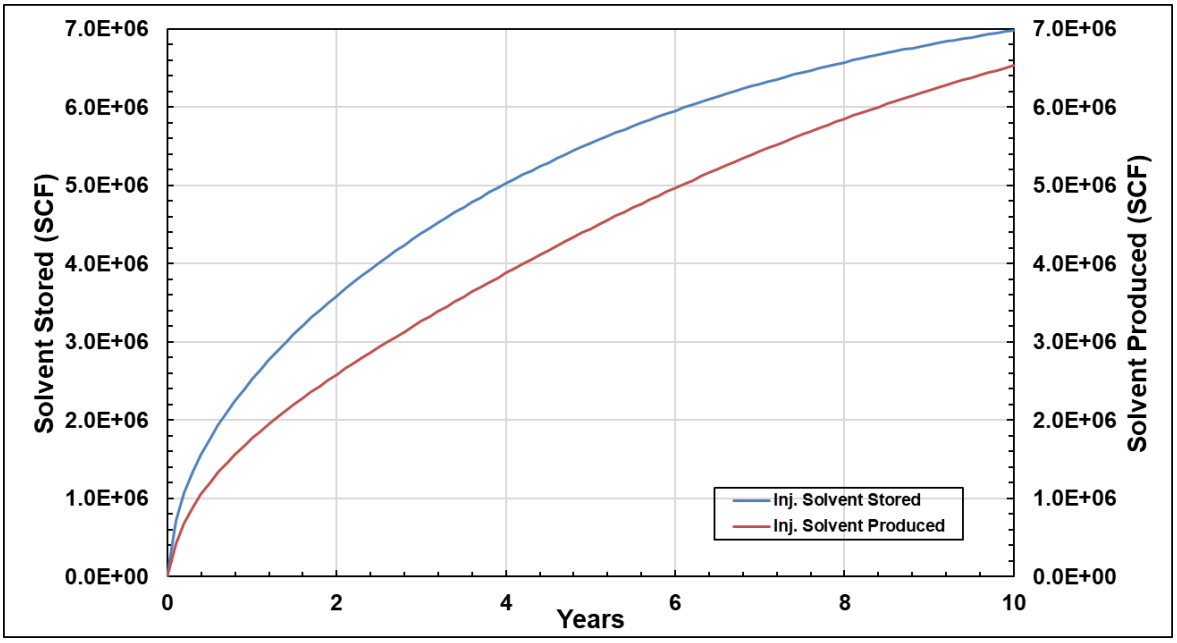

Figure 4.17 – Solvent stored and produced for a 10-year huff-n-puff injection process for the live oil and 90/10 CO_2-CH_4 solvent.

As the fracture volume is assumed to be replenished as soon as it is empty of solvent, we can calculate the required number of cycles, defined in **Eq. (4.2)**, as it is proportional to the volume produced and the pore volume of the fracture. **Figure 4.18** shows the number of cycles required as a function of time for the live oil and the three solvents.

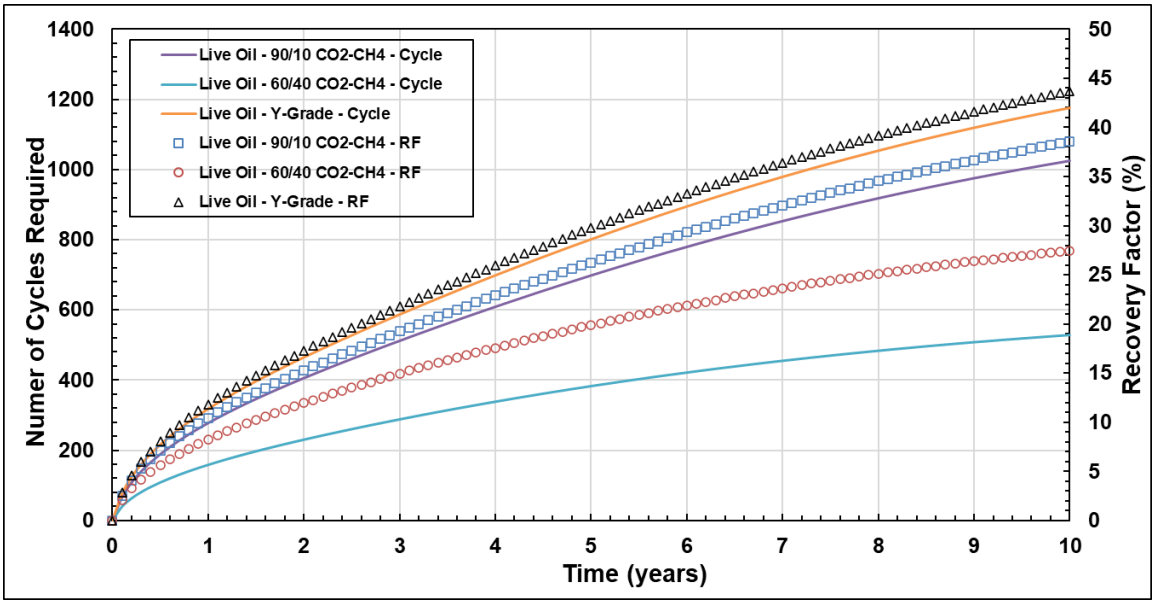

Figure 4.18 – Number of cycles required for a 10-year huff-n-puff injection process for the live oil and 90/10 CO_2-CH_4 solvent. Length of each cycle is not constant as the production eventually plateaus, as such, it will take longer to produce the same incremental amount of oil.

Although Y-grade is being produced at a lower concentration in comparison to the 90/10 CO_2-CH_4 solvent (0.572 solvent moles/total moles compared to 0.660 solvent moles/total moles), in 10 years, it results in higher number of cycles required. Y-grade is a liquid solvent, as such, once it is mixed with the oil, results in a higher liquid volume produced, leading to a greater number of cycles required.

Cycles as a function of time are dependent on the volume of the fracture, the effective diffusion coefficient, as well as the reservoir storativity. The scenario in Figure 4.18, is an example of a highly stimulated reservoir volume with an effective diffusion coefficient of 1.00×10^{-3} cm^2/s, as such, we see that solvent will have to be replenished daily to keep with the prediction above. To maintain with industry standards, solvent can be produced at a lower concentration, lowering the frequency of solvent reinjection.

We may assume that since Y-grade resulted in the highest oil recovery, it should be selected as the best solvent for this case scenario. Y-grade is a liquid solvent, it does not require for it to be compressed like CO_2, and there currently exists a surplus of natural gas liquids (Moody 2020), making it cheaper than alternatives. However, Y-grades require a greater number of cycles in comparison to lighter solvents such as 90/10 CO_2-CH_4 and 60/40 CO_2-CH_4, demanding greater volume of solvent to be used and more frequent stoppage times. The selection of best solvent in a huff-n-puff boils down to the cost (purchasing of the solvent, production halted due to stoppages) and revenue (volume of oil recovered, solvent recycled), and should be thoroughly analyzed.

4.2.4 Recovery Type Curves

Since a thermodynamic limit of recovery exists which cannot be exceeded even with greater producing times, a decrease in the time required to reach this limit must be analyzed such that production is substantial in a realistic amount of time. The best approach is to increase contact area, which may be displayed as an increase in diffusion coefficient. Or to decrease fracture spacing, which may be displayed either as a decrease in flow length or increased areal contribution of secondary and natural fractures (Theloy 2014).

Recovery factor can be plotted against a transform of time, allowing the impact of an increase in surface area, a decrease in fracture spacing, or an increase in effective diffusion coefficient to be assessed.

Figure 4.19 was created using a constant effective diffusion coefficient of 1×10^{-3} cm^2/s for the live oil with the 90/10 CO_2-CH_4 solvent as an example, while changing flow lengths and a project duration of 10 years. As we are simulating a single fracture and a single stimulated reservoir volume, the flow length can represent half the fracture spacing in a much

larger reservoir. At smaller fracture spacings, the time required to reach the maximum recovery factor is smaller than with longer flow lengths.

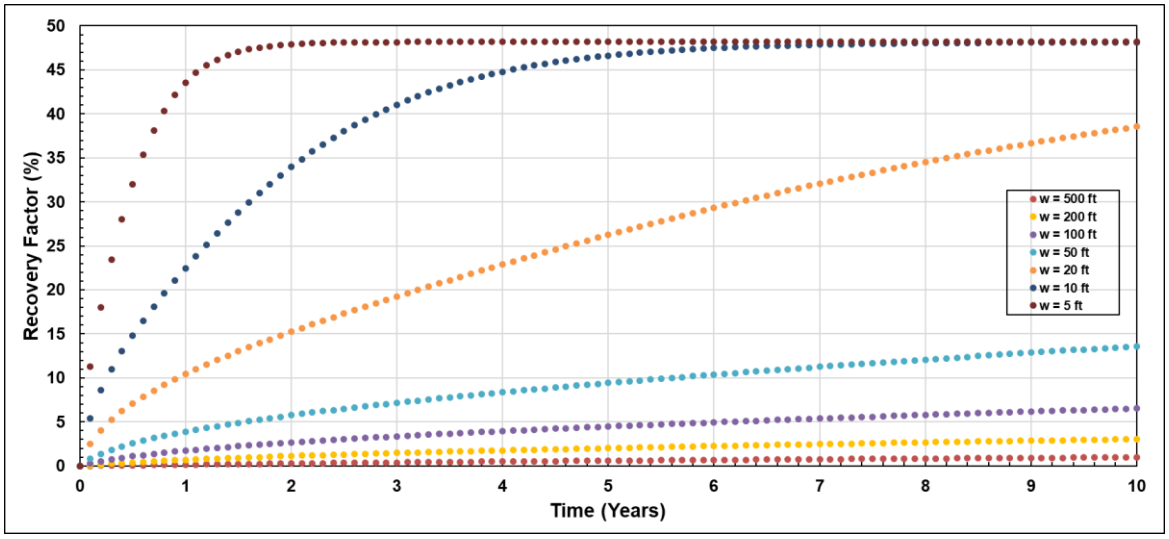

Figure 4.19 – Recovery factor for 10-year huff-n-puff processes of different flow length, using the live oil and 90/10 CO_2-CH_4 solvent as an example.

By plotting recovery as a function of $t/_{w^2}$, we can estimate recovery for a given time (years) regardless of fracture spacing (ft), providing with a preliminary tool to estimate the optimal number of fractures. **Figure 4.20** illustrates the recovery type curve created, for the live oil and the dead oil, with the three solvents.

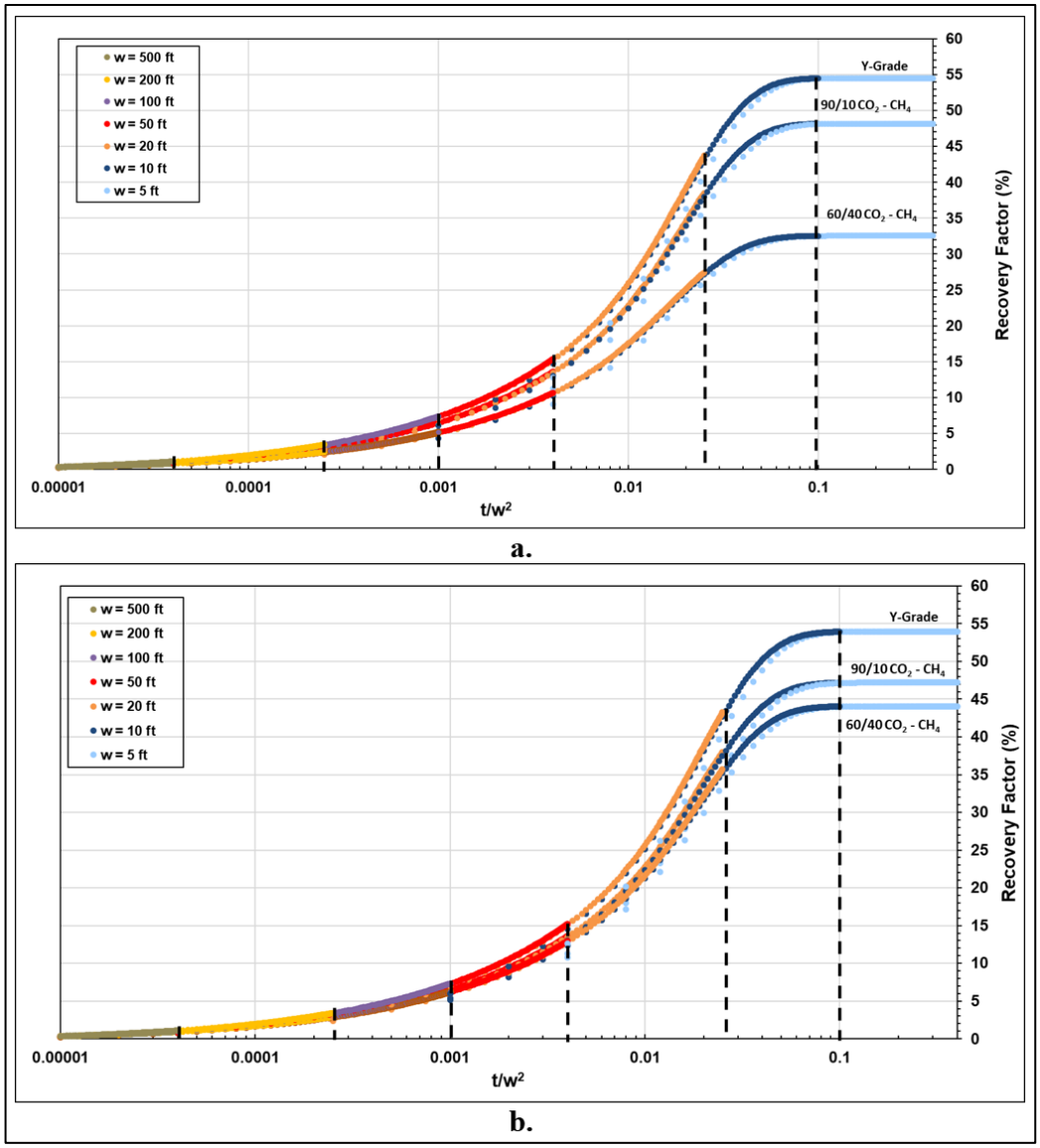

Figure 4.20 – Stimulated reservoir flow length type curve. Recovery as a function of t/w^2 (years/ft^2) for live (a.) and dead (b.) oil. Allows for prediction of recovery for a specific oil-solvent combination and any flow length at a constant effective diffusion coefficient.

Figure 4.21 was developed by keeping a constant flow length of twenty feet with variable diffusion coefficient, live oil with the 90/10 CO_2-CH_4 solvent**,** and a project duration of 10 years, as an example. The existence of secondary fractures, which increase the surface area of the primary fracture, appear as an increase in effective diffusion coefficient. If

secondary fractures exist, they result in a substantial increase in effective diffusion coefficient, and the time required to reach the maximum recovery decreases.

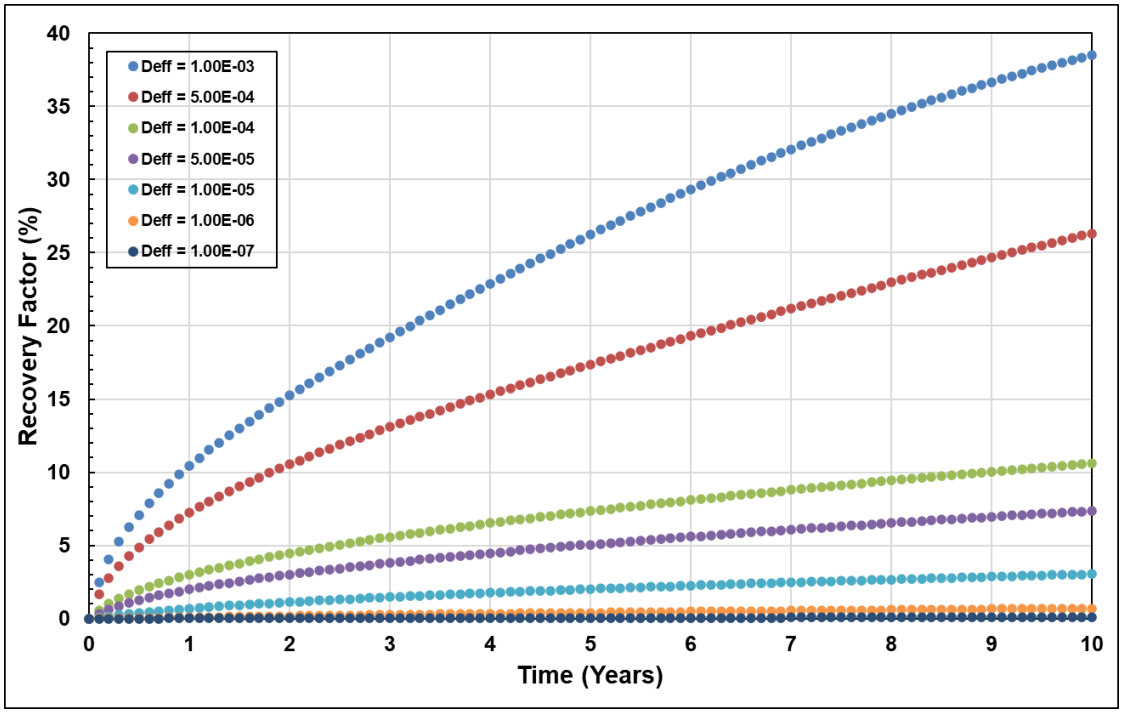

Figure 4.21 – Recovery factor for 10-year huff-n-puff processes of different effective diffusion coefficient, using the live oil and 90/10 CO_2-CH_4 solvent as an example.

By plotting recovery as a function of $t \times D_{eff}$, we can estimate recovery for a given time (years) regardless of effective diffusion coefficient. **Figure 4.22** illustrates the dimensionless recovery type curve created, for the live oil and dead oil, with the three solvents.

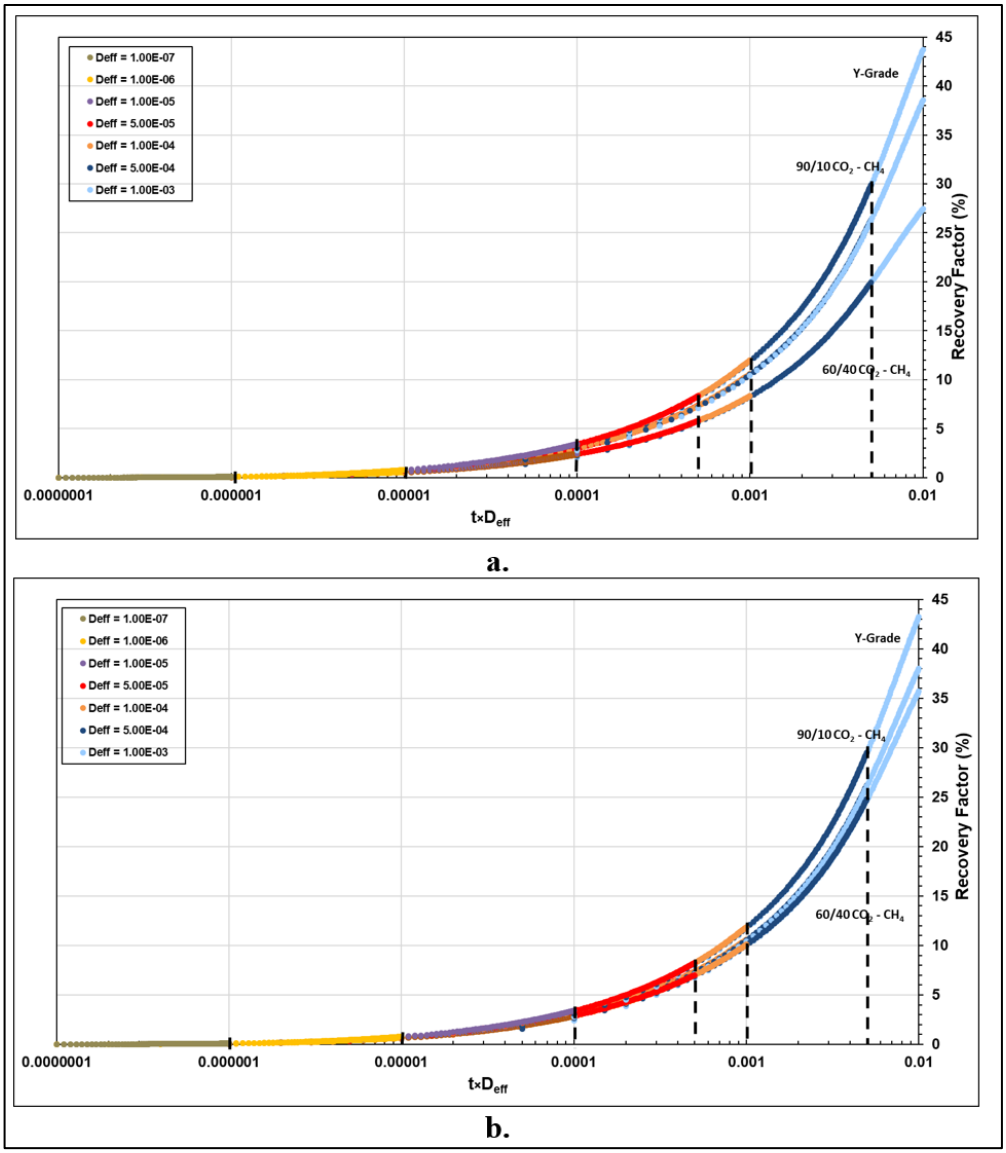

Figure 4.22 – Effective diffusion coefficient type curve. Recovery as a function of $t \times D_{eff}$ (years×cm^2/s) for live (a.) and dead (b.) oil. Allows for prediction of recovery for a specific oil-solvent combination and any effective diffusion coefficient at a constant flow length.

We can also create a type curve for Figure 3.12, or rather, a situation in which we are transforming the "shoe-box" matrix into an arrangement of rods to allow for greater fracture surface area. In such situation, as the number of rods is increased, the flow length of the reservoir decreases while the fracture surface area increases. By plotting recovery factor as a function of time (years) multiplied by fracture surface area (ft^2) and divided by flow length

(ft), **Figure 4.23** was created for the live oil (a.) and the dead oil (b.). Allowing for a prior estimation of recovery, given time, for any fracture surface area.

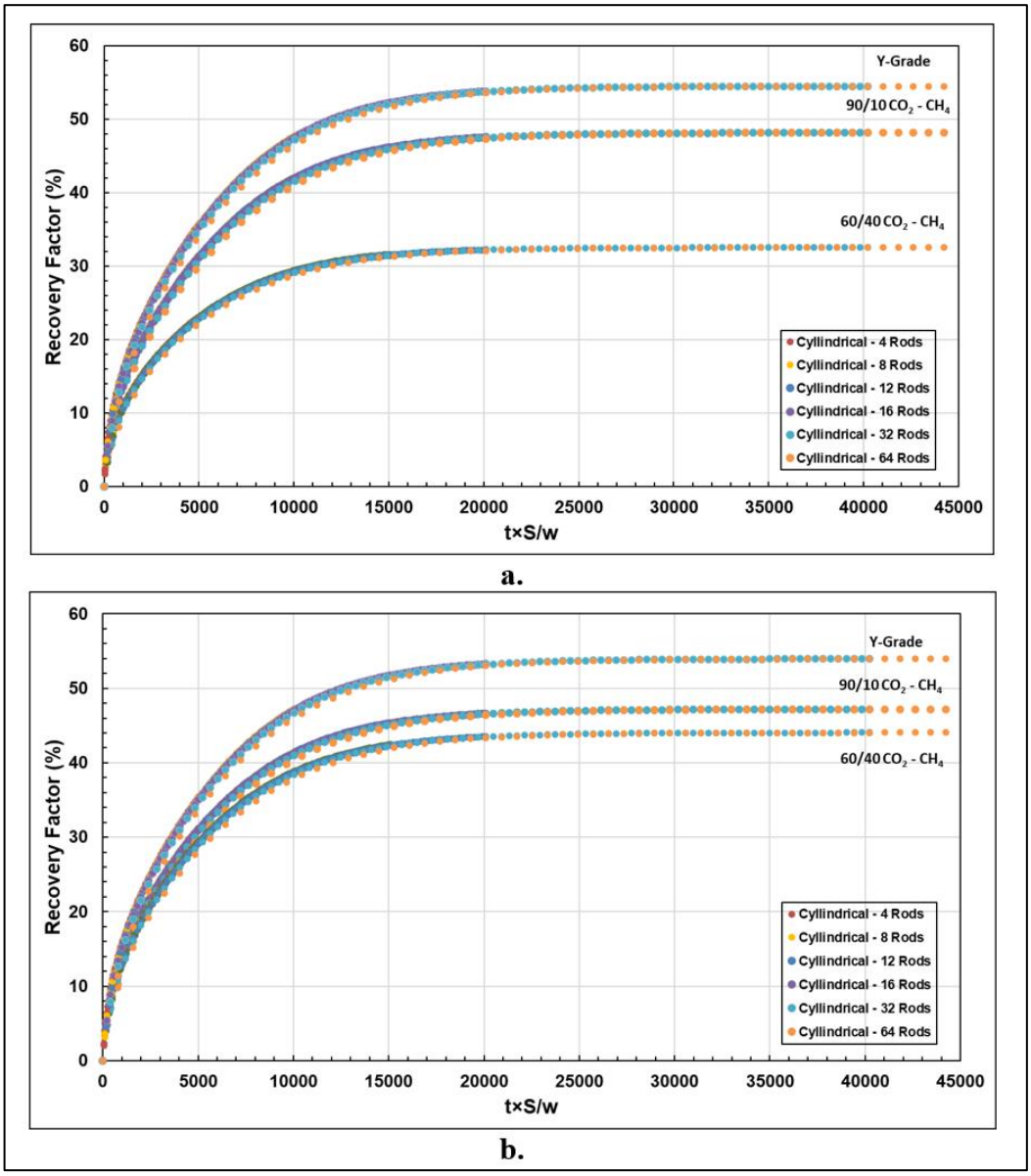

Figure 4.23 – Fracture surface area type curve. Recovery as a function of t×S/w (years/ft) for live (a.) and dead (b.) oil. Allows for prediction of recovery for a specific oil-solvent combination and any fracture surface area and flow length at a constant effective diffusion coefficient.

The type curves above can be used as a preliminary scale-up tool without requiring multiple simulations. We may estimate a recovery for any solvent-oil combination, at a given time based on the fracture surface area, fracture spacing, or effective diffusion coefficients.

CHAPTER V

CONCLUSIONS AND RECOMMENDATIONS

5.1 Conclusions

We developed a numerical simulator, estimating solvent-assisted recovery for unconventional plays provided an effective diffusion coefficient and a flow length. The following conclusions can be drawn from this work:

- Given solvent and oil composition, we can predict the maximum achievable recovery factor, based on mass balance coupled with thermodynamic phase equilibria.
- Preliminary analyses, such as maximum solvent concentration, realistic gas-oil ratio, and injected pore volume determination, can be used as a design and diagnostic tool to evaluate the maximum recovery factor for a specific oil-solvent combination.
- Number of cycles required in a huff-n-puff project may be estimated, given fracture volume, reservoir geometry and project duration.
- The solvent produced (which can be recycled back into the well) can be calculated from the swollen volume after flashing at standard conditions, and solvent stored can be calculated from the solvent concentration in the reservoir.
- Heavy solvents such as Y-Grades may be used as a substitute for commonly used injection gases such as CO_2 and CH_4, allowing unrefined gas liquids to be reinjected into the well, further improving production. Liquid solvents do not require to be compressed and there currently exists a surplus of natural gas liquids (Moody 2020), making it cheaper than alternatives. However, liquid solvents require a greater

number of cycles, demanding greater volume of solvent to be used and more frequent stoppage times.

5.2 Future Work and Recommendations

We focused on modeling and analyzing the fluid transport, thermodynamics, and limitations of solvent-assisted oil recovery in liquid-rich unconventional plays, in which the flow is limited by molecular diffusion.

To further improve the understanding of huff-n-puff processes in tight oil reservoirs, we recommend the following future work:

- Our simulator does not consider reservoirs that have oil initially in two-phases. Consequently, we are not analyzing two-phase behavior on the flow as solvent diffuses, as well as the impact capillary pressure will have on the properties of the mixture
- Further validation of number of cycles required for a huff-n-puff injection process, and solvent stored need to be performed using laboratory experiments. Experiment must be able to trace solvent and record solvent concentration within sample.
- We assume a range of realistic effective diffusion coefficients, based on stimulation of the reservoir, and oil-solvent interaction. There exist ample studies on the binary diffusion coefficient between CO2 and oil, including empirical models that may be used to calculate the coefficient for specific scenarios; however, the same cannot be said for multi-component diffusion. A more thorough analysis of effective diffusion coefficient should be done, such that, multi component diffusion can be taken into consideration.

- We are modeling the flow of solvent from the fracture to the matrix, and assume that the oil flows into the fracture solely based on the concentration gradient driven diffusion. The flow from the fracture to the surface, or rather, the production of oil will follow a different flow mechanism that should be analyzed, considering different production techniques, multilateral wells, flow assurance and fracture interference.

REFERENCES

Alfarge, Dheiaa, Mingzhen Wei, and Baojun Bai. 2017a. "Factors Affecting CO2-EOR in Shale-Oil Reservoirs: Numerical Simulation Study and Pilot Test." *Engergy Fuels* (American Chemical Society) 8462-8480.

Alfarge, Dheiaa, Mingzhen Wei, Baojun Bai, and Abdullah Almansour. 2017b. "Optimizing Injector-Producer Spacing for CO2 Injection in Unconventional Reservoirs of North America." *SPE Kingdom of Saudi Arabia Annual Technical Symposium and Exhibition.* Dammam: Society of Petroleum Engineers.

Burrows, Lauren C., Foad Haeri, Patricia Cvetic, Sean Sanguinito, Fan Shi, Deepak Tapriyal, Angela Goodman, and Robert M. Enick. 2020. "A Literature Review of CO2, Natural Gas, and Water-Based Fluids for Enhanced Oil Recovery in Unconventional Reservoirs." *Energy Fuels* (ACS Publications) 34: 5331-5380. doi:10.1021/acs.energyfuels.9b03658.

Elkady, Youssef, and Anthony R. Kovscek. 2020. "Multiscale study of CO2 impact on fluid transport and carbonate dissolution in Utica and Eagle Ford shale." *Journal of Petroleum Science and Engineering.* doi:10.1016/j.petrol.2020.107867.

Elturki, Mukhtar, and Abdulmohsin Imqam. 2020. "Application of Enhanced Oil Recovery Methods in Uncoventional Reservoirs: A Review and Data Analysis." *54th US Rock Mechanics/Geomechanics Symposium.* Golden: American Rock Mechanics Association.

Gale, Julia F. W., Stephen E. Laubach, Jon E. Olson, Peter Eichhubl, and András Fall. 2014. "Natural fractures in shale: A review and new observations." *AAPG Bulletin* (The American Association of Petroleum Geologistis) 98: 2165-2216.

Gamadi, T. D., J. J. Sheng, M. Y. Soliman, H. Menouar, M.C. Watson, and H. Emadibaladehi. 2014. "An Experimental Study of Cyclic CO2 Injection to Improve Shale Oil Recovery." *SPE Improved Oil Recovery Symposium.* Tulsa: Society of Petroleum Engineers.

Glorioso, John C., and Aquiles Rattia. 2012. "Unconventional Reservoirs: Basic Petrophysical Concepts for Shale Gas." *SPE/EAGE European Unconventional Resources Conference and Exhibition.* Vienna: Society of Petroleum Engineers.

Hawthorne, Steven B., Charles D. Gorecki, James A. Sorensen, Edward N. Steadman, John A. Harju, and Steve Melzer. 2013. "Hydrocarbon Mobilization Mechanisms from Upper, Middle, and Lower Bakken Reservoir Rocks Exposed to CO2." *Society of Petroleum Engineers.* doi:10.2118/167200-MS.

Hoteit, Hussein, and Abbas Firoozabadi. 2009. "Numerical Modeling of Diffusion in Fracture Media for Gas-Injection and -Recycling Schemes." *SPE Annual Technical Conference and Exhibition.* San Antonio: Society of Petroleum Engineers. doi:10.2118/103292-PA.

Jia, Bao, Hyun-Syung Tsau, and Reza Barati. 2019. "A review of the current progress of CO2 injection EOR and carbon storage in shale oil reservoirs." *Fuel.* doi:10.1016/j.fuel.2018.08.103.

Jia, Bao, Jyun-Syung Tsau, and Reza Barati. 2018. "Role of molecular diffusion in heterogeneous, naturally fractured shale reservoirs during CO2 huff-n-puff." *Journal of Petroleum Science and Engineering* 164: 31-42. doi:10.1016/j.petrol.2018.01.032.

Lake, Larry W., Russell Johns, Bill Rossen, and Gary Pope. 2014. *Fundamentals of Enhanced Oil Recovery.*

Lei, Qinghua, John-Paul Latham, and Chin-Fu Tsang. 2017. "The use of discrete fracture networks for modelling coupled geomechanical and hydrological behaviour of fractured rocks." *Computers and Geotechnics* (Elsevier Ltd.) 85: 151-176. doi:10.1016/j.compgeo.2016.12.024.

Liu, Guoqing, Tong Zhou, Fengxia Li, Yuanzhao Li, and Christine Ehlig-Economides. 2020. "Fracture Surface Area Estimation from Hydraulic-Fracture Treatment Pressure Falloff Data." *Society of Petroleum Engineers.*

Milad, Muhend, Radzuan Junin, Akhmal Sidek, Abdulmohsin Imwam, and Mohamed Tarhuni. 2021. "Huff-n-Puff Technology for Enhanced Oil Recovery in Shale/Tight Oil Reservoirs: Progress, Gaps, and Perspectives." *Energy Fuels* (ACS Publications) 35: 17279-17333. doi:10.1021/acs.energyfuels.1c02561.

Moody, Mark. 2020. *Using Natural Gas Liquids to Recover Unconventional Oil and Gas Resources.* Presentation, Battelle.

Perrin, Jack, and Emily Geary. 2019. *EIA adds new play production data to shale gas and tight oil reports.* February 2019. Accessed July 31, 2022. https://www.eia.gov/todayinenergy/detail.php?id=38372.

Pitman, Janet K., Leigh C. Price, and Julie A. LaFever. 2001. "Diagenesis and Fracture Development in the Bakken Formation, Williston Basin: Implications for Reservoir Quality in the Middle Member." U.S. Geological Survey Professional Paper 1653.

Prawira, Aliffa Raysha. 2021. *Evaluation of Minimum Miscibility and Effective Diffusion Coefficients for Design of Gas Assisted Recovery in Unconventional Liquid-Rich Reservoirs.* Masters Thesis, Texas A&M University.

Rachford, Jr., H. H., and J. D. Rice. 1952. "Procedure for Use of Electronic Digital Computers in Calculating Flash Vaporization Hydrocarbon Equilibrium." *J Pet Technol* 4 (10): 19. doi:10.2118/952327-G.

Robinson, D. B., and D. Y. Peng. 1976. "A New Two-Constant Equation of State Industrial and Engineering Chemistry: Fundamentals. Industrial & Engineering Chemistry Fundamentals." 15: 59-64.

Sahimi, Muhammad. 2011. *Flow and Transport in Porous Media and Fracture Rock.* 2nd. WILEY-VCH Verlag GmbH & Co. KGaA.

Scheibel, Edward G. 1954. "Liquid Diffusivities." *Industrial & Engineering Chemistry* 46: 2007-2008. doi:10.1021/ie50537a062.

Theloy, Cosima. 2014. "Integration of geological and technological factors influencing production the the Bakken play, Williston Basin." (ProQuest LLC).

Tianying, Jin. 2021. "Assessing the Impact on Hydrocarbon Production from Tight and Shale Plays by Depletion and Injection Using Thermodynamic and Transport Properties from Confined Spaces." https://hdl.handle.net/1969.1/193184.

Tovar, F.D., M.A. Barrufet, and D.S Shecter. 2018. "Gas Injection for EOR in Organic Rich Shales. Pat II: Mechanisms of Recovery." *SPE/AAPG/SEG Uncoventional Resources Technology Conference.* Houston, Texas. doi:10.15530/URTEC-2018-2903026.

Tovar, Francisco Deomar. 2017. *Gas Injection for Enhanced Oil Recovery in Organic Rich Shale Reservoirs.* PhD Thesis, Texas A&M University.

United States Energy Information Administration. July. *Oil and petroleum products explained.* 8 2022. Accessed 30 2022, July. https://www.eia.gov/energyexplained/oil-and-petroleum-products/where-our-oil-comes-from-in-depth.php.

United States Environmental Protection Agency. 2016. *Environmental Geophysics.* Accessed July 30, 2022. https://archive.epa.gov/esd/archive-geophysics/web/html/acoustic_logging.html.

Wilke, C. R., and Pin Chang. 1955. "Correlation of Diffusion Coefficients in Dilute Solutions." *AlChe* 1: 264-270. doi:10.1002/aic.690010222.

Yu, Long, Jinjie Wang, Chong Wang, and Daixin Chen. 2019. "Enhanced Tight Oil Recovery by Volume Fracturing in Chang 7 Reservoir: Experimental Study and Field Practice." *Energies* 12, no. 12: 2419. https://doi.org/10.3390/en12122419.

Yu, Wei, HamidReza Lashgari, and Kamy Sepehrnoori. 2014. "Simulation Study of CO2 Huff-n-Puff Process in Bakken Tight Oil Reservoirs." *SPE Western North American*

and Rocky Mountain Joint Regional Meeting. Denver: Society of Petroleum Engineering.

APPENDIX A

SOLVENT CONCENTRATION AFTER DIFFUSION

A.1 Average Solvent Concentration Following Huff-n-Puff Process

In Chapter III, we discuss a situation in which solvent is switched after the huff-n-puff process. The process had a project life of 20 years, after 5 years of injecting 90/10 CO_2-CH_4, the solvent was switched for a Y-Grade solvent and the process was run for 15 more years. However, following the initial 5 years, the solvent did not fully saturate the reservoir, such that it was entirely at the produced concentration, instead a concentration profile existed within the matrix, ranging from the maximum concentration at the matrix, and decreasing as we moved away from the fracture, illustrated in **Figure A.1**.

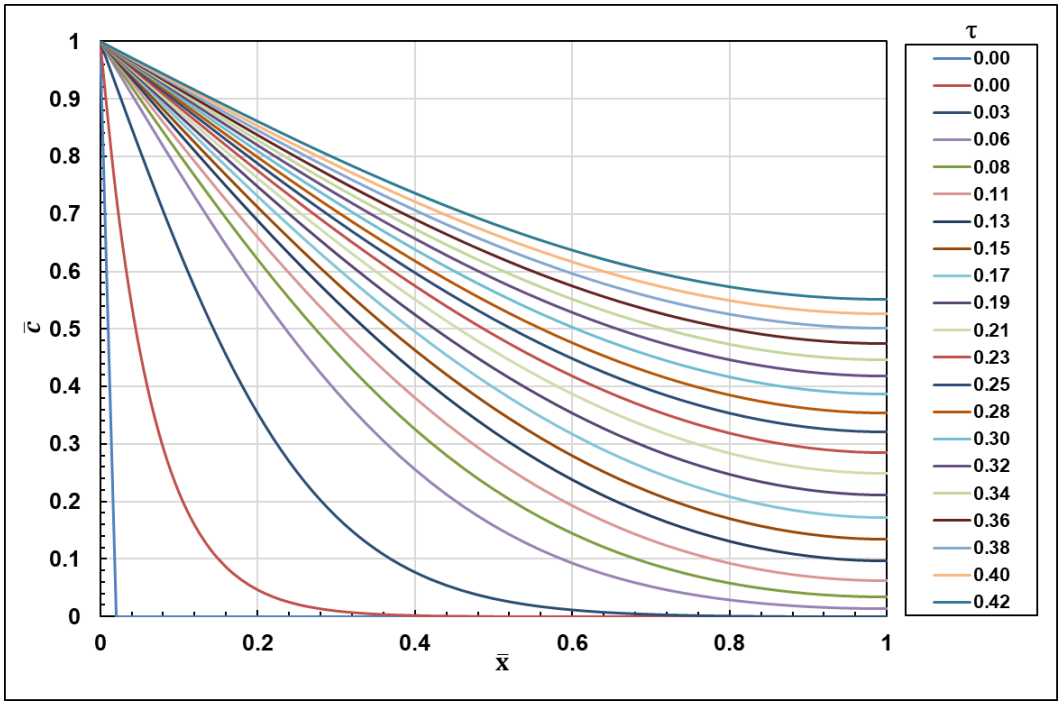

Figure A.1 – Dimensionless solvent concentration profile as a function of dimensionless width for the live oil and 90/10 CO_2-CH_4 solvent. τ = 0.42 (final

dimensionless time) illustrates solvent concentration profile left in the matrix after the predetermined 5 years.

We are interested in the final range of solvent concentrations. The solvent that is left in the reservoir functions as part of the oil for when the new solvent is introduced. We can estimate the concentration of the initial solvent by assuming that what is stored in the reservoir is equal to the average concentration of the solvent at the end time. Using the original molar fractions of each component making up the oil and the solvent, we combine them on a molar basis, creating a new oil for a different solvent to swell. We may also assume the lower or higher boundary as the solvent left, as such we may be underestimating and overestimating the concentration profile, respectively, and analyze the impact on recovery. **Figure A.2** illustrates the results of the 20-year process using the three different methodologies.

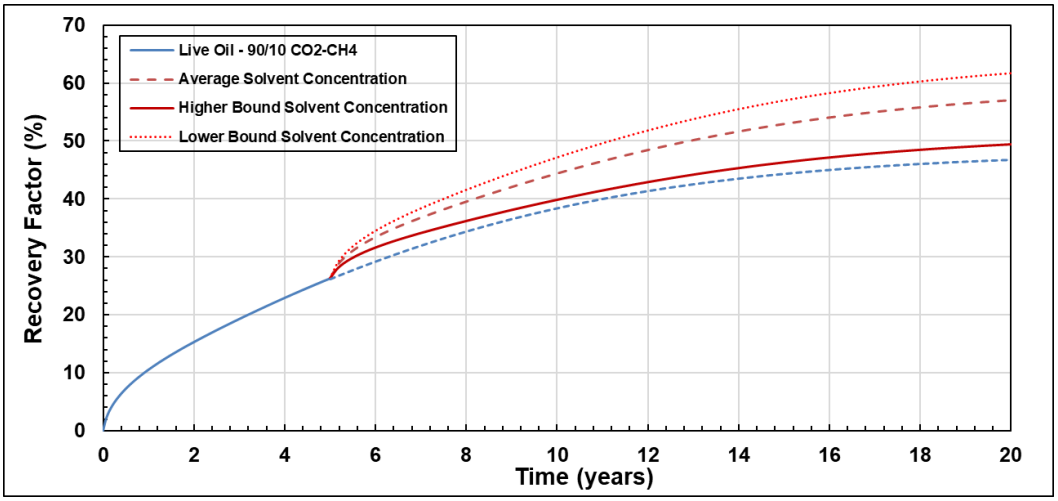

Figure A.2 – Recovery factor of 20-year huff-n-puff injection process, for the live oil. Including a solvent change after the initial 5 years of injection from 90/10 CO_2-CH_4 solvent to Y-Grade solvent for 15 more years. Depicting difference between using lower bound, higher bound and average of solvent profile in matrix after 5 years.

As expected, using either the lower bound or higher bound of the concentration profile resulted in an underestimation and an overestimation of the solvent concentration in

the matrix, leading to skewed recovery results. Using the lower bound of the solvent concentration profile led to an overestimation of the final recovery after the 15 years of Y-grade injection, as the original oil had only a small concentration of 90/10 CO_2-CH_4 solvent after the initial 5 years, allowing for a greater concentration of Y-grade to be used to maintain the constraint of 1.2 injected pore volumes. The opposite occurred when using the higher bound of the solvent concentration profile. We observed an underestimation of the recovery at the end of the 20-year process, in this case, the original oil was assumed to be fully saturated at the initial proposed concentration of 90/10 CO_2-CH_4 solvent, resulting in a lower concentration of Y-grade to be used while constraining the injected pore volumes to 1.2. While assuming the entire reservoir is at the average solvent concentration may lead to inaccurate results as well, it will serve as a better estimation than other methods.

APPENDIX B

INCLUSION OF ADVECTIVE TRANSPORT

B.1 Convection-Diffusion Flow

Our model allows for the inclusion of advective transport when considering the flow of oil from the matrix into the fractures. In Chapter II, we investigated the Peclet number, and concluded that due to the low fluid velocity caused by the low mobility in the nano pores, the Peclet number will be small (< 1) for unconventional reservoirs. As such, advection was assumed to be negligible, and the flow dominated by molecular diffusion. This appendix describes the equations used to include advective flow and illustrates the impact its inclusion has on the recovery factor of a huff-n-puff process.

Considering diffusion and advection-driven flow, we can expand Fick's second law of diffusion into the convection-diffusion equation (**Eq. (B.1)**). Once again, the change in concentration will be a product of the diffusion coefficient and the Laplacian of the concentration, as well as swelling-induced velocity in the opposite direction of flow, hindering diffusion.

$$\frac{\partial c}{\partial t} = D_{eff} \nabla^2 c - \nabla \cdot (c \vec{u}) \qquad \textbf{(B.1)}$$

Similarly, we consider one-dimensional flow, assuming that the fracture is the same height as the matrix and fully saturated with solvent. The flow will then be perpendicular to the length of the fracture. Eq. (B.1) can then be simplified to **Eq. (B.2)**.

$$\frac{\partial c}{\partial t} = D_{eff}\frac{\partial^2 c}{\partial x^2} - c\frac{\partial u}{\partial x} - u\frac{\partial c}{\partial x} \tag{B.2}$$

The volume expansion of the oil will cause a change in velocity, defined by the flow rate change over the cross-sectional area of the matrix. **Eq. (B.3)** shows the velocity change between two cells, where the term $c^{t+\Delta t}_{x+\Delta x}$ refers to the concentration at distance $x+\Delta x$ and time $t+\Delta t$.

$$\Delta u^{t+\Delta t}_{x+\Delta x} = \frac{\phi \Delta x}{(x+\Delta x)\,\Delta t}\left[f\left(\frac{c^{t+\Delta x}_{x+\Delta x} + c^{t+\Delta x}_{x}}{2}\right) - f\left(\frac{c^{t}_{x+\Delta x} + c^{t}_{x}}{2}\right)\right] \tag{B.3}$$

Boundary conditions (**Eq. (B.4)** and **Eq. (B.5)**) and initial conditions (**Eq. (B.6)** to **Eq. (B.8)**) will be the same as the model without advection, the only difference being the lack of the velocity term.

Dimensionless Boundary Conditions:

$$\bar{c} = 1, \text{ at } \bar{x} = 0 \tag{B.4}$$

$$\bar{u} = 0, \frac{d\bar{c}}{dx} = 0, \text{ at } \bar{x} = L \tag{B.5}$$

Dimensionless Initial Conditions:

$$\bar{c} = 1, \text{ at } \bar{x} = 0, \tau = 0 \tag{B.6}$$

$$\bar{c} = \bar{c}_i, \text{ at } \bar{x} > 0, \tau = 0 \tag{B.7}$$

$$\bar{u} = 0, \text{ at } \bar{x} = 1, \tau = 0 \tag{B.8}$$

We now substitute the dimensionless variables into the molecular diffusion equation (Eq. (B.2)), as shown in **Eq. (B.9)**.

$$\frac{\partial \bar{c}}{\partial \tau} = \frac{\partial^2 \bar{c}}{\partial \bar{x}^2} - \bar{c}\frac{\partial \bar{u}}{\partial \bar{x}} - \bar{u}\frac{\partial \bar{c}}{\partial \bar{x}} \quad \textbf{(B.9)}$$

We illustrated the impact advection has on the final recovery factor and the gross utilization factor (**Eq. (B.10)**), of a stimulated reservoir by continually increasing effective diffusion coefficient using the live oil and the 90/10 CO_2-CH_4 solvent as an example (**Figure B.1**). **Table B.1** shows the reservoir and fracture properties as well as the time constraint used for all simulated cases.

$$GUF = \frac{(Solvent\ Stored + Solvent\ Produced)}{Oil\ Produced} \quad \textbf{(B.10)}$$

Table B.1 – Diffusion simulation input, including stimulated reservoir and fracture porosity, length, width, height, pressure, temperature, and time constraint.

Stimulated Reservoir Properties		Fracture Properties	
ϕ_R (%)	10	ϕ_F (%)	40
l_R (ft)	200	l_F (ft)	200
w_R (ft)	20	w_F (ft)	2.5
h_R (ft)	200	h_F (ft)	200
P_R (psi)	3750	Constraint	
T_R (°F)	175	End Time (years)	10

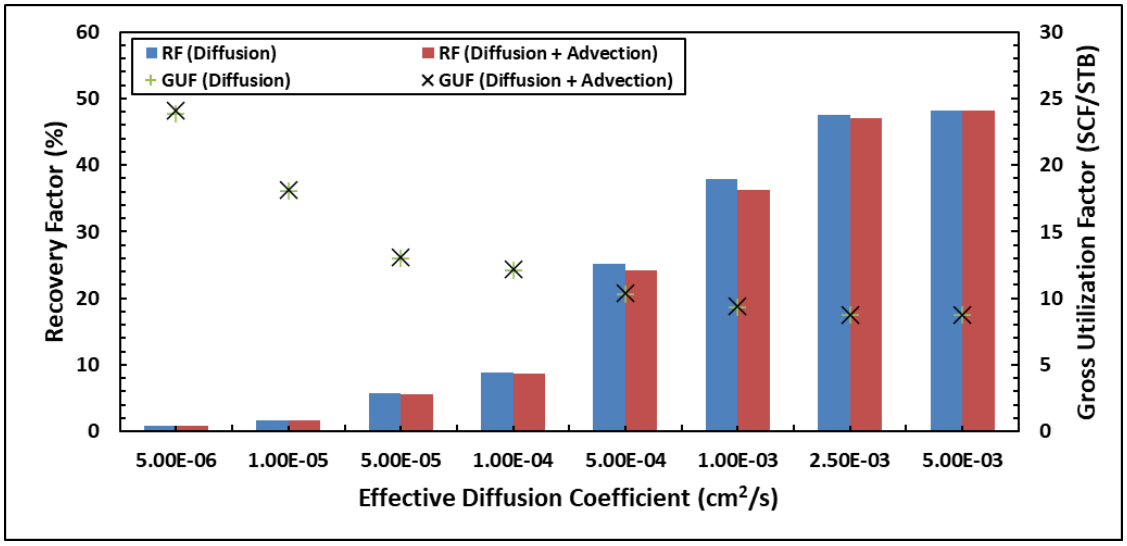

Figure B.1 – Impact of advective flow on final recovery factor and gross utilization factor, following 10 years of production of a reservoir at a pressure of 3750 psi and temperature of 175 °F.

Oil swelling caused by the solvent combination creates a velocity difference. However, as depicted by Figure B.1, the difference in recovery factor and gross utilization factor by considering this counter flow is minimal. The difference in recovery is the greatest at high effective diffusion coefficients, as the solvent is quickly swelling the oil, causing a high velocity profile in the opposite direction of the flow, slowing down diffusion. Yet, gross utilization factor is unaffected by the advective flow, rather, counter flow velocity is not impacting oil production such that a greater amount of solvent must be used. As such advection may be considered negligible.

APPENDIX C

OIL AND SOLVENT SEPARATION

C.1 Injection of solvent components included in original oil

In Chapter III, we stated that prior to calculating the recovery factor of oil, the solvent moles injected had to be separated from the oil moles in cases that the original oil included one or more solvent components. Failing to separate the moles will lead to recoveries greater than 100%. This appendix illustrates both scenarios, including the separation of the respective solvent moles from the oil prior to the flash, and not separating. As an example, we used Tianying (2021)'s live oil together with a solvent including components in the oil, injected at a constant solvent concentration of 0.7 solvent moles/total moles. **Table C.1** displays the solvent used for this example.

Table C.1 – Solvent used to illustrate proper separation of solvent moles before flashing. Noting that all three components are contained within the original Tianying (2021)'s live oil.

Injection Fluid Data	
Name	z_i
CO2	0.067
C4-6	0.133
F1	0.800

Once solvent has been added to the oil on a molar basis, we flash at standard temperature and pressure, providing with liquid and vapor compositions as well as the liquid and molar fractions. **Table C.2** illustrates the oil-solvent mixture after injection of solvent.

Table C.2 – Solvent/Oil combination calculations. Containing initial oil z_i, combined with CO_2, C_{4-6} and F1 solvent, and flash of mixture at standard conditions.

Component	Liquid - x_i	Vapor - y_i	Feed - z_i	initial oil z_i	Sol.	z_i	n_o	n_s	n_t
C1	7.00E-08	1.28E-05	4.00E-06	1.00E-05			5.89E-06		5.89E-06
N2	2.22E-08	1.29E-05	4.00E-06	1.00E-05			5.89E-06		5.89E-06
CO2	3.48E-03	1.24E-01	4.08E-02	1.98E-03	CO2	0.067	1.17E-03	5.89E-02	6.01E-02
N2C1	3.36E-03	6.33E-01	1.98E-01	4.94E-01			2.91E-01		2.91E-01
C2-3	1.10E-02	1.55E-01	5.53E-02	1.38E-01			8.15E-02		8.15E-02
C4-6	1.39E-01	8.78E-02	1.23E-01	1.09E-01	C4-6	0.133	6.41E-02	1.18E-01	1.82E-01
F1	8.14E-01	7.63E-04	5.63E-01	2.07E-01	F1	0.800	1.22E-01	7.07E-01	8.30E-01
F2	2.86E-02	7.06E-15	1.98E-02	4.94E-02			2.91E-02		2.91E-02

For simplification we then normalize the moles produced n_p, such that it equals 1. It is worth noting that regardless of the value of n_p, the final recovery is unaffected by it, as it is an intrinsic property. Using **Eq. (C.1)** to **Eq. (C.3)**, we calculate the moles in the vapor phase (n_v), in the liquid phase (n_s), and sum both phases providing the total moles (n_t) (**Table C.3**).

$$n_v = n_p \times y_i \times \left(1 - f_l\right) \quad \textbf{(C.1)}$$

$$n_l = n_p \times x_i \times f_l \quad \textbf{(C.2)}$$

$$n_t = n_v + n_l \quad \textbf{(C.3)}$$

Table C.3 – Solvent/Oil combination phase calculations. Separation of moles by phase, including vapor phase (n_v), liquid phase (n_l), as well as the addition of both moles, labeled as total moles (n_t).

Component	n_{feed}	n_v	n_l	n_t	f_l	f_v
C1	4.00E-06	3.95E-06	4.84E-08	4.00E-06	0.691	0.309
N2	4.00E-06	3.98E-06	1.54E-08	4.00E-06		
CO2	4.08E-02	3.84E-02	2.40E-03	4.08E-02		
N2C1	1.98E-01	1.95E-01	2.32E-03	1.98E-01		
C2-3	5.53E-02	4.77E-02	7.59E-03	5.53E-02		
C4-6	1.23E-01	2.71E-02	9.64E-02	1.23E-01		
F1	5.63E-01	2.36E-04	5.63E-01	5.63E-01		
F2	1.98E-02	2.18E-15	1.98E-02	1.98E-02		

We now separate the moles coming from the oil and the moles coming from the solvent in both phases, by calculating the percentage of the total moles coming from the oil (**Eq. (C.4)**). Multiplying vapor moles, or liquid moles by the % $n_{\text{from oil}}$, provides with the moles coming from the oil by phase (**Eq. (C.5)** and **Eq. (C.6)**). Subtracting vapor or liquid moles by the moles coming from the oil, results in the moles coming from the solvent. **Table C.4** illustrates the result of using the following equations on the test case.

$$\%\, n_{f\,rom\ oil} = z_i \times \frac{n_o}{n_{f\,eed}} \qquad \textbf{(C.4)}$$

$$n_{v\,(oil)} = n_v \times \%\, n_{f\,rom\ oil} \qquad \textbf{(C.5)}$$

$$n_{l\,(oil)} = n_l \times \%\, n_{f\,rom\ oil} \qquad \textbf{(C.6)}$$

$$n_{v\,(sol)} = n_v - n_{v\,(oil)} \qquad \textbf{(C.7)}$$

$$n_{l\,(sol)} = n_l - n_{l\,(oil)} \qquad \textbf{(C.8)}$$

Table C.4 – Separation of moles coming from the oil and moles coming from the solvent. Calculating % of moles coming from the oil. Highlighted liquid moles in red are then used to calculate recovery factor.

	Coming from the Oil		Coming from the Solvent		
Component	n_v (oil)	n_l (oil)	n_v (sol)	n_l (sol)	Oil %
C1	3.95E-06	4.84E-08	0.00E+00	0.00E+00	100%
N2	3.98E-06	1.54E-08	0.00E+00	0.00E+00	100%
CO2	7.47E-04	4.68E-05	3.76E-02	2.36E-03	1.95%
N2C1	1.95E-01	2.32E-03	0.00E+00	0.00E+00	100%
C2-3	4.77E-02	7.59E-03	0.00E+00	0.00E+00	100%
C4-6	9.54E-03	3.39E-02	1.76E-02	6.24E-02	35.2%
F1	3.47E-05	8.30E-02	2.01E-04	4.80E-01	14.7%
F2	2.18E-15	1.98E-02	0.00E+00	0.00E+00	100%
sum	2.53E-01	1.47E-01	5.54E-02	5.45E-01	

Finally, to avoid double counting the initial solvent moles already in the oil. We flash solely the liquid moles coming from the oil (**Table C.5**), and calculate the oil produced (**Eq. (C.9)**). Dividing the oil produced by the original oil in place, results in recovery factor. **Table**

C.6 illustrates the recovery factor using the methodology in this appendix, and the recovery factor not considering the separation of the solvent moles, at different solvent concentrations.

$$N_p = n_{l\,(oil)} \times V_{ml} \times f_l \qquad \textbf{(C.9)}$$

Table C.5 – Flash of separated liquid moles at standard conditions. From it, we acquire liquid molar volume and liquid fraction.

Data			Phase	Mol Fraction	Density (lb/ft^3)	Volume (cc)	Molar Vol. (ft^3/lbmol)
Temperature (°F)	60.0		Liquid	0.962	50.116	0.190	3.171
P (psia)	14.7		Gas	0.038	0.090	0.888	375.545
Component	Liquid - xi	Vapor - yi	Feed - zi				
C1	4.37E-08	7.61E-06	3.30E-07				
N2	4.90E-09	2.64E-06	1.05E-07				
CO2	1.38E-04	4.91E-03	3.19E-04				
N2C1	2.04E-03	3.66E-01	1.58E-02				
C2-3	3.49E-02	4.82E-01	5.18E-02				
C4-6	2.35E-01	1.47E-01	2.31E-01				
F1	5.88E-01	5.69E-04	5.66E-01				
F2	1.40E-01	3.32E-14	1.35E-01				

Table C.6 – Recovery factor at increasing solvent concentration, including separation of solvent moles and not. If moles are not separated, recovery factor will pass 100%.

	Sol. Concentration		
	0.60	0.70	0.80
RF %=	72.90%	83.03%	92.48%
RF % no sep.=	87.55%	118.27%	175.33%

At the original solvent concentration of 0.6, not accounting for the separation of the solvent will lead to a recovery factor difference of 15% (higher). The problem becomes more significant the higher the solvent concentration. Past a solvent concentration of 0.70, not separating solvent moles will lead to recoveries of over 100%, which is not possible; however, since the solvent injected contains oil components, the simulator must track the moles of every component and be able to separate solvent moles from initial oil moles.